

DISSERTATION

DEVELOPMENT OF A HYALURONAN-POLYETHYLENE COPOLYMER FOR  
USE IN ARTICULAR CARTILAGE REPAIR

Submitted by

Rachael Oldinski

Department of Mechanical Engineering

In partial fulfillment of the requirements

For the Degree of Doctor of Philosophy

Colorado State University

Fort Collins, Colorado

Spring 2009

UMI Number: 3374637

### INFORMATION TO USERS

The quality of this reproduction is dependent upon the quality of the copy submitted. Broken or indistinct print, colored or poor quality illustrations and photographs, print bleed-through, substandard margins, and improper alignment can adversely affect reproduction.

In the unlikely event that the author did not send a complete manuscript and there are missing pages, these will be noted. Also, if unauthorized copyright material had to be removed, a note will indicate the deletion.

**UMI<sup>®</sup>**

---

UMI Microform 3374637  
Copyright 2009 by ProQuest LLC  
All rights reserved. This microform edition is protected against  
unauthorized copying under Title 17, United States Code.

---

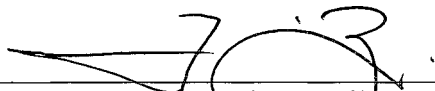
ProQuest LLC  
789 East Eisenhower Parkway  
P.O. Box 1346  
Ann Arbor, MI 48106-1346

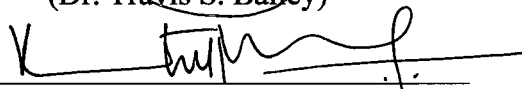
COLORADO STATE UNIVERSITY

December 15, 2008

WE HEREBY RECOMMEND THAT THE DISSERTATION PREPARED UNDER OUR SUPERVISION BY RACHAEL A. OLDINSKI ENTITLED [DEVELOPMENT OF A HYALURONAN-POLYETHYLENE COPOLYMER FOR USE IN ARTICULAR CARTILAGE REPAIR] BE ACCEPTED AS FULFILLING IN PART REQUIREMENTS FOR THE DEGREE OF DOCTOR OF PHILOSOPHY.

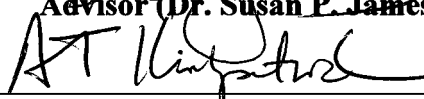
Committee on Graduate work

  
\_\_\_\_\_  
(Dr. Travis S. Bailey)

  
\_\_\_\_\_  
(Dr. Ketul C. Popat)

  
\_\_\_\_\_  
(Dr. Xianghong Qian)

  
\_\_\_\_\_  
Advisor (Dr. Susan P. James)

  
\_\_\_\_\_  
Department Head (Dr. Allan T. Kirkpatrick)

ABSTRACT OF DISSERTATION

DEVELOPMENT OF A HYALURONAN-POLYETHYLENE COPOLYMER FOR  
USE IN ARTICULAR CARTILAGE REPAIR

Articular cartilage is the connective tissue which covers the ends of long bones, providing a lubricious, hydrodynamic surface for articulation and energy dissipation. Articular cartilage has a limited ability to repair itself; once the native tissue has become damaged, either from injury or disease (e.g., arthritis), it is irreversible and the tissue will degrade with time resulting in joint pain. The goal of this research was to develop a permanent (i.e., non biodegradable/bioerodible) bioactive material and assess its applicability for articular cartilage repair and/or replacement. Utilizing two constituents, polyethylene (the 'gold standard' bearing material for total joint replacements) and hyaluronan (HA, a native component of articular cartilage), a hyaluronan-polyethylene graft copolymer (HA-*co*-HDPE) was developed. The novel HA-*co*-HDPE material was successfully synthesized using an interfacial polymerization reaction in a non-aqueous environment. Although the material has limited melt-processability, it is more processable than HA and was successfully compression molded into samples for physical, mechanical and *in vitro* biological characterization (e.g., swell ratio, dynamic mechanical analysis). HA-*co*-HDPE exploits the strength, rigidity and melt-processability associated with HDPE, and achieves increased osteogenic potential by incorporating the highly hydrophilic

biopolymer HA. In conclusion, the swelling, mechanical and degradation properties of the copolymer can be custom-optimized for biomedical applications by tailoring chemical or physical crosslinking strategies and varying the amount and molecular weights of HA and HDPE incorporated into the copolymer.

Rachael A. Oldinski  
Mechanical Engineering Department  
Colorado State University  
Fort Collins, CO 80523  
Spring 2009

## ACKNOWLEDGEMENTS

I would first like to thank my academic advisor and mentor, Dr. Susan James, for advancing my knowledge of polymer science and engineering and introducing me to the world of polymer chemistry. My gratitude and respect goes beyond limits; with her direction I achieved my goals successfully. Next, I would like to thank my committee members, Dr. Travis Bailey, Dr. Ketul Popat and Dr. Xianghong Qian, for providing input in support of my research within their respective fields of expertise. Also, this research presented in this thesis would not have been completed without the help and knowledge from various professional mentors: Dr. Herb Schwartz, Mrs. Rhonda Clark, Dr. Janine Campbell, and Mr. Frank Proch (Schwartz Biomedical); Dr. Eugene Chen, Dr. John Kisiday, Mr. Mike Karr, Dr. Pat McCurdy, Dr. Sandeep Kohli, and Dr. Don Heyse (CSU); Dr. Dennis Slatton, and Dr. Henri Wautier (Solvay Plastics). The following individuals motivated my research and without them I would not have accomplished as much as I did; I am very thankful for all of their effort and confidence throughout the past two and half years: Dr. Marisha Godek, Jeff Harris, Nate Johnson, Cody Cranson, Susan Yonemura, Jason Marini, Kari Luers, Tim Ruckh, Drew Henson, Trey Rodgers and David Prawel. Last, but certainly not least, I want to thank my husband, best friend, and inspiration, Keith Oldinski, for holding me together during the most stressful times and for keeping me grounded. Without you I would not have made it as far as I did.

## TABLE OF CONTENTS

Chapter 1: Background and Motivation.....	1
1.1 Introduction.....	1
1.2 Structure and Function of Articular Cartilage.....	1
1.2.1 Mechanical Properties of Articular Cartilage.....	2
1.3 Hyaluronan and HA Hydrogels.....	5
1.4 Synthetic Hydrogels for Articular Cartilage Repair.....	11
1.4.1 Characterization of Hydrogels.....	12
1.4.2 Mechanical Properties of Hydrogels.....	13
1.5 Cartilage, Hydrogel Properties Summary and Comparison.....	18
1.6 Polyethylene.....	19
1.6.1 PE Crosslinking.....	20
1.6.2 Antioxidants.....	22
1.7 Functionalized Polyolefins.....	24
1.7.1 Anhydride Esterification.....	26
1.8 Objectives and Specific Aims.....	27
1.9 References.....	29
Chapter 2: Synthesis and Characterization of HA- <i>co</i> -HDPE.....	36
2.1 Introduction.....	36
2.2 Materials and Methods.....	36

2.2.1 HA- <i>co</i> -HDPE Fabrication.....	37
2.2.2 HA- <i>co</i> -HDPE Melt Processing.....	40
2.2.3 Characterization Methods.....	44
2.2.4 Statistics.....	48
2.3 Results.....	49
2.4 Discussion.....	67
2.5 Conclusions.....	78
2.6 References.....	78
Chapter 3: Viscoelastic Characterization of HA- <i>co</i> -HDPE.....	82
3.1 Introduction.....	82
3.2 Materials and Methods.....	84
3.2.1 Dynamic Unconfined Compression.....	84
3.2.2 Dynamic Temperature Sweep.....	84
3.3 Results.....	85
3.3.1 Dynamic Unconfined Compression.....	85
3.3.2 Dynamic Temperature Sweep.....	89
3.4 Discussion.....	93
3.5 Conclusion.....	98
3.6 References.....	99
Chapter 4: <i>In Vitro</i> Biological Assessment of HA- <i>co</i> -HDPE.....	101
4.1 Introduction.....	101
4.2 Materials and Methods.....	102

4.2.1 HA- <i>co</i> -HDPE Fabrication.....	102
4.2.2 HA- <i>co</i> -HDPE Enzymatic Degradation.....	104
4.2.3 Secondary Origin Cell Study.....	105
4.2.4 Primary Origin Cell Study.....	108
4.2.5 Statistics.....	114
4.3 Results.....	115
4.3.1 Enzymatic Degradation.....	115
4.3.2 Secondary Origin Cell Study.....	116
4.3.3 Primary Origin Cell Study.....	117
4.4 Discussion.....	122
4.5 Conclusion.....	129
4.6 References.....	129

Appendix A

Appendix B

# **Chapter 1. Background and Motivation**

## **1.1 Introduction**

The following reviews the literature on stresses and strains measured in the knee joint and the mechanical properties of articular cartilage. Hydrogels and scaffolds designed for articular cartilage replacement are presented and various pertinent chemical and physical characterization methods, as well as mechanical experiments, are summarized. Information directly related to the chemical synthesis (i.e., copolymerization) of HA-co-HDPE is reviewed and preliminary data is presented on various polymer compositions and blends and the affects of such parameters on material properties. Finally, the research specific aims and hypothesis are presented followed by the research plan proposal.

## **1.2 Structure and Function of Articular Cartilage**

Cartilage is composed of chondrocytes and an extracellular matrix (ECM); the ECM mostly consists of proteoglycans (PGs), glycosaminoglycans (GAGs) such as hyaluronan (HA), type II collagen, glycoproteins (e.g., link proteins) and various mixtures of elastic fibers. The dominate load-bearing structural components in articular cartilage are the collagen molecules and negatively charged PGs.[1] The major PG in articular cartilage is aggrecan, found in huge multi-molecular aggregates comprised of numerous (greater than 100) monomers (i.e., chondroitin sulfate and keratin sulfate chains with N- and O-linked oligosaccharides) non-covalently bound to HA;[2] the non-covalent interaction between aggrecan molecules and HA can be disrupted by low pH, high ionic strength, or elevated shear forces.[3] HA plays a vital role in the swelling properties of aggrecan *in vivo*,

which stabilizes the ECM and forms the hydrated pressure-resistance gel which lubricates articulating joints. Aggrecan draws water into the tissue and creates a large osmotic swelling pressure, causing it to swell and expand (thus, aggrecan is restricted in its ability to move within the matrix and offers resistance to fluid flow), resulting in load-bearing properties critical to the biomechanics of articular cartilage. Aggrecan is also involved in mediating chondrocyte-chondrocyte and chondrocyte-matrix interactions. Link proteins, synthesized by chondrocytes, have the ability to interact with HA and a single aggrecan molecule. Together, aggrecan and HA play a role in cell-substratum adhesion.

Understanding the mechanism of lubrication of articulating surfaces *in vivo* is important; the goal is to mimic the superior tribological properties of natural joints. It has been suggested that during initial movement, a very viscous, aqueous layer protects articulating surfaces. Attenuated total reflection infrared (ATR-IR) was utilized for characterizing the composition of the superficial layer of articular cartilage.[4] ATR-IR reference materials were HA and dipalmitoyl phosphatidylcholine. It was shown via the ATR-IR analysis that HA is the decisive biomolecule that provides lubrication for articulating joints *in vivo*; the concentration of HA in synovial fluid is approximately 3 mg/mL. HA will be discussed in further detail later.

### 1.2.1 Mechanical Properties of Articular Cartilage

The mechanical properties of articular cartilage are difficult to assess and compare between testing methods because the tissue structure and properties vary depending on its location in the body. Mechanical testing is further complicated by the viscoelasticity,

poroelasticity, electromechanical forces and fluid flow, swelling behavior, and tissue prestresses.[5] A review of test methods and subsequent mechanical properties of the native articular cartilage follows so that properties of candidate copolymer materials can be compared to native cartilage.

Articular cartilage exhibits viscoelastic behaviors such as creep and stress relaxation in response to mechanical loading. Two dissipative mechanisms occur during loading: (a) fluid flow through the porous-permeable ECM creates a frictional drag force, and (b) the time-dependant swelling/deformation of the macromolecules (i.e., GAGs and PG aggregates). In response to an applied constant compressive load (or stress), articular cartilage will creep; in response to an applied constant compressive displacement (or strain), articular cartilage exhibits stress relaxation.[1] Stress relaxation and creep experiments may be performed under *confined* or *unconfined* compression; both of these experiments are used in conjunction with an isotropic homogeneous biphasic constitutive theory. The biphasic mixture theory assumes that articular cartilage is composed of two incompressible phases: an interstitial fluid phase and elastic solid matrix phase.

In static confined compression, a porous platen that allows fluid flow is used and the specimen experiences one-dimensional motion but multidimensional loading (due to the constraining sidewalls); two intrinsic material properties of the specimen can be determined: (a) the equilibrium confined compression aggregate modulus ( $H_A$ ), and (b) the hydraulic permeability ( $k$ ). The stress relaxation time constant ( $\tau$ ) can be defined by the compressive modulus, permeability and thickness ( $h$ ):  $\tau = h^2/H_A k$ . For all types of

articular cartilage, the elastic modulus ranges from 0.1 – 2.0 MPa, and the permeability ranges from  $(1.2 - 6.2) \times 10^{-16} \text{ m}^4/\text{N}\cdot\text{s}$ . [1] In static unconfined compression, a non-porous platen is used and the elastic modulus ( $E$ ), Poisson's ratio ( $\nu$ ), and hydraulic permeability can be determined; the equilibrium lateral expansion during stress relaxation or creep experiments can be measured directly using an optical method. These coefficients are also related to the shear modulus ( $\mu$ ) and aggregate modulus ( $H_A$ ) by  $\mu = E/[2(1 + \nu)]$  and  $H_A = [E(1 - \nu)]/[(1 + \nu)(1 - 2\nu)]$ . For all types of articular cartilage, the elastic modulus (which differs from the aggregate modulus) in compression ranges from 0.41 – 0.85 MPa, and the equilibrium Poisson's ratio ranges from 0.06 to 0.18. Unconfined compression can also be deformed dynamically, as described below, to determine the loss and storage moduli of viscoelastic materials such as cartilage.

Cartilage disks from the femoropatellar groove of 1-2 week old calves were subjected to cyclic shear deformation (0.01-1 Hz) at engineering strains of 0.4-1.6%. [6] Disks were compressed and allowed to reach equilibrium and subsequently subjected to continuous dynamic shear deformation (1%) at 0.1 Hz for 24 hours. The average engineering shear strain ( $\gamma$ ) in the samples were calculated by dividing the sample thickness ( $h$ ) into the product of the rotation angle ( $\theta$ ) and sample radius ( $R$ ); the average dynamic shear stress ( $\tau$ ) applied to the samples was calculated by dividing the torque ( $T$ ) by the product of the  $R$  and surface area ( $A$ ); the effective shear modulus ( $G$ ) was calculated by dividing  $\tau$  by  $\gamma$ . The  $G$  was in the range of 0.6-1.5 MPa for the cartilage explants at 10% axial offset strain and shear strains  $\leq 1\%$ . [6]

Table 1 summarizes the various mechanical properties known for healthy, native articular cartilage. It is important to keep in mind, however, that these values represent a range of properties determined from many different testing techniques for tissue samples from various locations of the anatomy. Coefficient of friction data (COF) can be found in Table 2 because the information was obtained from a hydrogel study.

**Table 1. Summary of articular cartilage mechanical properties.**

<b>Mechanical Property Tested</b>	<b>Property Value Range</b>
Elastic (Tensile) Modulus	5 – 25 MPa [1]
Elastic (Compressive) Modulus	0.41 – 0.85 MPa [1]
Aggregate Modulus	0.06 – 2.0 MPa [1, 7]
Shear Modulus	0.6 – 1.5 [6]
Toughness	130 kcal [5]
Poisson's Ratio	0.06 – 0.18 [1]

### 1.3 Hyaluronan and HA Hydrogels

HA is a biologically active polysaccharide or GAG that is found ubiquitously throughout the body. Due to its biocompatibility and semi-rigidity, HA is used for biomedical applications, including viscosupplementation and tissue engineering scaffolds, and in other clinical applications because of its unique physiochemical properties. The structure of the HA repeat unit is shown in Figure 1. The hydroxyl and carboxyl groups make this a very hydrophilic molecule – an important role of HA is moisture retention. The structure, degradation and material properties of HA are reviewed with the intention of utilizing HA in the development of an orthopaedic biomaterial.

As shown in Figure 1, HA is a linear charged polysaccharide consisting of repeating  $\beta$ -(1-4)-D-glucuronic acid and  $\beta$ -(1-3)-N-acetyl-D-glucosamine monomeric units.[8] The exact conformation of HA in aqueous solution is unknown, but dynamic hydrogen bonds

may exist. It is known that HA is highly water soluble over a very wide molecular weight range. The polymer chains begin to approach each other with an increase in molecular weight or concentration and interact hydrodynamically. High molecular weights lead to longer chains coiled into hydrodynamic spheres. Under normal physiological conditions (e.g., in the ECM), HA is believed to exist as crowded random coil molecules.[9] The structure of HA, either in aqueous solution or solid state, is theoretically determined using software simulations. An HA deca-saccharide has been modeled in aqueous solution; surrounded by 2000 water molecules, the total time period of 5 ns was simulated at 0.1-ps intervals.[10] Computational methods have shown that intramolecular hydrogen bond interactions exist across the glycosidic linkages.[10, 11] Hydrogen bonds stabilize the chain conformation in low energy regions.

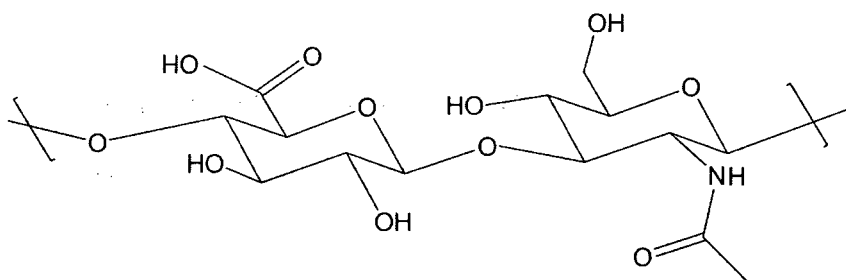


**Figure 1. Chemical structure of HA.**

HA consists of highly dynamic polymer chains; HA changes its conformation at the  $\beta$ -(1-4) linkage.[12] On average, HA is a highly extended polymer; however, the  $\beta$ -(1-4) is unstable and produces strong fluctuations in its molecular length. The glucuronic acid  $\text{OH}_3$  is particularly important in the HA structure and results in conformation fluctuations.[10] The helical conformations of HA strongly depend on counter ions, the pH, temperature and relative humidity of its environment.[11] The structure of HA has been compared to cellulose, also a polysaccharide.[12] In aqueous solution, the average

conformation that cellulose exhibits is highly extended and very close to that observed in crystal structures. One of the main differences between the HA and cellulose conformations is that the alternating  $\beta$ -(1-4) and  $\beta$ -(1-3) linkages in HA makes it a more mobile chain that is always changing its conformation, while the cellulose molecules, which lack the  $\beta$ -(1-4) linkage, are more rigid. Thus, cellulose is not water-soluble like HA and is a more structural material than HA.

Articular cartilage replacement materials should have mechanical, structural and biological properties similar to native tissue. Hydrogels do a good job of mimicking articular cartilage; similar to cartilage, hydrogels are three-dimensional hydrophilic networks capable of absorbing and retaining a large amount of water without dissolving.[13, 14] The use of HA in the development of hydrogels is advantageous because it is biocompatible and participates in numerous biological functions including joint lubrication and tissue connectivity.[15, 16] In its hydrated state, HA has the ability to bear compressive forces and plays a role in lubrication of articulating surfaces making it a natural choice for orthopaedic applications. Different crosslinking strategies have been explored to create insoluble and gel-like HA hydrogels, and to improve the mechanical properties. Physical crosslinking creates hydrogels through hydrophobic interaction, whereas chemical crosslinking exhibits new covalent intramolecular bonds that create an infinite network. A hydrophobic component can also be incorporated into the hydrogel to improve the structural integrity of the hydrogels.[13] Chemical modification (including chemical crosslinking) of HA can occur at three main positions: the hydroxyl at the C6 position of the *N*-acetylglucosamine; the carboxylic acid of the

glucuronic acid; and the –NH-position of the *N*-acetylglucosamine.[8] The hydroxyl group may be involved in sulfation, esterification (e.g., benzyl acid and anhydride) or periodate oxidation reactions. Due to the bio-degradation properties of HA, it is often utilized for tissue scaffolds.

Chemical crosslinking leads to a networked HA. One application of chemical crosslinking is the development of hydrogels. Another example is to alter the degradation properties of HA. Chemical crosslinking decreases the degradation rate (or increases the long-term stability) of HA – natural noncrosslinked HA is rapidly degraded in the body, turning over completely in less than 3 days;[17] the average turnover rate, however, depends on the initial molecular weight of the HA. Crosslinking also increases the mechanical properties, such as strength and modulus, of HA. Various degradation studies have been developed to test the effectiveness of an assortment of crosslinking methods. As with all polymer networks, the swelling properties of HA are altered by introducing crosslinks. Segura *et al.* studied the chemical crosslinking of HA at the carboxylic acid groups and/or hydroxyl groups using poly(ethylene glycol) diglycidyl ether.[18] The amount of crosslinker added was determined by calculating the molar ratio of hydroxyl groups in HA to epoxide groups in PEGDG; there are two epoxides in PEGDG and four hydroxyl groups per repeat unit of HA. The crosslinked polymer was a film when dry and a hydrogel when wet. Crosslinking at the carboxylic acid groups was verified via infrared spectrometry; the degree of crosslinking range was 12.5 – 100%. Enzyme degradation was tested using hyaluronidase (100 U/ml) during incubation at 37°C; complete degradation took 14 days. The water percentage in the HA hydrogels decreased from

98.5% for 12.5% crosslinked gels to 62.1% for 100% crosslinked gels. The complex modulus, measured by oscillatory tests, ranged from immeasurable for 12.5% crosslinked gels to 33.5 kPa for 100% crosslinked gels. A biuret isocyanate, derived from hexamethylene diisocyanate, was chosen by Zhang as a chemical crosslinker for HA because of its crosslinking location on the HA molecule; it crosslinks HA at the hydroxyl groups, not the carboxylic acid groups.[19, 20] This is important because the latter functional groups contribute to the lubricious properties of HA.

HA derivatives can also be fabricated without using chemical crosslinkers. In the development of an amphiphilic, hydrophobic HA, carboxylic groups were esterified with an alkyl halide (i.e., dodecyl or octadecyl bromide,  $C_{12}H_{25}$  or  $C_{18}H_{37}$ ) in a homogenous solution with dimethylsulfoxide (DMSO); sodium HA was preliminary transformed with tetrabutylammonium (TBA) salts.[21] The introduction of alkyl side chains was expected to disrupt intramolecular (i.e. hydrogen) bonding between HA molecules, thus rendering the amphiphilic HA chains more flexible compared to unmodified HA controls. The highly viscous hydrogel can also be modified by varying the degree of esterification, which also affects its water content.[22]

The HYAFF<sup>®</sup> 11 sponge are made of a linear hyaluronic acid derivative; the carboxyl groups on the glucuronic acid were esterified with benzyl groups (10-400  $\mu\text{m}$  pores, porosity 80%); ACPT<sup>™</sup> sponges are crosslinked derivatives of HA, in which the carboxylic acid groups were linked using an ester bond to the hydroxyl groups on different HA chains (10-300  $\mu\text{m}$  pores, porosity 85 and 86%).[23] The Young's modulus

was determined for all three types of sponges via unconfined compression in creep mode. The HYAFF<sup>®</sup> 11 sponge has a modulus of 42.1 kPa and the ACP<sup>™</sup> sponges had moduli of 8.2 and 7.6 kPa for the respective porosities. It was determined that both HYAFF<sup>®</sup> 11 and ACP<sup>™</sup> sponges were biocompatible; although both sponges were turned over *in vivo*, the ACP<sup>™</sup> sponges completely degraded in 2 weeks whereas HYAFF<sup>®</sup> 11 sponge completely degraded in 2 months.[24, 25] ACP<sup>™</sup> exhibits an increase in bone formation compared to HYAFF<sup>®</sup> 11, whereas the HYAFF<sup>®</sup> 11 sponge result in more hyaline-like and hypertrophic cartilage development.[24, 26] The disorganized fibrous cartilage is expected to show mechanical failure overtime because its mechanical properties are inferior to those of articular cartilage.

Hydrogels may be combined with porous scaffolding for full thickness osteochondral repair.[27] Techniques which have been developed to treat focal chondral lesions include abrasion arthroplasty, subchondral drilling, autologous osteochondral grafting, periosteal-perichondral grafting and chondrocyte transplantation. With the later techniques, pain and morbidity at the donor must be considered and multiple surgical procedures are required. Autograph, allograph, or synthetic materials may be employed for osteochondral repair. Autograph and allograph full thickness osteochondral plugs (including both the cartilage and the underlying bone) are harvested from a healthy site and implanted into a joint surface to replace excised damaged cartilage; various methods of implantation and different materials have been explored to reduce damage to surrounding tissue (i.e., cartilage and/or bone).[28] It has been shown that *in vitro* hyaluronic acid increases osteoblastic bone formation through increased mesenchymal cell differentiation and

migration.[29] Cavities were created on the right tibia of 10-11 month old New Zealand Albino rabbits; one of the cavities was filled with bone graft (positive control) and the other one was filled with hyaluronic acid and bone graft mixed together. Histological analysis was performed 20, 30 and 40 days after implantation. Fibrous tissue and fibrocartilage tissue were seen after 20 days in the experimental group. After 30 days new bone formation, with a thin stratum was observed. After 40 days all of the cavities exhibited new bone formation. The statistical scores were higher for the cavities treated with hyaluronic acid and bone graft.

#### **1.4 Synthetic Hydrogels for Articular Cartilage Repair**

The most popular hydrogel used in the development of artificial articular cartilage (i.e., permanent cartilage implants rather than scaffolds for cartilage regrowth) is made from poly(vinyl alcohol) hydrogel (PVA-H), which is a synthetic, non-degradable, biocompatible polymer. PVA-H can be synthesized by complexing with phenyl boronic acid,[30] dissolving in DMSO and repeatedly freezing and thawing,[31, 32] or crosslinking with sodium alginate.[33] The freeze-thaw method is the most straightforward process. A DMSO solution containing PVA is cooled below room temperature, upon which a gel is formed as a consequence of crystallization of the PVA molecules. The PVA gel is dried, annealed in silicon oil, and suspended in water, thus becoming PVA-H. PVA-H is geometrically stable and transparent. Water contents can range from 20 – 80%, depending on the annealing time and temperature and the porosity of the PVA-H, which decreases with an increase in DMSO concentration.[31, 32, 34, 35] Varying the water contents of PVA-H ultimately varies the physical and mechanical

properties of the hydrogel.

Full thickness artificial osteochondral plugs, formed into the shape of hemi-condyles,[36, 37] fabricated from PVA-H and titanium fiber mesh (TFM), demonstrated good structural stability by injecting molding the polymer into the TFM; implants showed firm attachment to canine femoral bone 12 months postoperatively.[38] However, the mechanical properties remain insufficient for use as an artificial articular cartilage. The shear strength between the PVA-H and the TFM was 2.2 MPa; the ultimate tensile strength and elastic tensile modulus of a PVA-H-20% were 20 and 160 MPa, respectively.[34] The shear modulus for both PVA-H-75% and PVA-H-80% was between 0.10 (10% strain) and 0.45 MPa (60% strain); the compressive moduli at 60% strain were between 0.7 and 18.4 MPa. The ultimate tensile strengths of the two hydrogels were 2.1 and 1.4 MPa, respectively.[32]

#### 1.4.1 Characterization of Hydrogels

Hydrogels can be designed to exhibit a wide variety of properties; synthetic and biological components may be used as constituents in the development of hydrogels. The following paragraphs discuss the characterization of hydrogels, such as those described above, and the ranges of properties that can be achieved with these different hydrogels are summarized.

The chemical and physical characterization of hydrogels is important in understanding the relationship between composition, processing and material properties. For example,

the amount of crosslinking or the degree of crystallinity will have affects on the swelling properties (i.e., water content) of hydrogels, thus affecting the mechanical properties (i.e., toughness). An intimate relationship exists between the mechanical properties of a hydrogel and its degree of swelling.[39] Increasing the concentration of a hydrogels hydrophilic constituent will increase the degree of swelling, which will lead to decrease in the mechanical strength of the hydrogel. Also, using changes in composition and processing to increase the degree of crosslinking or the percent crystallinity will result in a decrease in the degree of swelling, effectively increasing the mechanical strength. The degree of swelling can also be altered by adjusting the pH, ionic strength, and temperature of the swelling medium.

#### 1.4.2 Mechanical Properties of Hydrogels

The mechanical properties of hydrogels can be controlled by altering the comonomer or constituent concentration, increasing or decreasing the crosslink density, and changing the processing conditions. In addition to the confined and unconfined compression testing used to characterize cartilage that are described above, dynamic mechanical thermal analysis (DMTA) reveals the viscoelastic properties of hydrogel materials and articular cartilage. DMTA is also useful for characterizing a single type of polymer to determine the effects of composition, microstructure and processing on the thermomechanical response of the final material; this is particularly useful in understanding the behavior of polymer blends and copolymers with varying constituents. Changes in the alpha and beta transitions obtained from DMTA can be compared to those measured w/ DSC and TGA and these results can be used along with indirect measures of microstructure (e.g., x-ray diffraction, XRD) to infer the effect of composition and processing on structure and thus

properties. DMTA can also be used to find correlations between mechanical behavior and morphology by determining the network structure of polymers and polymer blends.

Quantitative information on the viscoelastic and rheological properties of a material can be determined by measuring the mechanical response of a sample as it is deformed under periodic stress or strain using a DMTA.[39] Static scans can be used to calculate Young's modulus and stress-strain curves, while dynamic scans can be used to calculate the complex viscosity and modulus for each data point and to look at changes in elasticity and lag with increasing stress. The complex dynamic modulus,  $G^*$  (shear) or  $E^*$  (tension/compression), is defined as the sum of the real (also elastic or storage) modulus,  $G'$  or  $E'$ , and the imaginary (also viscous or loss) modulus,  $G''$  or  $E''$ . For the case of shear loading:

$$G^* = G' + iG''$$

The ratio of  $G''$  to  $G'$  is known as  $\tan \delta$  (i.e., the damping factor);  $\tan \delta$  measures the ratio of the energy dissipated as heat to the maximum energy stored in the material during one cycle of oscillation. Measuring these values over a range of temperatures and frequencies characterizes the thermomechanical properties of a polymer; these changes can be described in terms of free volume or relaxation times. Polymer relaxations as a function of temperature are best obtained by doing time temperature scans (vary temperature or time at temperature) at a fixed frequency – this is also the best method for finding the glass transition temperature ( $T_g$ ) and detecting other transitions in materials. Upon heating, a semi-crystalline noncrosslinked polymer will go through six transitions: 1) local motions, 2) chain bending and stretching, 3) side group motion, 4) gradual main

chain motion (i.e.,  $T_g$ ), 5) large scale chain motion, and finally 6) chain slippage or flow (i.e.,  $T_m$ ). The temperature at which the maximum peak in the  $\tan \delta$  curve exists is known as the  $T_g$  or alpha transition; crystal-crystal slips can also cause alpha transitions, making  $T_g$  detection more difficult. The glass transition is the most commonly used method for establishing miscibility in polymer blends; broadening of the transition will occur if two polymers are miscible.[40] In this way, DMTA provides information regarding the interactions between polymers. Beta transitions are smaller peaks at lower temperatures. Frequency scans allow one to look at trends in the material and can be used to estimate changes in molecular weight and molecular weight distribution; the data can be used for time-temperature-superposition curve fabrication. In order to prevent water loss during DMTA the sample may be coated with petroleum gel or silicone vacuum grease (or in case of compression, submerged in water). Water loss limits the temperature range over which DMTA can be conducted on swollen hydrogels; extended frequency ranges may then be applied.

DMTA was performed on plain PVA at a frequency of 1 Hz, temperature range of 25-350°C, and a heating rate of 4°C/min.[40] DMA was performed on HA/PVA hydrogels employing parallel plate geometry on hydrated samples. Static dynamic tests were performed using a stress ratio of 150% at 1 Hz, at a rate of 50 mN/min, from 10 to 1000 mN. The  $T_g$  of PVA was 40-50°C (this value is known to change with variations in water content); the Young's modulus of the polymer after this transition was about  $10^8$  Pa. The  $T_m$  phase of PVA was 200-220°C and the sample began to decompose at about 300°C. The  $\tan \delta$  intensity related to the  $T_g$  of PVA only is about 0.4, which confirms that the

polymer is partly crystalline. The storage modulus for pure PVA-H was about  $8.0 \times 10^5$  Pa; this value increased with an increase in HA content up to 20% HA to a maximum value of  $1.2 \times 10^6$  Pa, but then decreased with increasing HA content to a value of  $4 \times 10^5$  Pa for 50% HA. The increase in modulus with HA contents up to 20% is related to the crystallization of PVA – HA provides additional nucleation sites for PVA crystallization. The Young's modulus of semi-crystalline polymers will increase after going through the  $T_g$  transition because the polymers crystallize due to an increase in mobility. It is also important to note the  $T_g$  and  $T_m$  of polymers will depend on the initial molecular weight; decreases in molecular weight will result in lower transition temperatures.

DMTA was also performed on plain PVA and PVA and methylcellulose (MC) (i.e., some of the hydroxyl groups are replaced with methoxyl groups) blend hydrogels.[41] Thin hydrogel films were heated from  $-20$  to  $260^\circ\text{C}$  at a rate of  $2^\circ\text{C}/\text{min}$  at a frequency of 1 Hz. The films were also subjected to sinusoidal deformation amplitude of  $5 \mu\text{m}$ . The ratio of PVA to MC was 20:80 and the water content was about 60%. The  $T_g$  occurred at  $85^\circ\text{C}$ , and the  $T_m$  transition occurred within the range of  $200$ - $260^\circ\text{C}$ . The DMTA scan of the PVA/MC hydrogel shows three peaks near those of PVA and one near the alpha peak of MC (at  $200^\circ\text{C}$ ); this data explains that the two polymers are only partially miscible.

Salubria™ samples (initial length = 6 mm) were placed between two impermeable, unlubricated platens in deionized water.[32] Samples may also be run in saline at room temperature.[42] Prior to each test, the samples were preloaded and cyclically preconditioned for 10 cycles between 1 and 10N to reduce the influence of surface

artifacts. Samples ( $n = 12$ ) were subsequently subjected to a compressive ramp up to 65% strain at a strain rate of  $100\% \text{min}^{-1}$  (i.e.,  $0.0167 \text{ s}^{-1}$ ). A second set of samples ( $n = 12$ ) was tested at a higher strain rate of  $1000\% \text{min}^{-1}$  (i.e.,  $0.1667 \text{ s}^{-1}$ ). The tangent slope was measured by calculating a line estimate for localized data at 10% increments from 10% to 60% strain.[32]

In another study, samples were compressed by 10% of measured thickness at a rate of 2% per second, and allowed to relax for 30 min (preliminary studies indicated that the gels reached steady-state well within this time). A 4% amplitude sinusoidal strain was then imposed for three cycles each at frequencies of 0.001, 0.01, 0.1, and 1.0 Hz (preliminary measurements indicated that the third cycle was adequately representative of the steady-state oscillatory response). The force response data from the third cycle of each frequency was analyzed using a Fast Fourier Transform algorithm (Matlab<sup>TM</sup>), and the amplitude of the first harmonic was used to calculate the dynamic stiffness (first harmonic of force divided by sample area, divided by applied test strain). It should be noted that the dynamic stiffness is not an intrinsic material property, but rather a functional measurement of the stiffness of a sample of specific dimensions at the indicated frequencies. Extraction of intrinsic material properties could be achieved by fitting a particular constitutive model to the recorded data, but additional tests would be required to determine those properties with a high degree of confidence.[42]

COF measurements were obtained using a pin-on-flat tester for five material combinations consisting of: PVA-H, alumina ceramic, ultra high molecular weight

polyethylene (UHMWPE), and bovine articular cartilage. Tests were run for 2,700 cycles with a sliding speed of 0.05 m/sec and a normal stress of 0.5 MPa in 37°C deionized water and  $\alpha$ -fraction calf serum (50:50); friction measurements were recorded at 5, 10, 15, 30 and 45 minutes. Approximate COF values for various combinations of materials/tissue were as follows: cartilage verse cartilage was 0.05; cartilage verse PVA-H was 0.1; cartilage verse alumina ceramics was 0.28; cartilage verse UHMWPE was 0.37; and PVA-H verse PVA-H was 0.74.[35]

### 1.5 Cartilage, Hydrogel Property Summary and Comparison

In the above paragraphs, the effects of degree of crosslinking or derivatization of HA, porosity, and processing methods on the material and mechanical properties of various hydrogels is presented. The mechanical properties of the previously discussed materials are summarized in Table 2 (n.a. = not available), which include the properties of native articular cartilage for comparison.

**Table 2. Mechanical properties of articular cartilage and HA-based and synthetic hydrogels.**

Mechanical Property	HYAFF <sup>®</sup> 11	ACP <sup>™</sup>	PVA-H	Articular Cartilage
Elastic (Tensile) Modulus	n.a.	n.a.	160 MPa [34]	5 – 25 MPa [1]
Elastic (Compressive) Modulus	42.1 kPa [43]	7.6 – 8.2 kPa [43]	0.7 – 18.4 MPa [32]	0.41 – 0.85 MPa [1]
Aggregate Modulus	n.a.	n.a.	n.a.	0.06 – 2.0 MPa [1, 7]
Shear Modulus	n.a.	n.a.	0.10 – 0.45 MPa [32]	0.6 – 1.5 MPa [6]
Toughness	n.a.	n.a.	n.a.	130 kcal [5]
COF (against itself)	n.a.	n.a.	0.74 [35]	0.05 [35]
Poisson's Ratio	n.a.	n.a.	n.a.	0.06 – 0.18[1]

The HA-derived and synthetic hydrogels summarized in Table 2 are much stiffer compared to native articular cartilage. The modulus mismatch may harm surrounding native tissue when implanted in vivo would ultimately result in failure of the implant. Therefore, there is a need to develop a material that is more compliant and more closely resembles the mechanical properties of articular cartilage, but is tough and durable and exhibits a low coefficient of friction against cartilage.

## **1.6 Polyethylene**

It was previously stated that hydrogel materials can be strengthened by the incorporation of a hydrophobic component. Polyethylene (PE) is a hydrophobic polymer that has been extensively utilized and researched for the orthopaedic industry. For this reason, it was hypothesized that creating a graft copolymer between HA and PE (HA-*co*-HDPE) would result in a material with better mechanical properties than HA alone. HA does not melt flow, thus it cannot be compression molded. PE is melt-processable and can be compression molded into parts with various properties. Furthermore, UHMWPE is a logical choice for blending with the HA-*co*-HDPE since it is an accepted biomaterial for joint replacement surgery. Polymer properties can be improved by blending different polymers without markedly changing the structure and function of the polymers themselves. Polymer blends involving UHMWPE and HDPE have been covered in the literature. The two polymers undergo co-crystallization due to similar  $T_m$  values.[44, 45] A 50:50 blend of UHMWPE and HDPE exhibits good chain entanglement; the tensile strength and tensile modulus of the blend were between the values for neat UHMWPE and neat HDPE.

### 1.6.1 PE Crosslinking

Currently, UHMWPE used in the orthopaedic industry for TJRs is crosslinked via gamma radiation to reduce wear *in vivo*. Chemical crosslinking of UHMWPE has also been investigated. Chemical crosslinking of UHMWPE improves *in vitro* and *in vivo* wear resistance. Crosslinking can be achieved chemically by silane or peroxides.[46] During the melt soak stage of compression molding, the peroxide decomposes and abstracts hydrogen atoms from the UHMWPE resulting in a combination of alkyl radicals.[47] Chemical crosslinking of UHMWPE in the melt, during compression molding, leads to reductions in crystallinity (more so than gamma radiation), resulting in better wear properties; however, reducing wear properties via crosslinking decreases mechanical property values. Chemical crosslinking with 0.3 to 0.5% (w/w) organic peroxides has been found to improve wear resistance by as much as 30% over unmodified resins, while reducing deformation under load. While crosslinking by gamma radiation potentially leads to polymer chain scission (i.e., degradation), no significant chain scission is observed in peroxide crosslinking.[43, 48] However, if undissociated peroxides are not eliminated *after* compression molding, they can also negatively effect the long-term stability of the implant, similar to remaining free radicals after radiation.[49]

Kurtz *et al.* compared 0.25% (w/w) dicumyl peroxide (DP) crosslinked UHMWPE to 150 kGray E-beam crosslinked UHMWPE.[50] Both crosslinking methods increased the tensile strength and decreased the ductility of the UHMWPE, as measured via a small punch test. It was also determined that chemical crosslinking in the melt decreased the size of the crystalline lamellae. Muratoglu *et al.* chemically crosslinked GUR 1050 with

0.2% (w/w) 2,5-Dimethyl-2,5-di-(tert-butyl-peroxy) hexyne-3 peroxide.[51] Chemical crosslinking was performed in the presence of an antioxidant, Irganox® 1010, at a concentration of 0.2% (w/w). The molecular weight between crosslinks ( $M_c$ ) was calculated by dividing the density of the crosslinked sample, approximated as  $0.92 \text{ g/cm}^3$ , by the crosslink density ( $d_x$ ), which was determined via swell ratio tests. The  $d_x$  was found to increase with increasing initial peroxide content. It was also found that the  $M_c$  dictated the wear properties, and was considered the utmost important material property defining wear behavior.[51]

Various UHMWPE resins were chemically crosslinked via a peroxide in an investigation by Shen *et al.*[52] GUR 412 (MW:  $2.5\text{-}3 \times 10^6$ ), GUR 413 (MW:  $3\text{-}4 \times 10^6$ ), and GUR 415 (MW:  $6 \times 10^6$ ) were chemically crosslinked with the chemical crosslinker, 2,5-dimethyl-2,5-bis(tert-butylperoxy)-3-hexyne.[47] The UHMWPE and an acetone solution of peroxide crosslinker were mixed together at room temperature to create a polymer slurry, which was then vacuum dried at room temperature to evaporate off the solvent.[47] Specimens examined included: (1) pure GUR 412, GUR 413 and GUR 415, that had been compression molded at  $170^\circ\text{C}$ ,  $220^\circ\text{C}$  and  $300^\circ\text{C}$  for 2 hours and then slowly cooled to room temperature; (2) slowly cooled GUR 415 that had been chemically crosslinked with varied peroxide concentrations at  $170^\circ\text{C}$ ; (3) quench-crystallized GUR 415 that was also crosslinked with varied peroxide concentrations at  $170^\circ\text{C}$ ; and (4) specimens (2) and (3) after irradiation. Uniform distribution of peroxide crosslinking was difficult to achieve for all samples, possibly due to inhomogeneous mixing of the UHMWPE resin and the peroxide. Chemically-induced crosslinks inhibited

recrystallization by stabilizing chain fragments. After compression molding at 300°C for two hours with slow cooling, a smoother, more uniform appearance was seen on the fracture surface for the three polymers compared to molding at 170°C and 220°C. Molding temperatures above 220°C were necessary for complete chain fusion particle interpenetration. Quenching led to an increase in the nucleation rate and a more homogeneous crystal distribution with fewer structural irregularities. One and 2% (w/w) peroxide crosslinked GUR 415 exhibited increased crystallinity and reduced lamellar thickness.[52] Control unmodified GUR 415 exhibited a 56% increase in crystallinity with irradiation.

### 1.6.2 Antioxidants

Due to the introduction of free radicals by DP and/or gamma radiation, oxidation through ageing is a concern for polymeric orthopaedic implants. However, the free radicals can be reduced and eliminated (i.e., quenched) with various thermal treatments after irradiation (i.e., melt quenching in a vacuum oven with argon purge). Remelting gamma-radiation crosslinked UHMWPE decreases the number of free radicals. After thermal-melt quenching, irradiated polymers are more oxidatively stable. The presence of an antioxidant (e.g., vitamin-E) traps free radicals by bonding to the molecules, disabling further oxidation.[53] In past reports, an antioxidant has been shown to reduce further oxidation by incorporation of the chemical (0.25%) with UHMWPE resin.[50] However, a decrease in  $d_x$  is seen if the UHMWPE is chemically crosslinked in the melt because primary free radicals are blocked by the antioxidant.[54] In this way, the resin may be compression molded in the presence of a chemical crosslinker and an antioxidant.

Vitamin E has gained popularity as an antioxidant to prevent oxidation of UHMWPE orthopaedic materials due to gamma radiation sterilization and crosslinking.[55-60] Vitamin E, or  $\alpha$ -tocopherol, is a phenolic antioxidant that traps residual free radicals. Vitamin E is biocompatible and therefore more acceptable to clinicians than Irganox® antioxidants;[61-63] for this reason vitamin E will be utilized instead of Irganox® for the prevention of oxidative degradation of HA-co-HDPE.

D,L- $\alpha$ -tocopherol is a known form of Vitamin E which has been shown to reduce oxidation of crosslinked UHMWPE.[56] Vitamin E ( $\alpha$ -tocopherol) was mixed with UHMWPE resin (0.4% (w/w)).[57, 61] UHMWPE TJR components treated with D,L- $\alpha$ -tocopherol (0.3% (w/w)) exhibit a reduction of wear compared to conventional UHMWPE.[58] Irradiation of UHMWPE constructs made from vitamin E doped resin showed a decrease in antioxidant content with an increase in radiation.[60] Diffusion of Vitamin E is an interesting new research field focused on treating irradiated UHMWPE constructs.[55] D,L- $\alpha$ -tocopherol was diffused with a final weight percent of 2-4% (w/w). Vitamin E has gained popularity for use in orthopaedic biomaterials in recent years.[59] D,L- $\alpha$ -tocopherol was used.[63] The vitamin E oil was dissolved in ethanol (50 g/L) and mixed with UHMWPE resin (0.8% (w/w)). Animal experiments were performed with D,L- $\alpha$ -tocopherol at a concentration of 0.8% (w/w) with UHMWPE.[62]

In summary, the standard mechanical properties of noncrosslinked UHMWPE used in the orthopaedic industry are: yield stress 22 MPa; ultimate tensile strength 40 MPa;

elongation to failure 353%. Due to the high strength, toughness and ductility of UHMWPE, it will be used to strengthen and toughen compression molded HA-co-HDPE.

### **1.7 Functionalized Polyolefins**

Maleated polymers have been shown to increase mechanical and physical properties of immiscible composites (e.g., cellulose and PE) by improving the interfacial interaction and or leading to covalent bonding between the components of composites.[64-71] The maleation of polyolefins, or grafting of maleic anhydride (MA) onto polyolefin chains, occurs through reactive blending, which can take place in an internal mixer or twin-screw extruder.[72] Multiple parameters can affect the degree of grafting, including the reactants concentration, the reaction temperature, the mixing speed,[73] and in some cases, the molar ratio of solvent to MA.[74] The temperature effect is complex and is best determined by the reaction constituents; an increase in mixing speed increases the degree of grafting and reduces the occurrence of side reactions (e.g. chain-branching/scission and crosslinking).[73] Dialkydic peroxides are employed as initiators due to their stability and half-life; DP is often chosen because its half-life is in the middle: too short of a half-life leads to chain scission as a result of a quick accumulation of free radicals and too long of a half-life reduces the efficiency of the grafting reaction, leaving unreacted initiator in the final product.[74] Adding DP results in a higher graft percent of MA.[75] The highest graft percents occur when DP was added after the polyolefin and the MA have mixed.

The distribution of MA to polyolefin has been reported as 3-4.0% (w/w). The

concentration of DP to the polyolefin falls between 0.25 to 0.5% (w/w). Rotor speeds were reported at 60 rpm for 10 minutes at 150°C.[72, 75] A solvent may also be added to the mixture.[74] A molar ratio of 0.5 of toluene to MA was used; an antioxidant was added at 0.2% (w/w) to reduce chain scission. The reaction was carried out at 190°C with a rotor speed of 60 rpm; MA (1.5-2% (w/w)) was added to polypropylene and mixed for 1 minute, then the DP (8400 ppm) was added and the reaction continued for 7 minutes. The degree of MA grafting was a 0.68%. After the maleation reaction has occurred, ungrafted (or unreacted) MA may be removed by titrating the reaction product into acetone and filtering out the polymer product.[75]

The goal of the reaction of functionalizing high density polyethylene (HDPE) with MA was to retain HDPE properties. Maleated HDPE was characterized via DSC, WAXD and DMA. The crystallinity (via DSC) was determined from equation of  $\%X_c = (\Delta H_f / \text{theoretical } \Delta H_f) \times 100$ , using theoretical  $\Delta H_f = 7.919$  kJ/mol. Tensile tests were conducted at strain rate 50 mm/min; samples were 0.4 mm thick and 4 mm wide. DMA was conducted on a DDV-II-EA machine at amplitude of 0.200 and a programmed scanning rate of 2°C/min. The highest graft % MA achieved was 1.59%.[76] The crystallinity of PE in the PE-MA samples showed gradual lowering with an increase in MA graft %; this is expected due to the intrusion of the bulky MA groups in the crystallite formation. The melting temperature of the PE-MA samples also decreased slightly with an increasing amount of grafted MA; this is a direct result of the lowering PE crystallinity and a greater extent of supercooling and hence, a lower crystallization temperature. The yield strength was also shown to decrease, due to a decrease in the PE

chain stiffness with the introduction of MA groups. Thin films of a maleated linear low density polyethylene (MA-g-LLDPE) and starch copolymer were pressed at 170°C (approximately 60°C above the MA-g-LLDPE melt temperature); the thin films were approximately 1 mm thick.[77] Tensile strength and strain were determined following ASTM D638. MA-g-LLDPE showed a reduced tensile strength and elongation to failure compared to neat LLDPE; copolymers showed superior properties compared to blends of starch and LLDPE (both tensile strength and elongation to failure decrease as the amount of starch is increased). Hydrogels must be completely immersed in a water bath (also buffered solution or saline) that is thermally regulated during the tensile tests.[39]

#### 1.7.1 Anhydride Esterification

The esterification between MA and starch was performed at the same time as the maleation of poly(lactic acid) (PLA).[65] The ratio of PLA/starch was 55/45. MA and the initiator (2,5-bis(*tert*-butylperoxy)-2,5 dimethylhexane) were added into the PLA/starch system at various concentrations and the blend was mixed for 10 min. The mixture was then reacted by running through a twin-screw extruder, with a screw diameter of 19.1 mm and a length-to-diameter ratio of 25/1. Temperatures of the extruder were set at 125, 185, and 185 °C from feed inlet to die, respectively. Tensile tests showed that the compatibilized mixture was stronger than composites without the addition of MA. The interfacial reaction between maleated linear low density polyethylenes (MA-g-LLDPE) (0.3 and 3.0 weight % MA) and starch (starch contents were 0, 10, 20, 30 and 40 weight %) has been observed using FTIR.[77] All components were vacuum dried at 90°C for approximately 8 hours; blending was performed in a rheomixer at 180°C at 60 rpm for 10

minutes. Vibration bands at 1865 and 1780  $\text{cm}^{-1}$  are associated with anhydride groups, 1710  $\text{cm}^{-1}$  is associated with carboxylic acid (left over from the reaction and also hydrolyzed anhydride groups); the vibration band at 1730  $\text{cm}^{-1}$  was associated with the ester formation between the maleic anhydride and hydroxyl groups on the starch. Hydrolyzed anhydride groups can be converted back through drying at elevated temperatures (above the melt).

Commercially available synthetic biomaterials for total joint and hemi-arthroplasties and repair of articular cartilage lesions, which lack the chemical and physical complexity that confers the properties of native articular cartilage, fail to recapitulate the extraordinary physical and biological properties of natural articular cartilage. The development of a novel copolymer designed to exploit the properties of a naturally occurring biocompatible biopolymer (i.e., HA) in combination with the current “gold standard” synthetic material for joint arthroplasties (i.e., PE) is discussed in the following sections. Specifically, the copolymer exploits the strength, rigidity and melt-processability associated with HDPE, and promises improved biomaterial lubricity, biocompatibility and longevity by incorporating the highly hydrophilic biopolymer HA. Further, the swelling, mechanical and degradation properties of the copolymer can be custom-optimized by tailoring chemical or physical crosslinking strategies and varying the amount of HA and HDPE incorporated into the copolymer.

### **1.8 Objectives and Specific Aims**

The long term goal of this research is to develop a hyaluronan-graft-polyethylene copolymer (HA-*co*-HDPE) for use as a permanent osteochondral plug or partial

resurfacing implant. The specific goal of the proposed dissertation is to determine how copolymer composition and processing affect the properties relevant to its use in partial resurfacing implants.

The objectives of this research are to evaluate the material properties of a novel HA-*co*-HDPE copolymer, and to produce a material which can be further developed for various uses throughout the biomedical engineering field, with the primary focus on articular cartilage replacement. The proposed research will expand on past work by manipulating physical and mechanical properties for the desired application. Kurkowski's Master of Science thesis describes in detail the development of HA-*co*-HDPE and the implications for its use.[78] The affects of varying the processing methods of the HA-*co*-HDPE copolymer on the microstructure and material properties of a HA-*co*-DHPE hydrogel will also be investigated.

Specific aims include:

1. To synthesize and compression mold a melt-processable biosynthetic copolymer of HA and PE over a range of molecular morphologies, network characteristics, and compositions.
2. To physically and chemically characterize the biosynthetic material.
3. To evaluate the viscoelastic properties relative to current hydrogel biomaterials for articular cartilage replacement and the native tissue.
4. To evaluate the short-term and long-term *in vitro* biological assessment of the biosynthetic material.

## 1.9 References

1. Mow VC, Guo XE. Mechano-electrochemical properties of articular cartilage: their inhomogeneities and anisotropies. *Annual Review of Biomedical Engineering* 2002;4:175-172.
2. Kiani C, Chen L, Wu YJ, Yee AJ, Yang BB. Structure and function of aggrecan. *Cell Research* 2002;12(1):19-32.
3. Roughley PJ, Lee ER. Cartilage Proteoglycans: Structure and Potential Functions. *Microscopy Research and Technique* 1994;28:385-397.
4. Crockett R, Grubelnik A, Roos S, Dora C, Born W, Troxler H. Biochemical composition of the superficial layer of articular cartilage. *Journal of Biomedical Materials Research* 2007;82A:958-964.
5. Silver FH, Bradica G. Mechanobiology of cartilage: how do internal and external stresses affect mechanochemical transduction and elastic energy storage? *Biomechan Model Mechanobiol* 2002;1 219-238.
6. Frank EH, Jin M, Loening AM, Levenston ME, Grodzinsky AJ. A versatile shear and compression apparatus for mechanical stimulation of tissue culture explants. *Journal of Biomechanics* 2000;33:1523-1527.
7. Wang H, Ateshian G. The normal stress effect and equilibrium friction coefficient of articular cartilage under steady frictional shear. *Journal of Biomechanics* 1997;30 (8):771-776.
8. Rinaudo M. Main properties and current applications of some polysaccharides as biomaterials. *Polymer International* 2008;57:397-430.
9. Cowman MK, Matsuoka S. Experimental approaches to hyaluronan structure. *Carbohydrate Research* 2005;340:791-809.
10. Almond A, Brass A, Sheehan JK. Oligosaccharides as model systems for understanding water-biopolymer interaction: Hydrated dynamics of a hyaluronan decamer. *Journal of Physical Chemistry B* 2000;104:5634-5640.
11. Haxaire K, Braccini I, Milas M, Rinaudo M, Perez S. Conformational behavior of hyaluronan in relation to its physical properties as probed by molecular modeling. *Glycobiology* 2000;10(6):587-594.
12. Almond A, Sheehan JK. Predicting the molecular shape of polysaccharides from dynamic interactions with water. *Glycobiology* 2003;13(4):255-264.
13. Ambrosio L, De Santis R, Nicolais L. Composite hydrogels for implants. *Proc Instn Mech Engrs* 1998;212 (H):93-99.

14. Nakayama A, Kakugo A, Gong JP, Osada Y, Takai M, Erata T, et al. High mechanical strength double-network hydrogel with bacterial cellulose. *Advanced Functional Materials* 2004;14(11):1124-1128.
15. Noble PW. Hyaluronan and its catabolic products in tissue injury and repair. *Matrix Biology* 2002;21(1):25-29.
16. Toole BP. Hyaluronan: From extracellular glue to pericellular cue. *Nature Reviews Cancer* 2004;4(7):528-539.
17. Coleman PJ, Scott D, Ray J, Mason RM, Levick JR. Hyaluronan secretion into the synovial cavity of rabbit knees and comparison with albumin turnover. *The Journal of Physiology* 1997;503(3):645-656.
18. Segura T, Anderson BC, Chung PH, Webber RE, Shull KR, Shea LD. Crosslinked hyaluronic acid hydrogels: a strategy to functionalize and pattern. *Biomaterials* 2005;26(4):359-371.
19. Zhang M. Surface Modification of Ultra High Molecular Weight Polyethylene With Hyaluronan For Total Joint Replacement Application [Doctor of Philosophy Mechanical Engineering]: Colorado State University Dissertation; 2004.
20. Zhang M, James SP. Silylation of hyaluronan to improve hydrophobicity and reactivity for improved processing and derivatization. *Polymer* 2005;46:3639-3648.
21. Pelletier S, Hubert P, Lopicque F, Payan E, Dellacherie E. Amphiphilic derivatives of sodium alginate and hyaluronate: synthesis and physico-chemical properties of aqueous dilute solutions. *Carbohydrate Polymers* 2000;43:343-349.
22. Pelletier S, Hubert P, Payan E, Choplin L, Dellacherie E. Amphiphilic derivatives of sodium alginate and hyaluronate for cartilage repair: Rheological properties. *Journal of Biomedical Materials Research* 2001;54:102-108.
23. Solchaga LA, Dennis JE, Goldberg VM, Caplan AI. Hyaluronic acid-based polymers as cell carriers for tissue-engineered repair of bone and cartilage. *Journal of Orthopaedic Research* 1999;17:205-213.
24. Solchaga LA, Temenoff JS, Gao J, Mikos AG, Caplan AI, Goldberg VM. Repair of osteochondral defects with hyaluronan- and polyester-based scaffolds. *OsteoArthritis and Cartilage* 2005;13:297-309.
25. Gao J, Dennis JE, Solchaga LA, Goldberg VM, Caplan AI. Repair of Osteochondral Defect with Tissue-Engineered Two-Phase Composite Material of Injectable Calcium Phosphate and Hyaluronan Sponge. *Tissue Engineering* 2002;8 (5):827-837.
26. Allison DD, Grande-Allen KJ. Review. Hyaluronan: A Powerful Tissue Engineering Tool. *Tissue Engineering* 2006;12(8):2131-2140.

27. Lu HH, Jiang J, Hung CT, Guo XE, Ateshian G, inventors. Polymer-ceramic-hydrogel composite scaffold for osteochondral repair. NY/USA, 2006 2005/03/04/.
28. McKay WF, inventor. Shaped osteochondral grafts and methods of using same. IN/USA, 2006 2005/04/30/.
29. Aslan M, Simsek Gk, Dayi E. The effect of hyaluronic acid-supplemented bone graft in bone healing: Experimental study in rabbits. *Journal of Biomaterials Applications* 2006;20:209-220.
30. Hari PR, Sreenivasan K. Preparation of polyvinyl alcohol hydrogel through the selective complexation of amorphous phase. *Journal of Applied Polymer Science* 2001;82:143-149.
31. Noguchi T, Yamamuro T, Oka M, Kumar P, Kotoura Y, Hyon S-H, et al. Poly(vinyl alcohol) hydrogel as an artificial articular cartilage: Evaluation of biocompatibility. *Journal of Applied Biomaterials* 1991;2:101-107.
32. Stammen JA, Williams S, Ku DN, Guldberg RE. Mechanical properties of a novel PVA hydrogel in shear and unconfined compression. *Biomaterials* 2001;22:799-806.
33. Fujii H, Abe M, Oka K, inventors; Kuraray Co.,Ltd., assignee. Polyvinyl alcohol hydrogel and process for producing the same. Japan Patent No. 6139963, 2000 1997/11/20/.
34. Chang Y-S, Oka M, Gu H-O, Kobayashi M, Toguchida J, Nakamura T, et al. Histologic comparison of tibial articular surfaces against rigid materials and artificial articular cartilage. *Journal of Biomedical Materials Research* 1997;37:51-59.
35. Ushio K, Oka M, Hyon S-H, Yura S, Toguchida J, Nakamura T. Partial hemiarthroplasty for the treatment of osteonecrosis of the femoral head. *The Journal of Bone and Joint Surgery* 2003;85-B(6):922-930.
36. Zhai H, Xu W, Guo H, Zhou Z, Shen S, Song Q. Preparation and characterization of PE and PE-g-MAH/montmorillonite nanocomposites. *European Polymer Journal* 2004;40:2539-2545.
37. Schmieding R, inventor. Osteochondral repair using plug fashioned from whole distal femur or condyle formed of hydrogel composition. Washington DC, USA, 2004 2003/08/12/.
38. Oka M. Biomechanics and repair of articular cartilage. *Journal of Orthopaedic Science* 2001;6:448-456.
39. Anseth KS, Bowman CN, Brannon-Peppas L. Review: Mechanical properties of hydrogels and their experimental determination. *Biomaterials* 1996;17:1647-1657.

40. Cascone MG. Dynamic-mechanical properties of bioartificial polymeric materials. *Polymer International* 1997;43:55-69.
41. Park JS, Park JW, Ruckenstein E. Thermal and dynamic mechanical analysis of PVA/MC blend hydrogels. *Polymer* 2001;42 (4271):4280.
42. Hunter CJ, Mouw JK, Levenston ME. Dynamic compression of chondrocyte-seeded fibrin gels: effects on matrix accumulation and mechanical stiffness. *OsteoArthritis and Cartilage* 2004;12(117-130).
43. Stein HL. Ultra High Molecular Weight Polyethylene (UHMWPE). *Guide to Engineering Plastics Families: Thermoplastic Resins*. Materials Park: ASMInternational, 1999. p. 167-171.
44. Lim KKK, Ishak ZAM, Ishiaku US, Fuad AMY, Yusof AH, Czigany T, et al. High-Density Polyethylene/Ultrahigh-Molecular-Weight Polyethylene Blend. I. The Processing, Thermal, and Mechanical Properties. *J Appl Polym Sci* 2005;97 413-425.
45. Boscoletto AB, Franco R, Scapin M, Tavan M. An Investigation on Rheological and Impact Behaviour of High Density and Ultra High Molecular Weight Polyethylene Mixtures. *European Polymer Journal* 1997;33(1):97-105.
46. Kurtz SM, Muratoglu OK, Evans M, Edidin AA. Advances in the processing, sterilization, and crosslinking of ultra-high molecular weight polyethylene for total joint arthroplasty. *Biomaterials* 1999;20:1659-1688.
47. Shen FW, McKellop HA, Salovey R. Irradiation of Chemically Crosslinked Ultrahigh Molecular Weight Polyethylene. *Journal of Polymer Science: Part B: Polymer Physics* 1996;34:1063-1077.
48. Narkis M, Raiter I, Shkolnik S, Siegmann A, Eyerer P. Structure and Tensile Behavior of Irradiation- and Peroxide-Crosslinked Polyethylenes. *JMacromolSci- Phys* 1987;B 26(1):37-58.
49. Lewis G. Properties of crosslinked ultra-high-molecular-weight polyethylene. *Biomaterials* 2001;22:371-401.
50. Kurtz SM, Pruitt LA, Jewett CW, Foulds JR, Edidin AA. Radiation and chemical crosslinking promote strain hardening behavior and molecular alignment in ultra high molecular weight polyethylene during multi-axial loading conditions. *Biomaterials* 1999;20 1449-1462.
51. Muratoglu OK, Bragdon CR, O'Conner DO, Jasty M, Harris WH, Gul R, et al. Unified wear model for highly crosslinked ultra-high molecular weight polyethylenes (UHMWPE). *Biomaterials* 1999;20:1463-1470.
52. Shen FW, McKellop HA, Salovey R. Morphology of chemically crosslinked ultrahigh molecular weight polyethylene. *Journal of Biomedical Materials Research* 1998;41 71-78.

53. Costa L, Jacobson K, Bracco P, Brach del Prever EM. Oxidation of orthopaedic UHMWPE. *Biomaterials* 2002;23:1613-1624.
54. Oral E, Greenbaum ES, Malhi AS, Harris WH, Muratoglu OK. Characterization of irradiated blends of  $\alpha$ -tocopherol and UHMWPE. *Biomaterials* 2005;26:6657-6663.
55. Oral E, Wannomae KK, Rowell SL, Muratoglu OK. Diffusion of vitamin E in ultra-high molecular weight polyethylene. *Biomaterials* 2007;28:5225-5237.
56. Wolf C, Maninger J, Lederer K, Fröhlich-Smounig H, Gamse T, Marr R. Stabilisation of crosslinked ultra-high molecular weight polyethylene (UHMW-PE)-acetabular components with  $\alpha$ -tocopherol. *Journal of Materials Science Materials in Medicine* 2006;17:1323-1331.
57. Wolf C, Macho C, Lederer K. Accelerated ageing experiments with crosslinked and conventional ultra-high molecular weight polyethylene (UHMW-PE) stabilised with  $\alpha$ -tocopherol for total joint arthroplasty. *Journal of Materials Science Materials in Medicine* 2006;17:1333-1340.
58. Teramura S, Sakoda H, Terao T, Endo MM, Fujiwara K, Tomita N. Reduction of wear volume from ultrahigh molecular weight polyethylene knee components by the addition of vitamin E. *Journal of Orthopaedic Research* 2007.
59. Reno F, Caplan AI. UHMWPE and vitamin E bioactivity: An emerging perspective. *Biomaterials* 2006;27:3039-3043.
60. Bracco P, Brunella V, Zanetti M, Luda MP, Costa L. Stabilisation of ultra-high molecular weight polyethylene with Vitamin E. *Polymer Degradation and Stability* 2007;92:2155-2162.
61. Oral E, Rowell SL, Muratoglu OK. The effect of  $\alpha$ -tocopherol on the oxidation and free radical decay in irradiated UHMWPE. *Biomaterials* 2006;27:5580-5587.
62. Wolf C, Lederer K, Bergmeister H, Losert U, Bück P. Animal experiments with ultra-high molecular weight polyethylene (UHMW-PE) stabilised with  $\alpha$ -tocopherol used for articulating surfaces in joint endoprostheses. *Journal of Materials Science Materials in Medicine* 2006;17:1341-1347.
63. Wolf C, Lederer K, Pfragner R, Schauenstein K, Ingolic E, Siegl V. Biocompatibility of ultra-high molecular weight polyethylene (UHMW-PE) stabilized with  $\alpha$ -tocopherol used for joint endoprostheses assessed in vitro. *Journal of Materials Science Materials in Medicine* 2007;18:1247-1252.
64. Zhou J, Yan F. Effect of Polyethylene-graft-Maleic Anhydride as a Compatibilizer on the Mechanical and Tribological Behaviors of Ultrahigh-Molecular-Weight Polyethylene/Copper Composites. *J Appl Polym Sci* 2004;93:948-955.

65. Zhang J, Sun X. Mechanical Properties of Poly(lactic acid)/Starch Composites Compatibilized by Maleic Anhydride. *Biomacromolecules* 2004;5:1446-1451.
66. Yoshimura T, Matsuo K, Fujioka R. Novel Biodegradable Superabsorbent Hydrogels Derived from Cotton Cellulose and Succinic Anhydride: Synthesis and Characterization. *J Appl Polym Sci* 2006;99:3251-3256.
67. Qiu W, Endo T, Hirotsu T. A novel technique for preparing of maleic anhydride grafted polyethylene. *European Polymer Journal* 2005;41:1979-1984.
68. Pompe T, Zschoche S, Herold N, Salchert K, Gouzy M, Sperling C, et al. Maleic Anhydride Copolymers - A Versatile Platform for Molecular Biosurface Engineering. *Biomacromolecules* 2003;4:1072-1079.
69. Park J, Park K. Improvement of the physical properties of reprocessed paper by using biological treatment with modified cellulase. *Bioresource Technology* 2001;79:91-94.
70. Chandra R, Rustgi R. Biodegradation of maleated linear low-density polyethylene and starch blends. *Polymer Degradation and Stability* 1997;56:185-202.
71. Lu B, Chung TC. Synthesis of Maleic Anhydride Grafted Polyethylene and Polypropylene, with Controlled Molecular Structures. *Journal of Polymer Science: Part A: Polymer Chemistry* 2000;38:1337-1343.
72. Magaraphan R, Skularriya R, Kohjiya S. Morphological study of LLDPE-NR reactive blending with maleic anhydride. *Journal of Applied Polymer Science* 2007;105:1914.
73. Sheshkali HRZ, Assempour H, Nazockdast H. Parameters affecting the grafting reaction and side reactions involved in the free-radical melt grafting of maleic anhydride onto high-density polyethylene. *Journal of Applied Polymer Science* 2007;105:1869.
74. Krause-Sammartino LE, Lucas JC, Reboredo MM, Aranguren MI. Maleic anhydride grafting of polypropylene: peroxide and solvent effects. *Plastics, Rubber and Composites* 2006;35(3):117.
75. Aghjeh MKR, Nazockdast H, Assempour H. Parameters affecting the free-radical melt grafting of maleic anhydride onto linear low-density polyethylene in an internal mixer. *Journal of Applied Polymer Science* 2006;99:141.
76. Wang Y, Ji D, Yang C, Zhang H, Qin C. Structure and Properties of Maleated High-Density Polyethylene. *Journal of Applied Polymer Science* 1994;52:1411-1417.

77. Yoo SI, Lee TY, Yoon J-S, Lee I-M, Kim M-N, Lee HS. Interfacial adhesion Reaction of Polyethylene and Starch Blends Using Maleated Polyethylene Reactive Compatibilizer. *Journal of Applied Polymer Science* 2002;83:767-776.

78. Kurkowski RA. Chemical crosslinking, compatibilization, and direct molding of an ultra high molecular weight polyethylene and hyaluronic acid microcomposite. Fort Collins: Colorado State University Thesis; 2007.

## Chapter 2: Synthesis and Characterization of HA-*co*-HDPE

### 2.1 Introduction

Hyaluronan (HA) is the simplest glycosaminoglycan; it is non-sulphated, unbranched and immunologically inert.[1] Maleic anhydride *graft* high density polyethylene (MA-*g*-HDPE) was selected for use as the functionalized hydrophobic polymeric component of a HA and HDPE copolymer; HA-*co*-HDPE is the result of an esterification reaction between the MA and hydroxyl functional groups on the HA. This copolymer is melt processable and thus amenable to direct molding. This property allows HA-*co*-HDPE to be compression molded into a variety of shapes, including porous scaffolds or fully dense components. The long term goal is to increase the equilibrium water content and increase the crosslink density to form a structurally sound lubricious biomaterial for repairing or replacing damaged articular cartilage. It is hypothesized is that by adjusting the molecular weights of the PE and HA portions of the copolymer the mechanical properties can be optimized for permanent articular cartilage implants. In order to test this hypothesis, a melt-processable biosynthetic copolymer of HA and PE will be synthesized over a range of molecular morphologies, network characteristics, and compositions, and will be physically and chemically characterized.

### 2.2 Materials and Methods

Two MA-*g*-HDPE (molecular weight: 121.5 kg/mol, 0.36 graft % MA, Solvay Plastics; 15 kg/mol, 3.0 graft % MA, Sigma-Aldrich) materials were used in the synthesis of HA-*co*-HDPE. Sodium HA (molecular weight: 650 kDa and 1.5 MDa) was purchased from

Genzyme Corporation. High density polyethylene (HDPE, molecular weight unknown) and ultra high molecular weight polyethylene (UHMWPE, molecular weight: 1-3 Mg/mol) were generous gifts of DePuy Orthopaedics. Hexadecyltrimethylammonium bromide (CTAB), NaCl, poly(hexamethylene diisocyanate), dibutyltin diisothiocyanate (tin), vitamin E and anhydrous DMSO were purchased from Sigma-Aldrich. Absolute (200 proof) ethyl alcohol was purchased from AAPER. Xylenes and acetone were purchased from Fisher and dried by refluxing over CaCl and CaSO<sub>4</sub>, respectively. Xylenes and acetone were distilled under dry N<sub>2</sub>. [2, 3] All water was distilled, deionized, and UV sterilized. All chemicals were used as received unless otherwise specified.

### 2.2.1 HA-co-HDPE Fabrication

Complexation methods for sodium HA with CTAB have been described.[4-13] HA-CTA and MA-g-HDPE are the two constituents of the graft copolymer HA-co-HDPE. A 0.1% (w/v) solution of MA-g-HDPE in xylenes was refluxed for 2 hours at 110°C (for 15 kg/mol) or 135°C (for 121.5 kg/mol) under a dry N<sub>2</sub> atmosphere ensuring all of the MA-g-HDPE had gone into solution. HA-CTA was dissolved in DMSO at 110°C (0.5% (w/v)). The MA-g-HDPE solution was added to the HA-CTA solution via a heated cannula under dry N<sub>2</sub> flow.[3] After reacting under vigorous mixing for 12 hours the viscous gel product and supernatant were vacuum dried at 50°C for 72 hours. The reaction products remaining after vacuum drying were subjected to hydrolysis, which generated an ion exchange, resulting in the removal of CTA<sup>+</sup> side groups.[4]

A 0.2M NaCl aqueous solution was added to the HA-CTA-*co*-HDPE product while stirring at room temperature. After 1 hour an excess of ethyl alcohol was added to the HA-*co*-HDPE and salt solution, causing the HA-*co*-HDPE to precipitate out. The precipitate was pelleted by centrifugation, washed with ethyl alcohol 5 times to remove CTA<sup>+</sup>Cl<sup>-</sup> salt, and vacuum dried at room temperature for 48 hours (or until no change in weight was observed). The HA-*co*-HDPE was re-suspended in water, washed with acetone to remove residual NaCl, and vacuum dried at room temperature for 24 hours (or until no change in weight was observed). A schematic of the product HA-*co*-HDPE is shown in Figure 1.

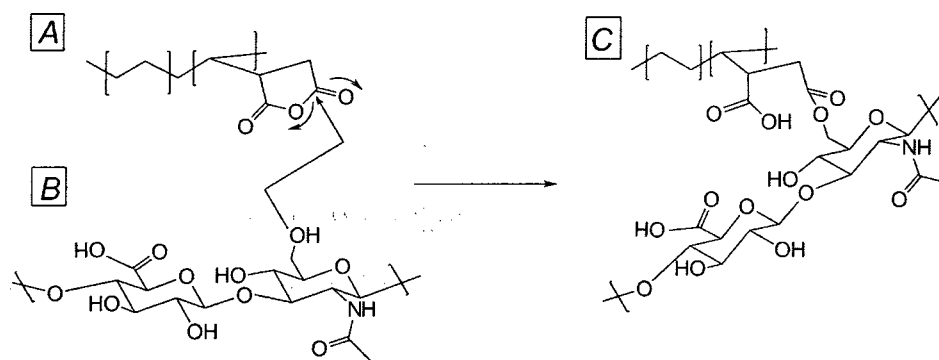


**Figure 1. Esterification reaction involving MA-g-HDPE and HA.**

HA-*co*-HDPE with different theoretical weight percentages of HA were fabricated, using the 121.5 kg/mol MA-g-HDPE, in order to observe the effects of different weight percentages of HA: 85% (85-HA) and 98% (98-HA), respectively, assuming 100% conversion. Also, HA-*co*-HDPE was fabricated from the 15 kg/mol MA-g-HDPE with 28, 40, 50, 60 and 90% (w/w) HA (28-HA, 40-HA, 50-HA, 60-HA, 90-HA). The weight ratios of HA and HDPE were determined from the original weight of each constituent, MA-g-HDPE and HA-CTA. The chemical equations used to calculate the moles of HA

and HDPE employed in the synthesis of HA-CTA-*co*-HDPE and HA-*co*-HDPE, are shown below:

$$\frac{\text{mass\_HA}}{\text{Mw\_HA}} \cdot \frac{\text{Mw\_HA}}{\text{Mw\_repeat\_unit}} \cdot \frac{4(\text{OH})}{1\_repeat\_unit} := \text{moles\_HA}$$

$$\frac{\text{mass\_HDPE}}{\text{Mw\_HDPE}} \cdot \frac{\text{Mw\_HDPE}}{\text{Mw\_repeat\_unit}} \cdot \frac{3}{100} := \text{moles\_HDPE}$$

$$97 \cdot \left( 28 \cdot \frac{\text{g}}{\text{mol}} \right) + 3 \cdot \left( 126 \cdot \frac{\text{g}}{\text{mol}} \right) \div 100 := \text{Mw\_repeat\_unit of HDPE}$$

Two negative control reactions were included and carried out using identical methods to those described above. (In one reaction, unmodified HDPE was used in place of MA-*g*-HDPE and added to the HA-CTA DMSO solution. In the other reaction, DMSO was used without the addition of HA-CTA).

Chemical crosslinking of the HA portion of the copolymer powder was accomplished via a poly(hexamethylene diisocyanate) crosslinker to yield crosslinked HA-*co*-HDPE powder (XL HA-*co*-HDPE).[4, 7] One gram of HA-*co*-HDPE powder was placed into a small beaker, and 50 mL of a 2.0% (v/v) poly(hexamethylene diisocyanate), a 10% (v/v) poly(hexamethylene diisocyanate), or a 2.0% (v/v) poly(hexamethylene diisocyanate) with the addition of a tin catalyst acetone solution were added under dry N<sub>2</sub>. The specimens were soaked in the respective solutions for 10 minutes or 24 hours at room temperature for 10 minutes then placed in a vacuum oven at 50°C for 3 hours to cure the crosslinker. The chemically crosslinked copolymer was centrifuged, washed with acetone 5 times to remove residual uncured crosslinker, then vacuum dried at room temperature for 24 hours (or until no change in weight was observed). The solubility of HA-*co*-HDPE

and XL HA-*co*-HDPE was tested at 24, 50 and 80°C in acetone, xylenes, water, hexanes, ethanol, THF and DMSO.

### 2.2.2 HA-*co*-HDPE Melt Processing

To determine if the HA-*co*-HDPE powder could be compression molded 0.5 g of HA-*co*-HDPE powder were placed in a 25 mm cylindrical inner diameter (I.D.) stainless steel mold, Figure 2, with polyimide mold release film placed between the powder and the plungers. The mold was placed in a vacuum bag and sealed. Air within the vacuum bag was evacuated by applying a vacuum pressure of -25 in Hg (gauge). The vacuum bag was subsequently flushed with dry N<sub>2</sub>, and a vacuum pressure of -25 in Hg (gauge) was applied. The vacuum bag was filled with dry N<sub>2</sub> three times. A vacuum pressure of -25 in Hg (gauge) was maintained during the entire compression molding cycle. XL HA-*co*-HDPE powder was prepared for compression molding in the same fashion as HA-*co*-HDPE.

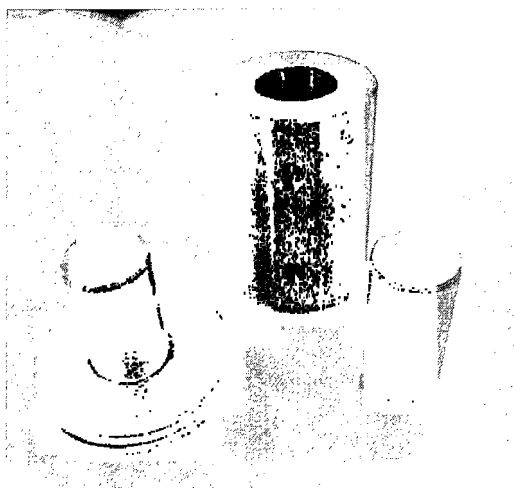


**Figure 2. Stainless steel mold utilized in the compression molding of HA-*co*-HDPE.**

The compression molding cycles for both HA-*co*-HDPE and XL HA-*co*-HDPE, fabricated from two different MA-*g*-HDPE polymers, is shown in Figure 3;[14] the melt

soak temperature was approximately 10-15°C above the average  $T_m$ , corresponding to the different copolymer batches, which was deduced from DSC results. Following compression molding, the HA-co-HDPE and XL HA-co-HDPE pucks were placed in a water bath for 48 hours at room temperature.

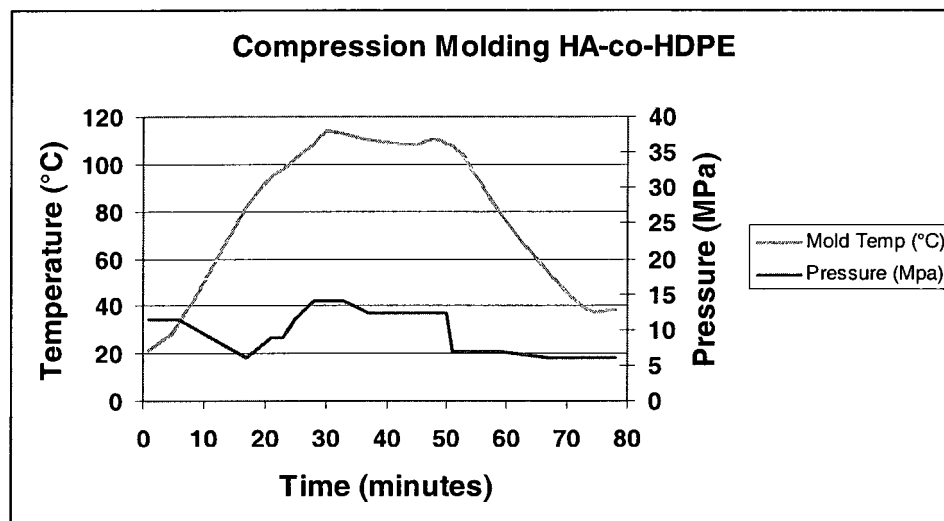


Figure 3. Compression molding cycle for HA-co-HDPE powder.

Three grams of MA-g-HDPE (molecular weight 15 kg/mol) was heated in a glass Petri® dish in an inert atmosphere (vacuum bag) to 120°C using the compression molding press; the samples (n=1 for each group) were held at the melt temperature for 10 minutes. One sample was immediately placed in freezing water (0°C) while the other sample was left on the platens as they slowly cooled to room temperature. These 2 different cooling rates are included with the cooling rate determined by the current molding cycle in Figure 4.

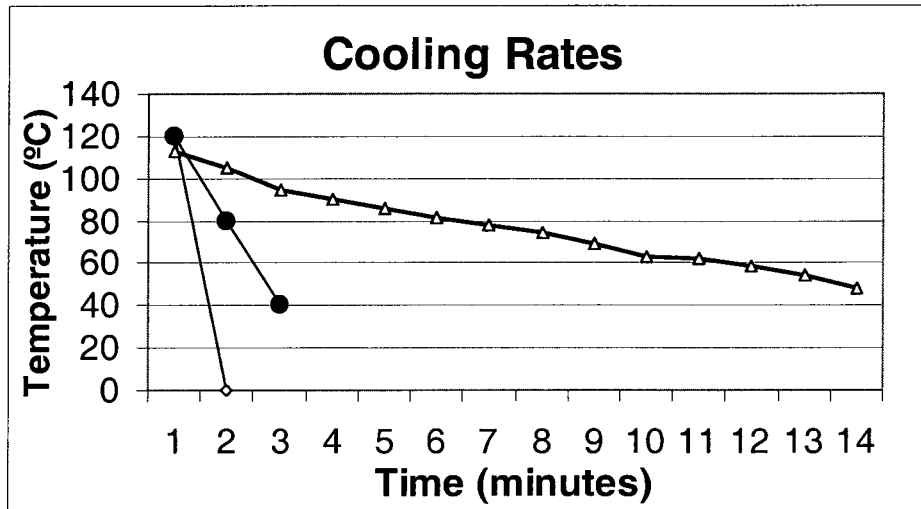


Figure 4. Various cooling rates of compression molding mold for MA-g-HDPE (15 kg/mol).

A compression molding cycle was developed for blend composites which contain high molecular weight PEs (i.e., UHMWPE and MA-g-HDPE (0.3% MA)). The desired melt soak parameters are listed below in Table 1. *UHMWPE resin will be compression molded using these target parameters to obtain a graphical depiction of the compression molding cycle in its entirety.*

Table 1. Compression molding cycle melt soak stage parameters for HA-co-HDPE samples and composite blends.

	Old Parameters	New Parameters
Melt Soak Temperature	120°C	154°C
Melt Soak Time	10 minutes	20 minutes
Average Melt Soak Pressure	8 MPa	8 MPa

HA-co-HDPE was fabricated from 640 kDa HA and 15 kg/mol MA-g-HDPE (3% MA), with a theoretical final weight ratio of 50:50 and 10:90. The HA-co-HDPE (50:50 weight ratio only) and UHMWPE (GUR 1020) powders were blended together via a cryogrinder. Weight ratios of the HA-co-HDPE and UHMWPE powders were 90:10, 75:25, and 60:40. Compression molding took place under vacuum; the parameters were 150°C and 110°C and 18 MPa and 14 MPa for 20 minutes (n=1 for each UHMWPE blend and n=1

for 100% HA-*co*-HDPE control); see Figure 5 for compression molding cycles used to melt process HA-*co*-HDPE and UHMWPE powder blends.

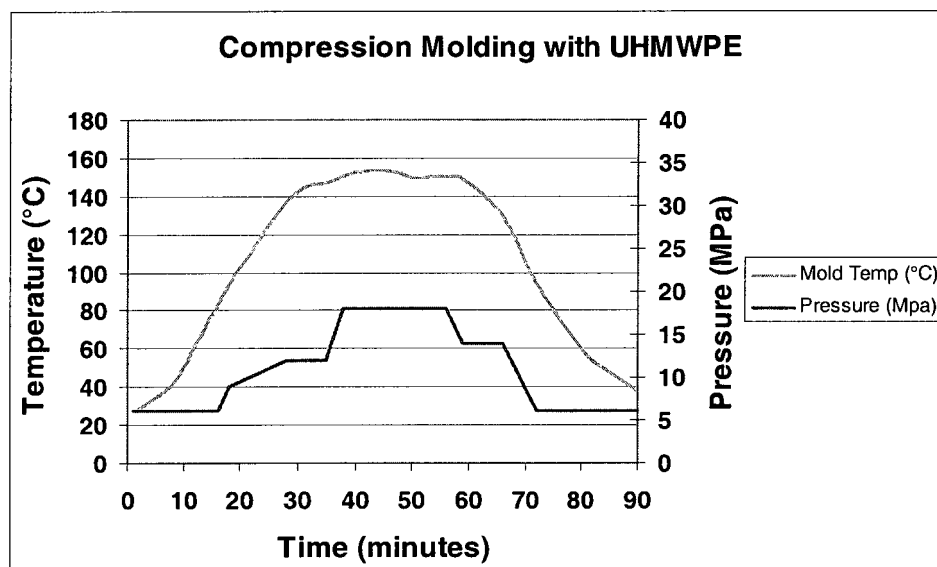


Figure 5. Compression molding cycle for HA-*co*-HDPE and UHMWPE powder blends.

Some of the HA-*co*-HDPE and UHMWPE compression molded samples were additionally treated with HA and PE chemical crosslinkers. One group (labeled HA XL) was placed in 10% (v/v) poly(diisocyanate) and acetone solution for 10 minutes, removed from the solution and placed in a 50°C vacuum oven for 3 hours to cure the crosslinker. Then the group samples were rinsed with acetone and vacuum dried at -25 in Hg (gauge) for 12 hours. Another group was pre-treated with 0.5% (w/w) dicumyl peroxide (DP) and 0.03% (w/w) vitamin E prior to compression molding. The final group (labeled HA XL DP/E) included the two previous steps, which involved chemical crosslinking both the HA and PE portions of the HA-*co*-HDPE and UHMWPE composites. Some of the compression molded HA-*co*-HDPE samples were also chemically crosslinked. One group was soaked in 10% (v/v) poly(diisocyanate) and acetone solution for 24 hours and the

other group was soaked in 10% poly(diisocyanate) plus dibutyltin dilaurate (a reaction catalyst) acetone solution for 24 hours. Both samples were then cured in a 50°C vacuum oven for 3 hours to cure the crosslinker. Then the group samples were rinsed with acetone and vacuum dried at -25 in Hg (gauge) for 12 hours.

**Table 2. Identification labels for the various sample groups and their respective constituents.**

<b>Sample Identification</b>	<b>Sample Constituents</b>
A	HA-co-HDPE (40% HA, MW = 1.5 MDa)
B	HA-co-HDPE (50% HA, MW = 1.5 MDa)
C	HA-co-HDPE (60% HA, MW = 1.5 MDa)
D	HA-co-HDPE (50% HA, MW = 650 kDa)
E	Treated HA-co-HDPE (50% HA, MW = 1.5 MDa)
F	HA-co-HDPE (50% HA, MW = 1.5 MDa) + UHMWPE
G	HA-co-HDPE (50% HA, MW = 1.5 MDa) + treated UHMWPE
H	HA-co-HDPE (50% HA, MW = 1.5 MDa) + treated MA-g-HDPE (3.0%)
I	HA-co-HDPE (50% HA, MW = 1.5 MDa) + treated MA-g-HDPE (0.3%)

### 2.2.3 Characterization Methods

A Nicolet Magna-IR 760 spectrometer (E.S.P.) was used to record Fourier Transform infrared spectroscopy (FTIR) data. Sample powder (2% (w/w)) was ground, mixed with KBr, and pressed into pellets for analysis. Transmission absorption spectra were collected over a range of 600-4000  $\text{cm}^{-1}$  at a resolution of 4  $\text{cm}^{-1}$  after 128 scans. Various HA-co-HDPE were analyzed, and three scans per group were combined to determine average peak values.

X-ray photoelectron spectroscopy (XPS) qualitative analysis was performed using a PHI 5800 spectrometer. The instrument was equipped with a monochromatic Al K $\alpha$  (1486.6eV) X-ray source. Data acquisition/processing were performed using MultiPak Spectrum ESCA software. Measurements were taken with an electron takeoff angle of 45° from the surface normal (sampling depth approximately 60 Å); a low energy (5 eV) electron gun was used for charge neutralization on the non-conductive samples. Elemental compositions were determined from 10-1100 eV survey scans acquired with a pass energy of 93.9 eV. The high resolution spectra (C1s, N1s) were obtained at a pass energy of 23.5 eV. Component peak analysis of high resolution spectra was performed using MultiPak Spectrum ESCA software. XPS analysis was performed on HA-co-HDPE, fabricated from 121.5 kg/mol MA-g-HDPE, for 98-HA with a sample size of one spectrum per group.

Elemental analysis was performed at Galbraith Laboratories. The carbon, oxygen, and nitrogen content were determined using inductively coupled plasma optical emission spectroscopy (ICP-OES), after peroxide fusion in a Parr bomb. Samples of HA-co-HDPE, fabricated with 121.5 kg/mol, with 85-HA and 98-HA were analyzed (n=1).

Solid state nuclear magnetic resonance (ssNMR) was performed by Process NMR Associates, LLC (Danbury, CT) on control and test powder samples; a 50:50 weight ratio of maleated *graft* HDPE (MA-g-HDPE) and HA was used as the control. This control sample was compared to 85-HA and 98-HA HA-co-HDPE. Data was obtained on a Varian Unity Plus 200 spectrometer operating at a frequency of 50.297 MHz for <sup>13</sup>C and

299.96 MHz for  $^1\text{H}$ . A 7 mm Supersonic MAS probe by Doty Scientific was utilized for the experiments. The VACP-MAS experiments were performed utilizing the variable amplitude cross polarization pulse sequence in order to reduce the effects of spin modulation on the quantitative nature of the experiment.  $^{13}\text{C}$  SPMAS experiments were performed with gated high power decoupling. Magic angle spinning was employed at a rate of around 5.4 kHz.

The percent crystallinity ( $\%X_c$ ) and melting temperature ( $T_m$ ) of the copolymer was measured by means of a TA Instruments differential scanning calorimeter (DSC) 2920 in a dry  $\text{N}_2$  atmosphere per ASTM D3418-03. Samples were heated from  $24^\circ\text{C}$  to  $180^\circ\text{C}$  at a rate of  $10^\circ\text{C}/\text{minute}$ , held at equilibrium for 1 minute, cooled to  $24^\circ\text{C}$  at a rate of  $10^\circ\text{C}/\text{minute}$ , re-heated from  $24^\circ\text{C}$  to  $180^\circ\text{C}$  at a rate of  $10^\circ\text{C}/\text{minute}$ , held at equilibrium for one minute, and air cooled to room temperature (all with  $\text{N}_2$  atmosphere). The heat of fusion ( $H_f$ ) was calculated by integrating the DSC endotherm from the second heating curve from  $80$  to  $160^\circ\text{C}$ . The  $H_f$  of 100% crystalline HDPE was determined to be  $288 \text{ J/g}$ . [15, 16] The  $\%X_c$  was calculated by dividing the  $H_f$  of the sample by  $288 \text{ J/g}$  (because the 100% crystalline  $H_f$  of the graft copolymer is unknown) and multiplying by 100. DSC was used to characterize 3 specimens from each compression molded puck. The samples were heated from room temperature to  $200^\circ\text{C}$ , cooled back down to  $0^\circ\text{C}$ , then heated to  $200^\circ\text{C}$ ; the heating and cooling rates were  $10^\circ\text{C}/\text{minute}$ . Data was collected from the second heating curve; HA-co-HDPE and powder blend data was analyzed by integrating from  $50$ - $150^\circ\text{C}$  and UHMWPE data was analyzed by integrating  $65$ - $165^\circ\text{C}$ .

The degradation temperatures ( $T_d$ ) of the powder samples were determined using a TA Instruments thermogravimetric analyzer (TGA) 2950 at a heating rate of 10°C/minute in helium. Masses of individual specimens ranged from 5-15 mg. All variations of the HA-*co*-HDPE copolymer were analyzed. TGA was also performed on HA-*co*-HDPE powders (50-HA, 15 kg/mol MA-*g*-HDPE) treated with 0.3% vitamin E; one powder sample was heated to 150°C and another powder sample was heated to 170°C and both were held constant at the respective temperature for 20 minutes. The weight percent lost during that time was then compared to untreated HA-*co*-HDPE powders. Finally, TGA was performed to determine the purity (or amount of copolymerized HA) and excess HA (free HA, not covalently linked to HDPE or itself) in various HA-*co*-HDPE formulations. TGA was performed on 10-HA, 28-HA and 50-HA HA-*co*-HDPE after processing (in powder form), after soaking in a 50:50 water:xylenes solution and vacuum drying, and after centrifuge collection. All reported average values and standard deviations for % $X_c$ ,  $T_m$ , and  $T_d$  were calculated from a sample size of three per group.

Hydrolyzed HA-CTA, refluxed MA-*g*-HDPE, and HA-*co*-HDPE dry powders, fabricated with 121.5 kg/mol MA-*g*-HDPE, were placed onto scanning electron microscopy (SEM) specimen holders with carbon double-sided tape and surfaces were coated with 5 nm of gold. Powders were stored in a desiccated vacuum prior to imaging; images were taken using a JOEL JSM-6500F field emission SEM. Images were taken at 180x, obtained at 15 keV. Compression molded HA-*co*-HDPE and MA-*g*-HDPE, 15 kg/mol, were also viewed via SEM at 200, 2000, and 5000x and obtained at 15 keV. Half of the compression

molded sample was soaked in distilled water for 36 hours and subsequently vacuum dried at room temperature for 72 hours before examination.

HA-co-HDPE samples, XL HA-co-HDPE samples and HA-co-HDPE:UHMWPE samples were punched out of 3 mm thick pucks with a 4 mm diameter biopsy punch for swell ratio experiments. Specimens were dried in 50°C vacuum oven at -25 in Hg (gauge) for at least 24 hours prior to the experiment. The original weights of sample specimens were recorded for swelling experiments at this time. The specimens were then swelled in PBS for 24 hours at 37°C in a shaker oven. The specimens were removed from solution, blotted with a paper towel, and the wet weight was recorded. The specimens were placed in a vacuum oven for 24 hours at 50°C under -25 in Hg. The dry weight was also recorded for specimens containing UHMWPE after vacuum drying; this value was used to calculate the lost material, or the weight percentage that was lost to the environment (i.e., solution). Water content was calculated as the increase in weight percent using the following equation:

$$\text{Increase in weight, \%} = (\text{wet weight} - \text{conditioned weight}) / \text{conditioned weight} \times 100$$

#### 2.2.4 Statistics

Statistics were analyzed using Statistical Analysis Software (SAS® Institute Inc.). A normality test was performed; all swelling data was normal. An ANOVA test with a 95% confidence interval ( $\alpha=0.5$ ) was performed; multiple comparisons were performed using

the least square means. The average value and standard error of the mean (s.e.m.) for each experimental and control group population was calculated.

### 2.3 Results

An interfacial polymerization reaction utilizing two immiscible solvents, DMSO and xylenes, was used to synthesize the novel HA-*co*-HDPE, a graft copolymer.[17] Under vigorous mixing the HA-CTA and MA-*g*-HDPE formed a covalently bound crosslinked network via esterification.[18] Maleated HDPE was incorporated to precisely adjust the physiochemical properties of HA: to produce a hydrophilic, thermoplastic HA, and to enhance the mechanical properties of HA. The reaction between MA-*g*-HDPE and HA-CTA was carried out successfully in an inert atmosphere (see Figure 6) forming the gel graft copolymer HA-CTA-*co*-HDPE.

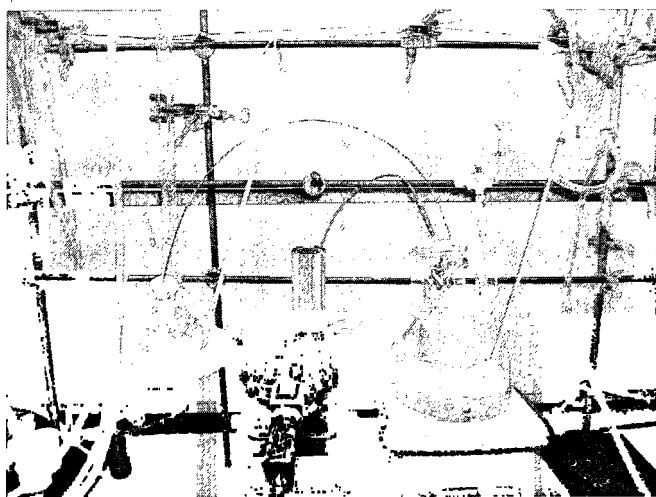
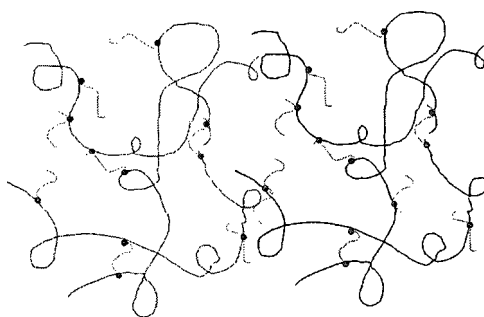


Figure 6. Reaction set up for HA-*co*-HDPE synthesis.

The esterification reaction between the anhydride and hydroxyl functional groups does not produce any water. At the very instant the MA-*g*-HDPE solution was added to the HA-CTA solution, a viscous gel formed. After a few minutes (when the combined

solution temperature equilibrated at 110°C) any unreacted MA-*g*-HDPE (121.5 kg/mol) came out of solution and further reaction with the HA-CTA was unlikely; however, the 15 kg/mol MA-*g*-HDPE remained in solution (due to its  $T_m$  of 90°C). The reaction yields for the HA-*co*-HDPE copolymers, made with the two different MA-*g*-HDPE (121.5 kg/mol and 15 kg/mol), were on average 65 and 95%, respectively. A white, fluffy, porous powder was generated via hydrolysis, in which HA-CTA-*co*-HDPE converted to HA-*co*-HDPE. The hydrolysis procedure for HA-CTA-*co*-HDPE and its derivatives was adapted from the same hydrolysis procedure HA-CTA, and any unreacted HA molecules will precipitate out of solution along with the HA-*co*-HDPE; in other words, currently no methods are known which could be applied to purifying the HA-*co*-HDPE (i.e., removing unreacted constituents). The removal of DMSO was the result of its miscibility with water. Upon hydration, the HA-*co*-HDPE (both with the HA portion unintentionally and intentionally chemically crosslinked) behaved like a hydrogel; the liquid prevented the polymer network from collapsing into a compact mass, and the network retained the liquid. A schematic of the network structure of HA-*co*-HDPE (fabricated from 1.5 MDa HA and 15 kg/mol MA-*g*-HDPE) is shown in Figure 7; one can imagine how changing the length of the HA chains and/or the length of the HDPE chains would change the resulting structure and networked (i.e., HDPE acting as chemical crosslinker) the polymer is. The graft percent of MA on HDPE used in the initial reaction will also affect this since the MA groups on the HDPE are what can form the covalent linkages (shown as red dots in Figure 7) with HA; when a single HDPE chain is covalently bound to two or more HA chains, the HA chains are effectively crosslinked by the HDPE. A SEM image of HA-*co*-HDPE, fabricated with 121.5 kg/mol MA-*g*-HDPE, 98-HA, is shown in Figure 8.



**Figure 7. Schematic of the HA-co-HDPE network structure: black lines – HA; light blue lines –HDPE; red dots – covalent bonds between HA and HDPE. Crystallinity of HDPE is not shown.**

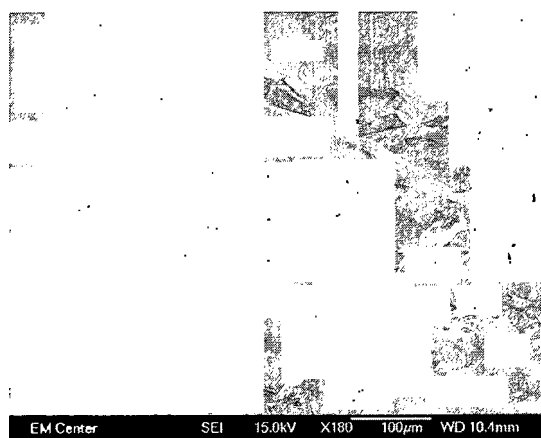


**Figure 8. SEM image of HA-co-HDPE (121.5 kg/mol MA-g-HDPE, 98-HA).**

HA-co-HDPE and XL HA-co-HDPE were both insoluble in acetone, water, xylenes, ethanol, hexanes, THF and DMSO at 24, 50 and 80°C; thus, it was difficult to characterize HA-co-HDPE and XL HA-co-HDPE using standard analytical techniques due to the insoluble nature of the copolymer. HA-co-HDPE neither unmodified nor XL HA-co-HDPE is soluble in any typical organic solvent, which hinders the use of solution dependent polymer characterization methods.

To determine if an esterification occurred between HA hydroxyl groups and MA functional groups, an FTIR spectra overlay of HA-co-HDPE, refluxed MA-g-HDPE (15 kg/mol) and a blend of MA-g-HDPE and HA was constructed (see Figure 9).

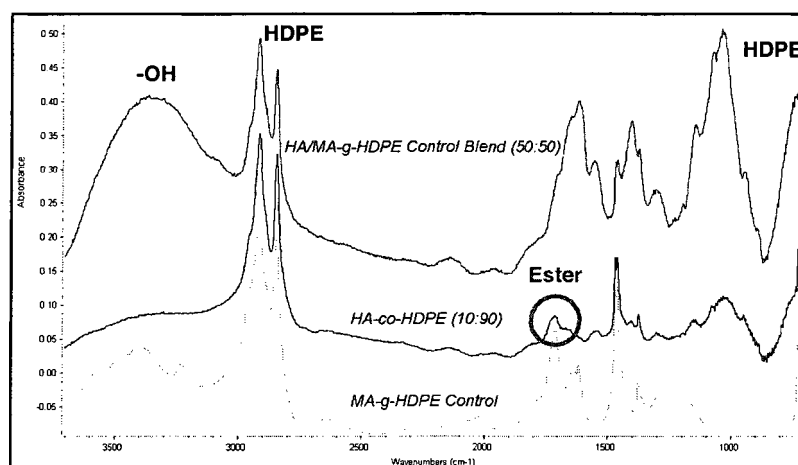


**Figure 9. FTIR spectra overlay of HA-co-HDPE ((10:90) = 10-HA, [10:1] 50-HA, [1:1] = 10-HA) and graft copolymer constituents.**

The FTIR spectrum of HA-co-HDPE closely resembles the FTIR spectra of HDPE resin and HA, the major constituents of the graft copolymer. The peak associated with hydroxyl functional groups did show a shift between sodium HA, HA-co-HDPE (85-HA and 98-HA), from 3405 to 3427 and 3371  $\text{cm}^{-1}$  respectively. Virtually no shift in the frequency of  $\text{-CH}_3$  and  $\text{-CH}_2$  groups, 2919 and 2918  $\text{cm}^{-1}$ ; however, the area integrated under the peak did increase from the addition of HDPE. An additional peak at 2850  $\text{cm}^{-1}$  is associated with methyl groups from the HDPE. The peaks at 1616, 1418, 1321, and 1160  $\text{cm}^{-1}$  shifted slightly from HA to the copolymer at 1620, 1410, 1320, and 1155  $\text{cm}^{-1}$ . The peak at 1032  $\text{cm}^{-1}$  increased to 1046  $\text{cm}^{-1}$  in the copolymer. No other new peaks appeared in the copolymer spectrum compared to the spectra of HA and HDPE. The graft copolymer spectra do, however, show noticeable peaks in the anhydride/ester region, 1779 and 1846  $\text{cm}^{-1}$ . [19, 20] The peaks in the HA-co-HDPE materials (see part B) are shaped differently compared to the controls, which may indicate an increase in the ester peak due to the copolymerization reaction.

High resolution XPS was performed on HA-co-HDPE, fabricated with 121.5 kg/mol MA-g-HDPE, (98-HA) to identify what elements and functional groups were present in each graft copolymer (see Figure 10).[21] XPS results showed that the hydrolysis method was not effective in removing all of the ammonium salt.

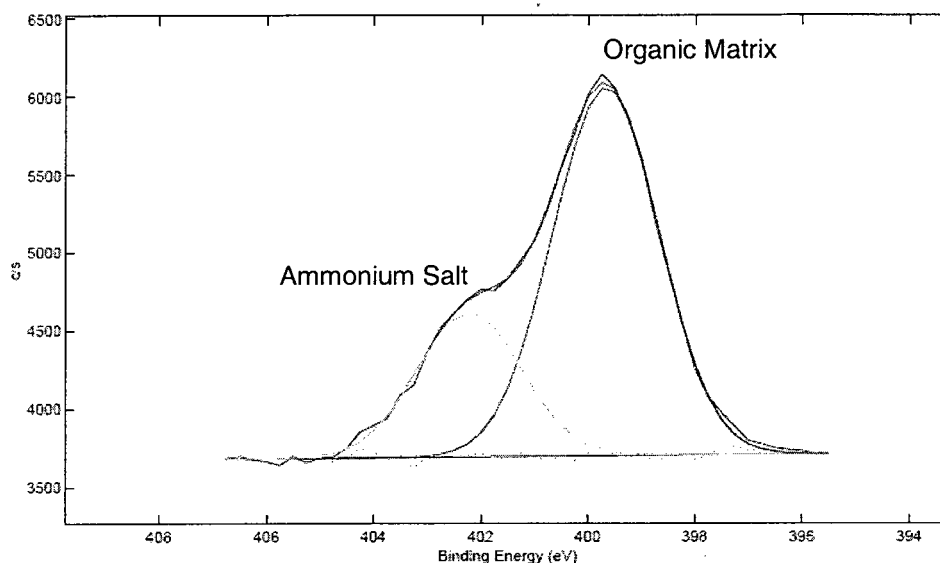


**Figure 10. XPS N<sub>1s</sub> high resolution spectrum for 98-HA HA-co-HDPE.**

Elemental analysis data for HA-co-HDPE, fabricated with 121.5 kg/mol MA-g-HDPE, 85-HA and 98-HA, are shown in Table 3; as the weight percentage of HA increases, weight percentages of oxygen and nitrogen also increase. The results from elemental analysis showed that the carbon percentage calculated for the copolymers was lower than expected for both HA-co-HDPE batches. It was also shown that the oxygen and nitrogen had lower percentage values for the copolymer with 85-HA versus the copolymer with 98-HA.

**Table 3. Elemental analysis data of HA-co-HDPE copolymer of different molar ratios.**

Sample ID	Analysis	Theoretical Weight %	Results
HA-co-HDPE (98% HA)	C	42.67	36.15 %
	O	43.08	43.30 %
	N	3.43	2.82 %
HA-co-HDPE (85% HA)	C	48.61	40.30 %
	O	37.14	37.88 %
	N	2.95	2.58 %

The spectral features associated with a  $^{13}\text{C}$  ssNMR spectrum are shown in Table 4, which were used to assign chemical bonds to peaks shown on the ssNMR spectra.

**Table 4.  $^{13}\text{C}$  solid state nuclear magnetic resonance spectral features.**

Chemical Shift Range	Carbon Type
0-20 ppm	Methyl Carbons ( $\text{CH}_3$ )
20-40 ppm	Methylene Carbons ( $\text{CH}_2$ )
60-80 ppm	Ether Carbons (C-O)
100-120 ppm	Fluorinated Carbon ( $\text{CF}_2$ )
100-160 ppm	Nitrile Carbon (CN) or Olefin
160-180 ppm	Carboxyl Carbon (C=O) Esters, Amides
180-190 ppm	Carboxyl Carbon (C=O) Acids
190-200 ppm	Aldehyde Carbon
200-220 ppm	Ketone Carbon

Figure 11 (see next page) shows  $^{13}\text{C}$  ssNMR spectra for the control and copolymer samples.

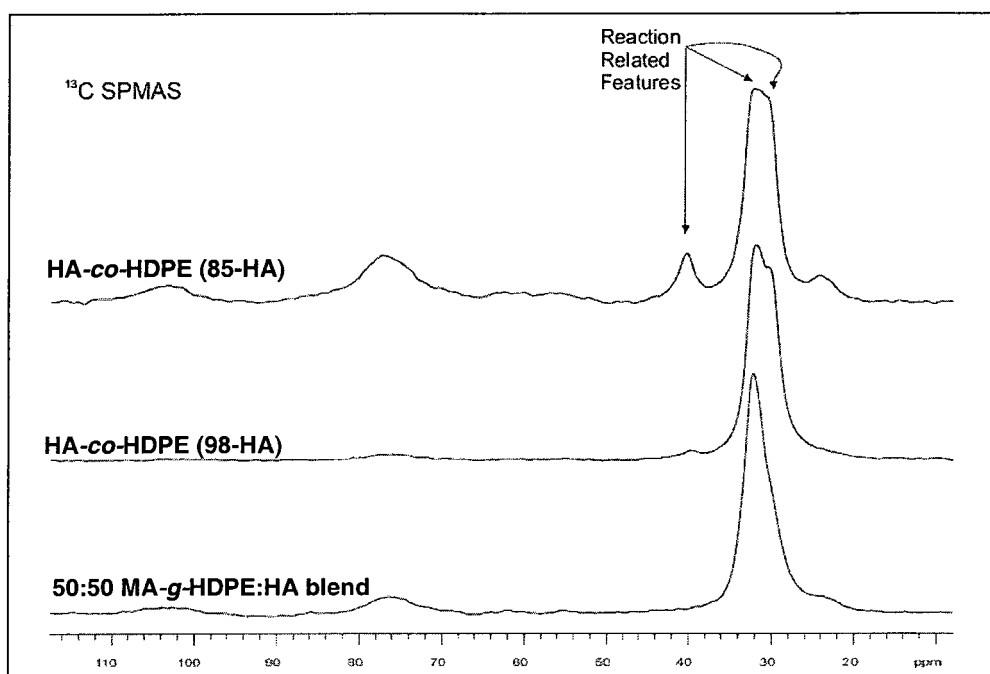


Figure 11.  $^{13}\text{C}$  solid state nuclear magnetic resonance spectra.

In Figure 11, peaks at 110-50 ppm represent chemical bonds that are associated exclusively with HA; the peaks at ~35-20 ppm represent carbon-carbon and carbon-hydrogen bonds associated primarily with HDPE ( $\text{CH}_2$ ,  $\text{CH}_3$ ) due to its high crystalline nature and also carbon bonds ( $\text{CH}$ ,  $\text{CH}_3$ ) present in HA. The shift in signal intensities (peaks >50 ppm) between the control blend spectrum (*bottom*) and 85-HA HA-*co*-HDPE (*top*), and the 98-HA HA-*co*-HDPE spectrum (*middle*) indicates a higher HA content in the control blend and 85-HA copolymer compared to the 98-HA copolymer. This result was expected given that weight calculations for the copolymer were based on a theoretical 100 percent conversion reaction—an *ideal* case. The difference in the peak shape/intensity at ~40-20 ppm between the control and HA-*co*-HDPE samples is indicative of a change in crystallinity; the HA-*co*-HDPE samples are more crystalline than the control. The contact array for the 85-HA sample is shown in Figure 12 and the relaxation time data is shown in Figure 13.

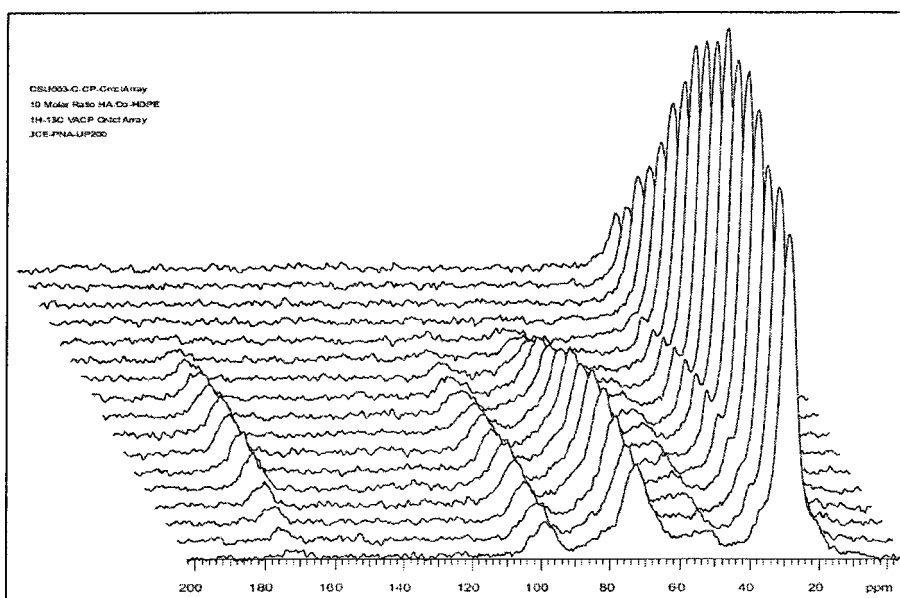


Figure 12. Contact time array from solid state nuclear magnetic resonance of HA-co-HDPE (85-HA).

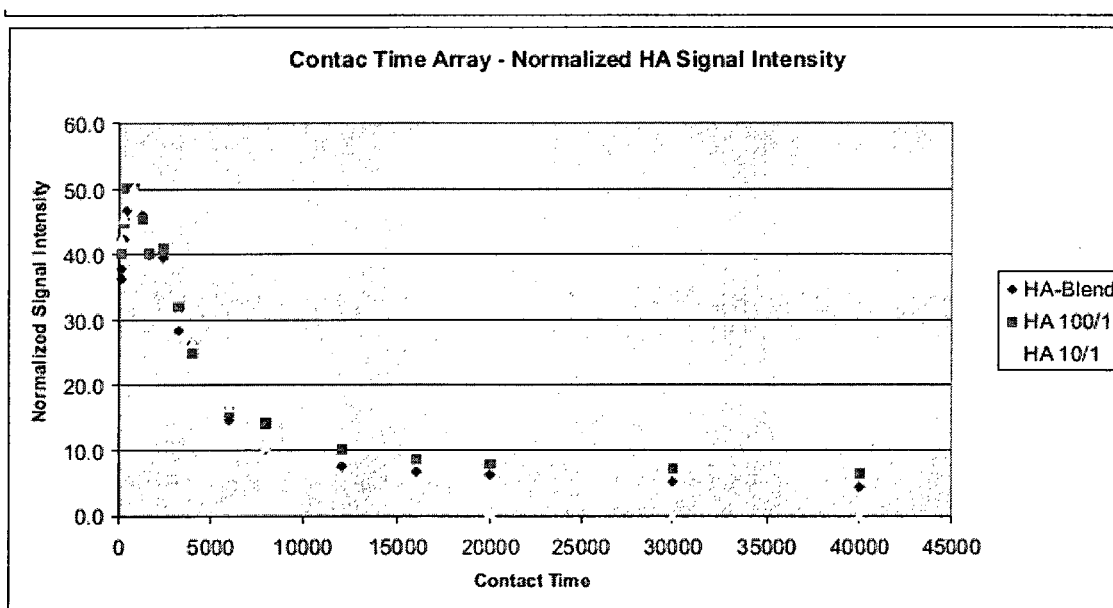


Figure 13. Relaxation time profiles of contact time arrays from solid state nuclear magnetic resonance: the control sample (50:50 weight ratio MA-g-HDPE:HA powder blend) (blue diamond); 98-HA HA-co-HDPE (pink square); 85-HA HA-co-HDPE (yellow triangle).

The HDPE crystalline phase was observed more selectively due to the stronger  $^1\text{H}$ - $^1\text{H}$  dipole coupling that exists in a rigid crystalline matrix. The segmental backbone motions present in amorphous HDPE phases effectively reduce the  $^1\text{H}$ - $^1\text{H}$  couplings so that amorphous phases were less intense in the NMR spectrum than they actually are.

The  $T_m$  and  $\%X_c$  of the graft copolymers and their constituents were determined from DSC. Representative DSC melt endotherm curves for HA-*co*-HDPE (85-HA and 98-HA, made from 121.5 kg/mol MA-*g*-HDPE), refluxed MA-*g*-HDPE, a powder blend of HA-*co*-HDPE and refluxed MA-*g*-HDPE (121.5 kg/mol), are shown in Figure 14. DSC scans of HA-*co*-HDPE (theoretical weight percent of HA is 50%) and a control blend of HA and MA-*g*-HDPE are shown in Figure 15 and 16; the MA-*g*-HDPE was 15 kg/mol.

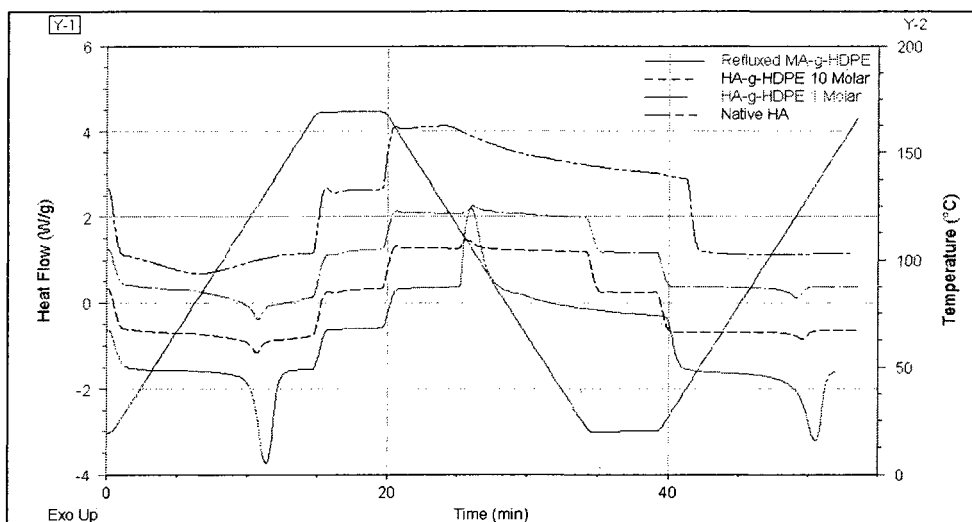


Figure 14. DSC scan overlay of MA-*g*-HDPE, HA, MA-*g*-HDPE/HA blend, and HA-*co*-HDPE.

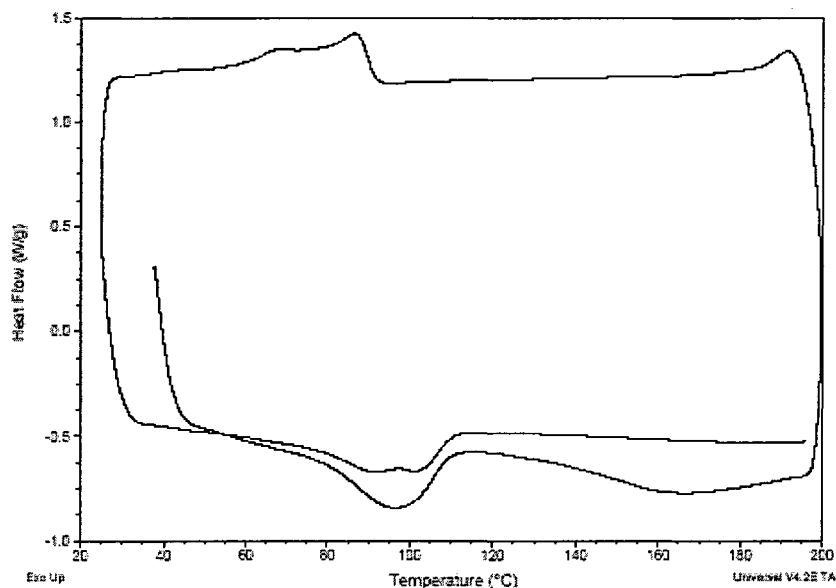


Figure 15. DSC scan of HA-*co*-HDPE, 50-HA, fabricated with 15 kg/mol MA-*g*-HDPE.

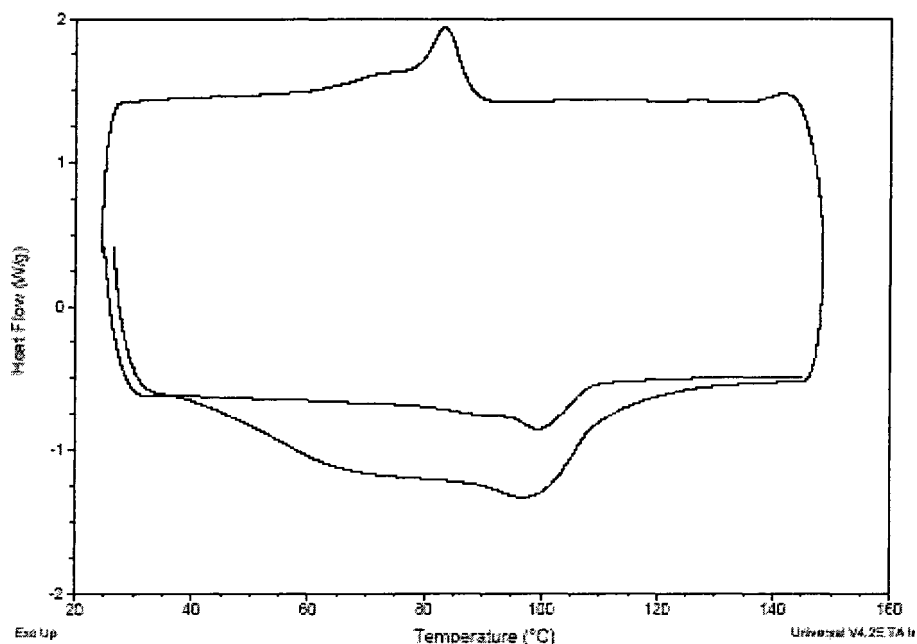


Figure 16. DSC scan of a 50:50 control blend of HA and MA-g-HDPE, 15 kg/mol.

Compression molding the novel graft copolymer, exhibiting intentionally non-crosslinked and crosslinked HA portions, was successful at temperatures 10-15°C above the  $T_m$  of the respective weight percents HA. Figure 17 represents the material property data (e.g.,  $T_m$  and  $\%X_c$ ) comparing the two different cooling rates (the control was the DSC data of MA-g-HDPE, which had a controlled cooling rate of 10°C). It was determined that the cooling rate of the MA-g-HDPE (molecular weight 15 kg/mol) does not significantly affect the  $T_m$  and  $\%X_c$  of the compression molded samples.

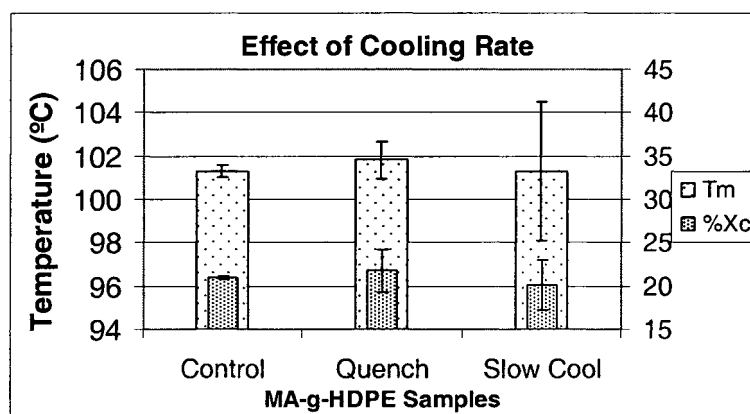
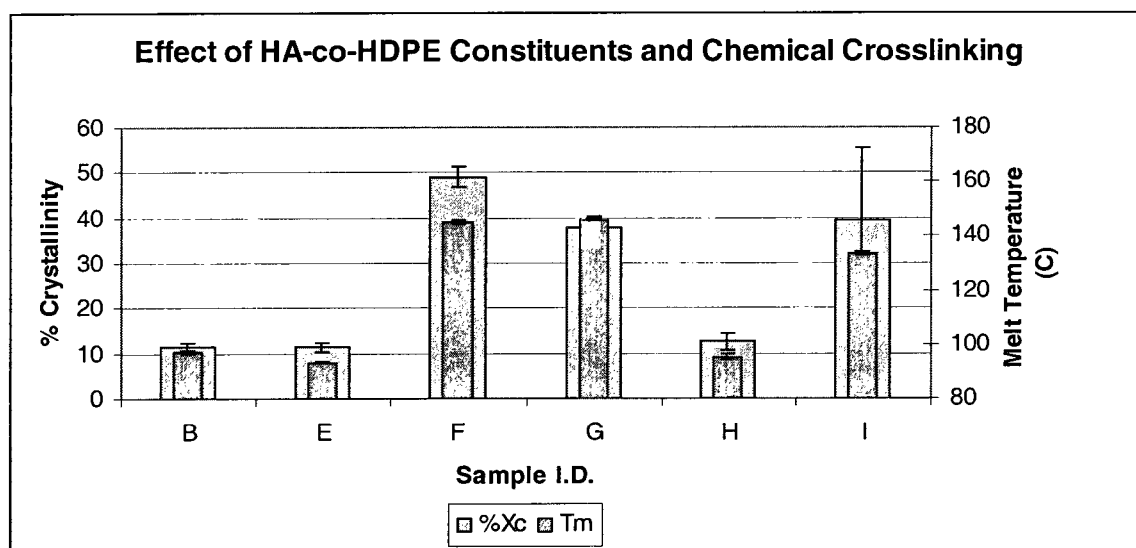


Figure 17. The effect of compression molding cooling rate for MA-g-HDPE (15 kg/mol).

The cooling rate does not have an effect on the  $\%X_c$  of MA-g-HDPE (with a molecular weight of 15 kg/mol) that was melted on a hot platen. MA-g-HDPE cannot be compression molded by itself because of its low molecular weight and results in a pool of fluid material; when copolymerized with HA, it has an increased to flow and maintains shape after molding. This is why the DSC sample of MA-g-HDPE was used for a control due to a similar heating method – resin is allowed to melt flow past its melting temperature and is cooled at a controlled, measurable rate. Crystallinity and melting temperature calculated for various HA-co-HDPE samples/blends are shown in Figure 18, below.



**Figure 18. Degrees of crystallinity and melt temperatures for various HA-co-HDPE compression molded samples and composite blends. Refer to Table 2 for detailed specimen information (average  $\pm$  standard error of the mean).**

FTIR analysis was conducted on HA-co-HDPE before and after DSC analysis; the spectra are shown below in Figure 19.

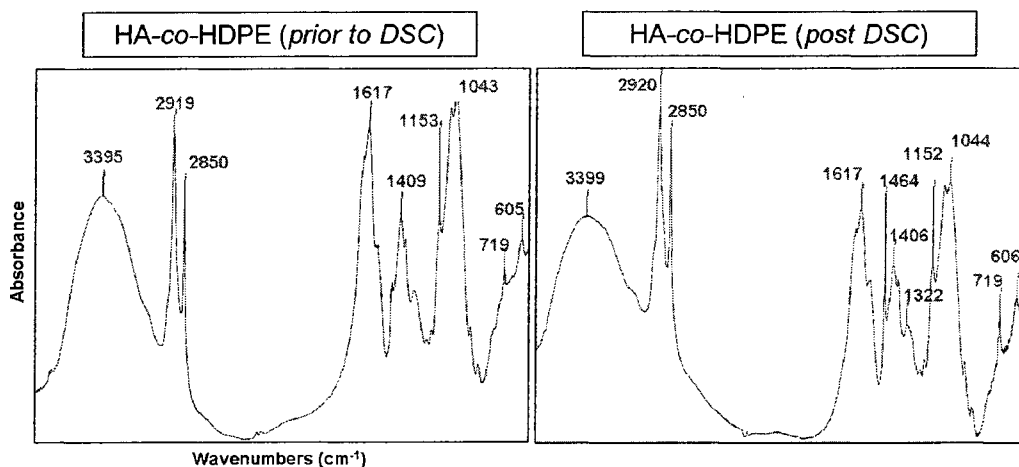


**Figure 19. FTIR analysis of HA-co-HDPE pre- and post-thermal analysis via DSC.**

Crystallinity and melting temperature calculated for various HA-co-HDPE (50-HA) and HA-co-HDPE:UHMWPE powder blends (using the 50-HA copolymer) are shown in Figure 20, below.

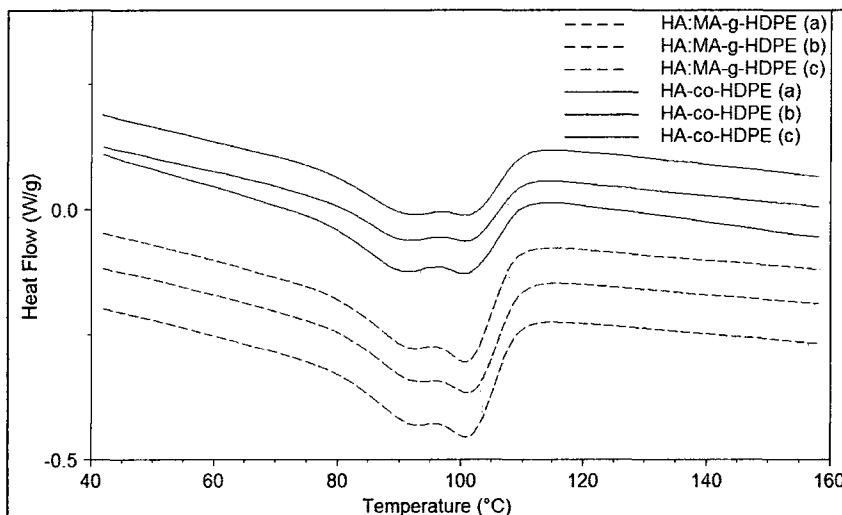


**Figure 20. DSC scan overlay for HA-co-HDPE (50-HA) and MA-g-HDPE control blends, 50:50 weight ratios (second heating curve).**

Crystallinity and melting temperature calculated for various HA-co-HDPE (50-HA) and HA-co-HDPE:UHMWPE powder blends (using the 50-HA copolymer) are shown in Figure 21, on the next page.

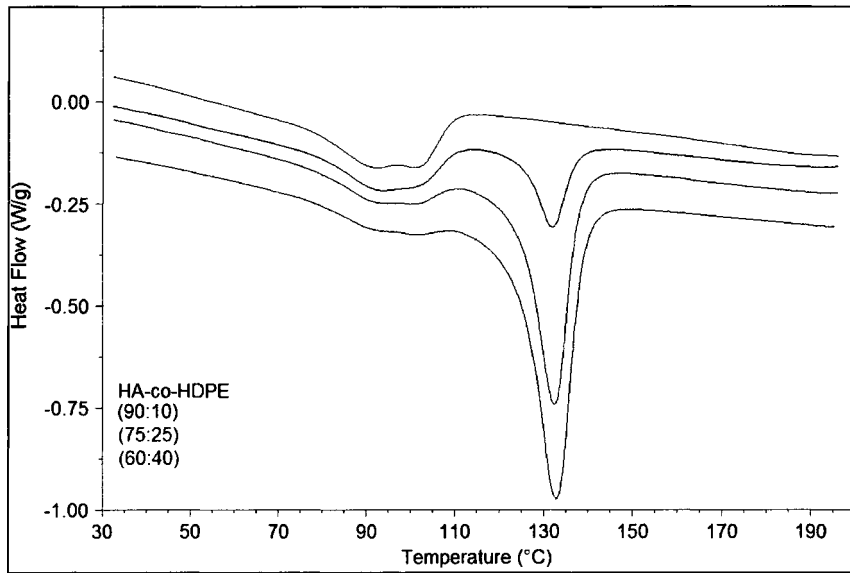


Figure 21. DSC scan overlay for HA-co-HDPE and UHMWPE powder blends (second heating curve).

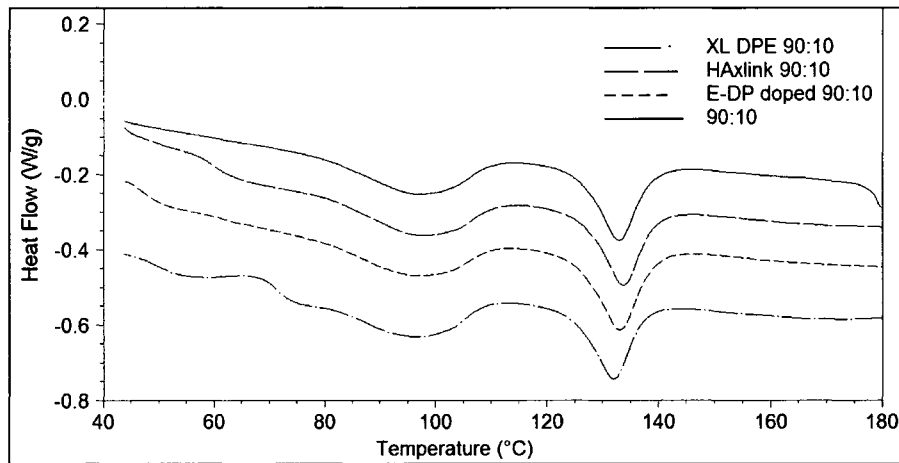


Figure 22. DSC scan overlay for HA-co-HDPE:UHMWPE (90:10) powder blend and the effects of compression molding and chemical crosslinking.

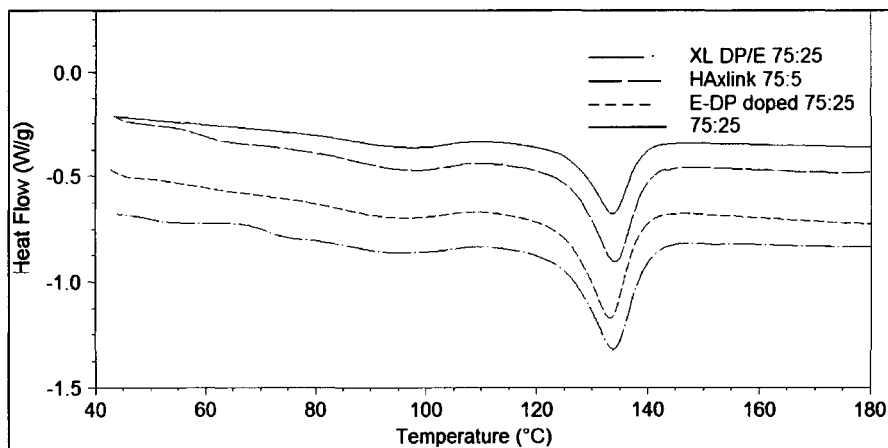


Figure 23. DSC scan overlay for HA-co-HDPE:UHMWPE (75:25) powder blend and the effects of compression molding and chemical crosslinking.

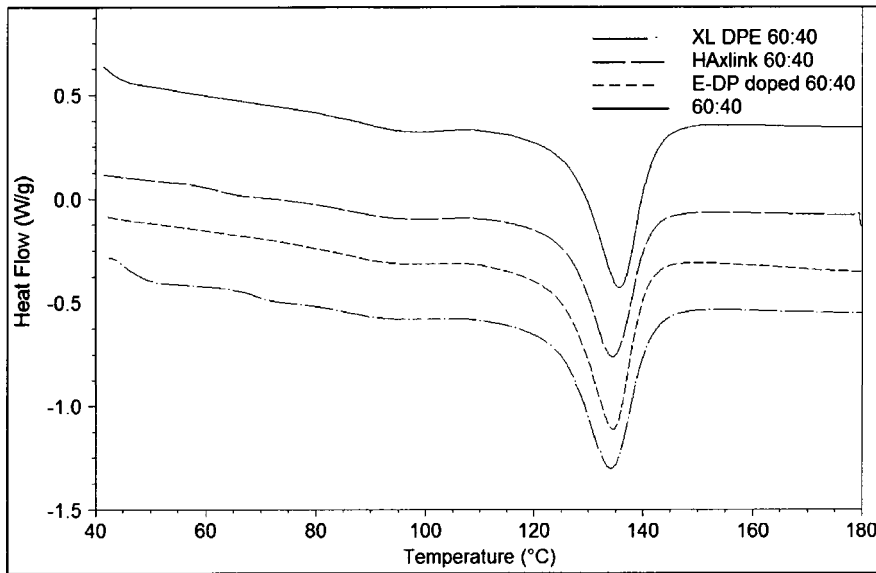


Figure 24. DSC scan overlay for HA-co-HDPE:UHMWPE (60:40) powder blend and the effects of compression molding and chemical crosslinking.

SEM images of compression molded 50-HA HA-co-HDPE are shown in Figure 25; macrostructure was compared between compression molded samples and samples that had been swollen in water and subsequently dried for SEM analysis.

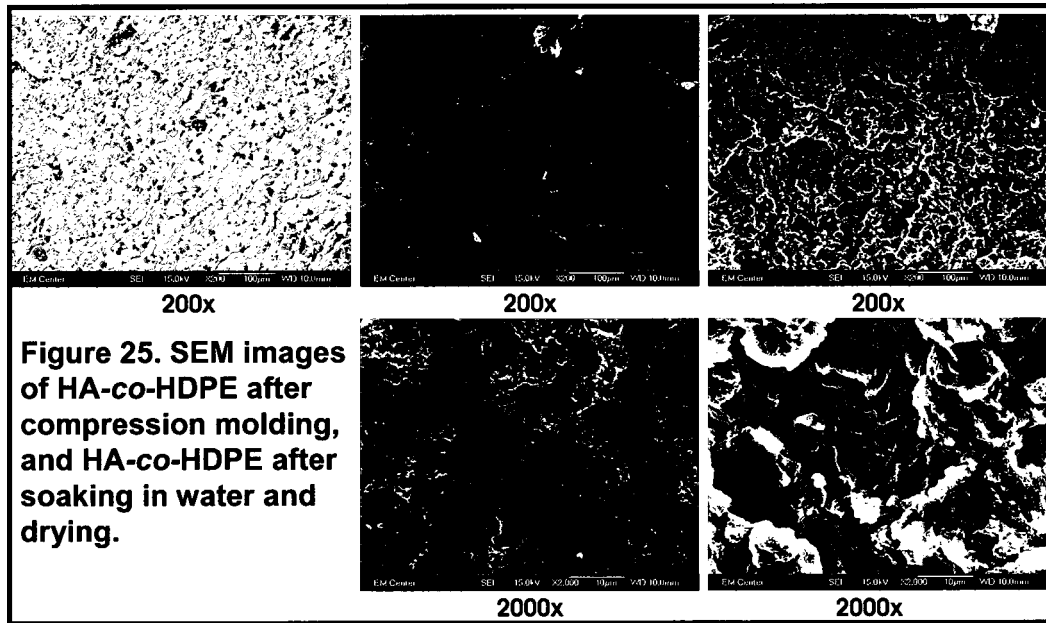


Figure 25. SEM images of HA-co-HDPE after compression molding, and HA-co-HDPE after soaking in water and drying.

From the TGA scans in Figure 26 it is shown how the esterification reaction between HA and HDPE affects the degradation profiles of the two constituent polymers. This method

was thus used to identify if a reaction occurred between HA and MA-g-HDPE. TGA was also used to determine the approximate weight ratios of the constituent materials in the final product, compared to the theoretical weight ratios calculated prior to the reaction.

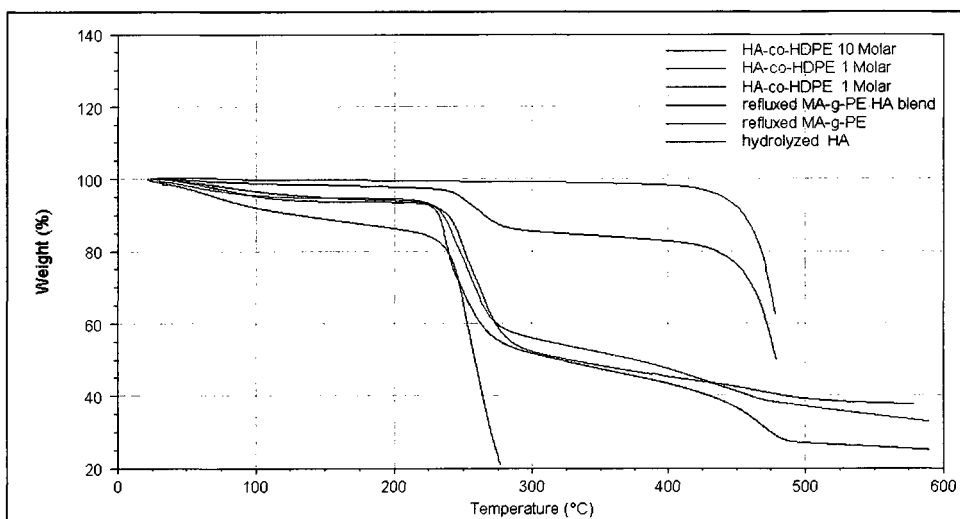


Figure 26. TGA scan of HA-co-HDPE and the graft copolymer constituents.

The effect of the addition of vitamin E was tested and the TGA scans are shown in Figure 27.

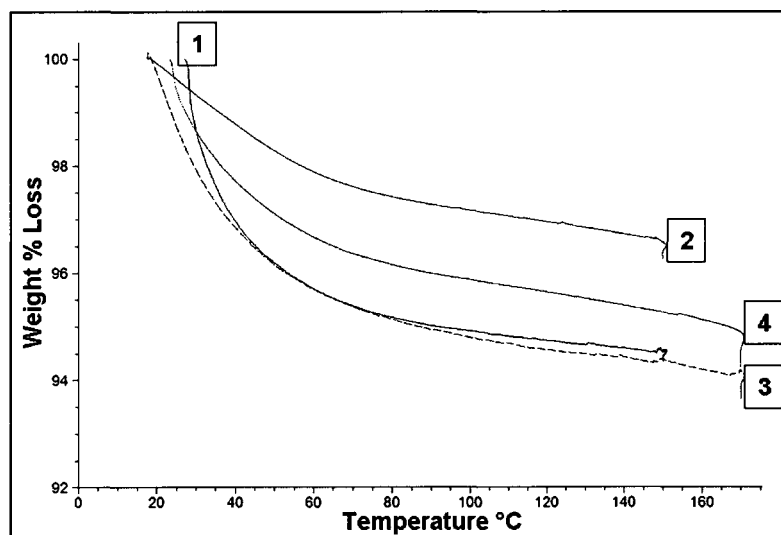
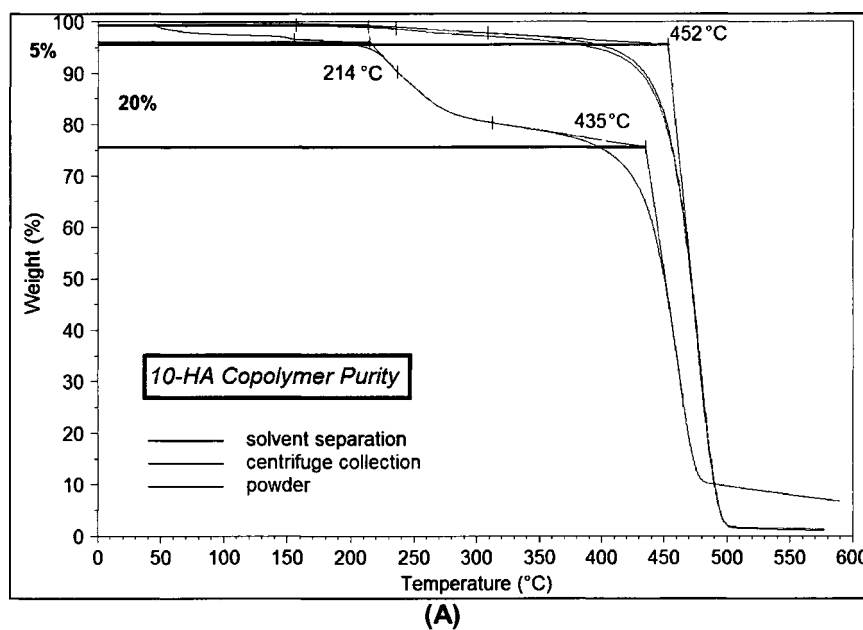


Figure 27. TGA scan of HA-co-HDPE untreated (1,3) and treated with 0.3% vitamin E (2,4).

The TGA scans represent the four different samples: 1) HA-*co*-HDPE held at 150°C, 2) HA-*co*-HDPE doped with vitamin E held at 150°C, 3) HA-*co*-HDPE held at 170°C, and 4) HA-*co*-HDPE doped with vitamin E held at 170°C. An n=1 powder sample represents each TGA scan. The scans in Figure 27 show that the HA-*co*-HDPE treated with vitamin E degrades less, based on weight % lost during heating, compared to untreated samples. This effect is seen for powders held for 20 minutes at 150°C and 170°C. Therefore, the addition of vitamin E is advantageous to decreasing the amount of HA degradation during the compression molding of HA-*co*-HDPE.

TGA was utilized to approximate the purity (i.e., the amount of HA and PE covalently bound to each other in the networked copolymer) of the 10-HA, 28-HA, and 50-HA HA-*co*-HDPE materials. The scans for the three different copolymer materials are shown below in Figure 28.



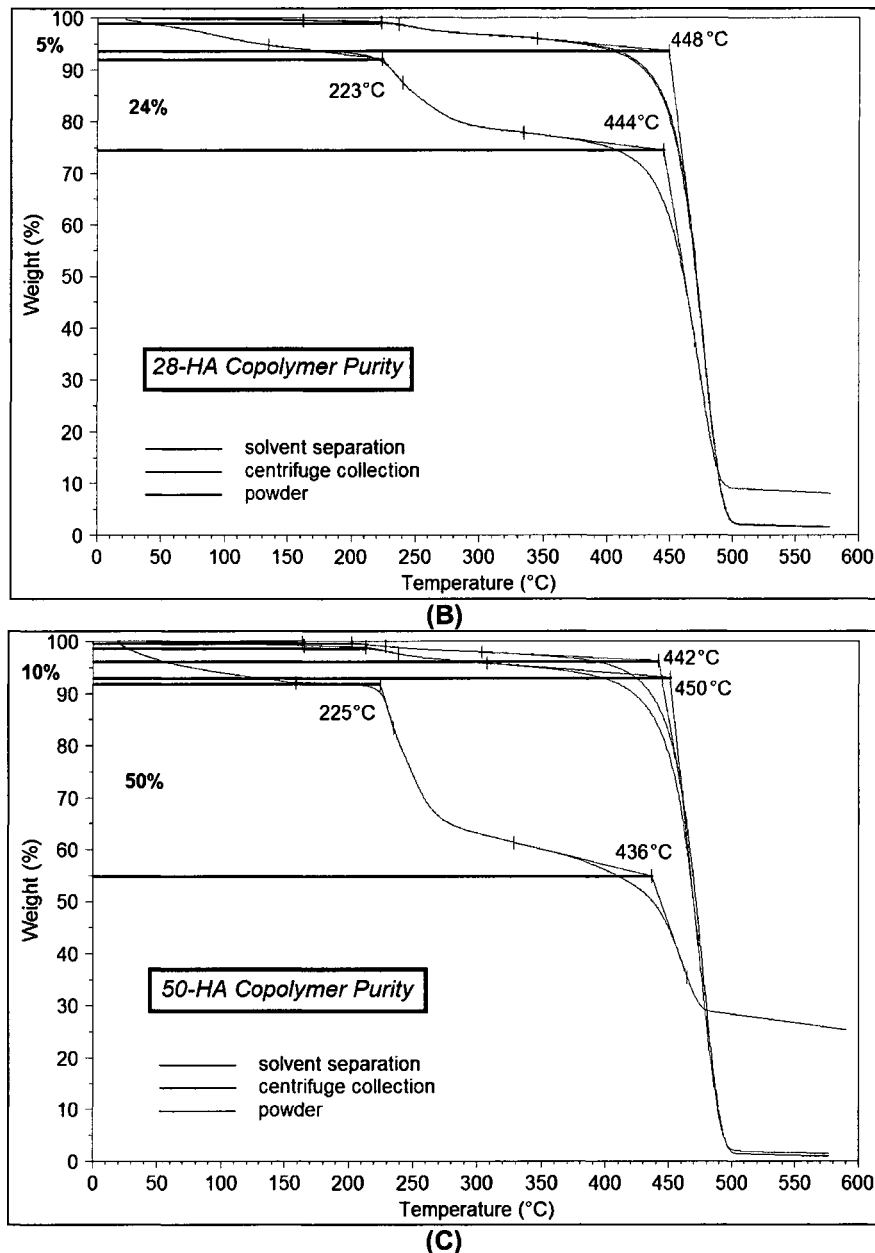


Figure 28. TGA scans of 10-HA (A), 28-HA (B) and 50-HA (C) HA-co-HDPE showing an overlay of various untreated and washed copolymer powders.

The water content data for HA-co-HDPE, XL HA-co-HDPE and HA-co-HDPE:UHMWPE blend composites (see Table 2) are shown in Figures 29-31. There was no significant difference between groups ( $p = 0.8625$ ) with varying weight percents of HA (see Figure 29); however, there was a significant difference between 50% HA weight percent groups ( $p < 0.01$ ) with different molecular weights of HA (see Figure 29). There

was no significant difference between groups with varying weight percents of HA (see Figure 31).

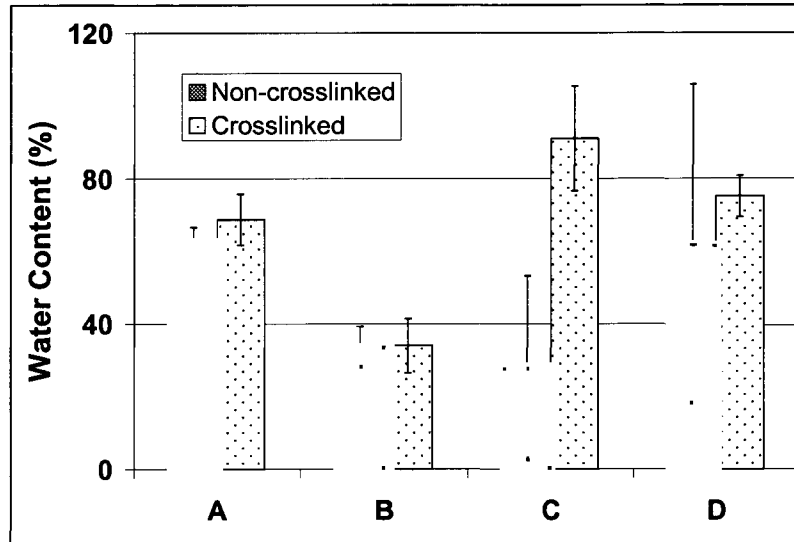


Figure 29. Water content after 24 hour soak for HA-co-HDPE fabricated with various weight ratios of the polymeric constituents (average  $\pm$  standard error of the mean): A is 40-HA (1.5 MDa), B is 50-HA (1.5 MDa), C is 60-HA (1.5 MDa), and D is 50-HA (650 kDa). Also see Table 2.

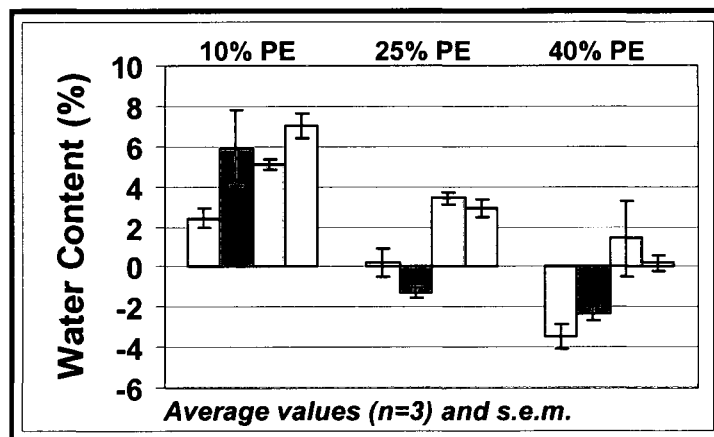
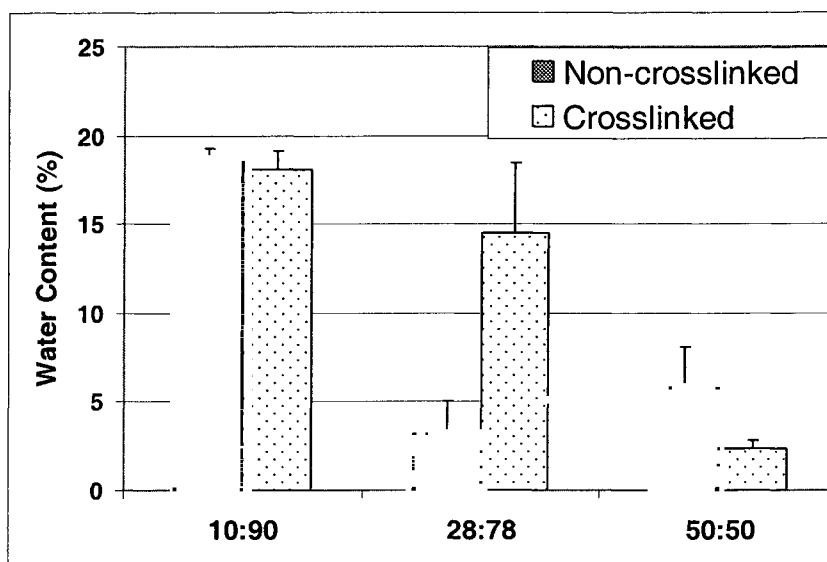


Figure 30. Water content for various compression molded HA-co-HDPE:UHMWPE powder blend composites; experiment was conducted in PBS at 37°C for 24 hours; compression molded powder blends are labeled by weight percent UHMWPE (PE).



**Figure 31. Water content percentages for various compression molded HA-co-HDPE powders (10-HA, 28-HA and 50-HA by weight); experiment was conducted in PBS at 37°C for 24 hours.**

## 2.4 Discussion

The fabrication of HA-co-HDPE was successful; however, the consistency of the reaction varied between the different copolymer batch types. The weight ratios of HA-co-HDPE constituents that were calculated before the reaction occurred varied slightly from the reaction product TGA-derived weight ratios. These differences, which are seen only for certain weight ratios of HA-co-HDPE constituents, may be explained with further characterization and may be affected by the morphology of certain constituent weight percentages. Altering the molecular weight of the HA and HDPE constituents, altering the graft percent of MA, and altering the weight percentage of HA in the HA-co-HDPE copolymer resulted in materials with various physical properties. Increasing the graft percent of MA onto the HDPE backbone helped to create a more homogeneous HA-co-HDPE network. Regarding the microstructure, it is preferred to incorporate a low

molecular weight HA and high molecular weight maleated polyethylene to obtain a microstructure that is further bioinspired by the structure of articular cartilage.

The lack of solubility precludes the measurement of molecular weight, for example. Also, HA degrades at high temperatures, consequently high temperature solutions were also not feasible. Thus, circumstantial evidence has played a vital role in confirming the synthesis of HA-*co*-HDPE and XL HA-*co*-HDPE. Increasing the amount of time samples soaked in the crosslinking solution did increase the degree of crosslinking. The crosslinking was more effective because more crosslinker was able to diffuse through the powder slurry/sample thickness. The tin catalyst, however, was unsuccessful in significantly increasing the degree of crosslinking of the HA-*co*-HDPE materials. Water soluble crosslinkers would be an appropriate avenue for further investigation, especially in the case of drug delivery or various *in vivo* applications.

Molecular spectroscopy provides direct methods for studying polymer structures and their mutual interactions. Synthetic and biological polymers present a particularly difficult problem for molecular characterization due to the multi-component nature of the systems. In practice, no single spectroscopic or analytical technique is sufficient for the complete determination of all of the structure and distribution. Traditionally, IR spectroscopy has been one of the most popular physical methods in characterizing polymers; it is one of the simplest and fastest methods for the identification of compounds.[22] FTIR provides chemical structural information on polymers that is suitable for qualitative identification. Due to the low graft percents of MA groups, any

identifiable peaks associated with cyclic anhydrides were not seen on the FTIR spectra, and therefore it is not likely that any formed ester bond would appear on a FTIR spectrum. The relatively high molecular weight of HA also contributed to the difficulty in identifying newly produced ester peaks, since the ester carbonyl ( $\text{C=O}$ ) exists on every HA repeat unit. Also, due to the large weight percent of HA, hydrogen bonding was likely occurring and the carbonyl peak was interfering with the absorption of the characteristic ester band.

The hydrolysis procedure was successful in removing DMSO, as shown in the FTIR and XPS spectra, but not all of the ammonium salts were removed (Figures 9 and 10). The incomplete removal of ammonium salts may be the result of the amphiphilic graft copolymer; the ammonium salts are most likely trapped in the crosslinked network of the graft copolymer. The hydrolysis procedure for HA-CTA-*co*-HDPE and its derivatives was adapted from the same hydrolysis procedure HA-CTA, and any unreacted HA molecules will precipitate out of solution along with the HA-*co*-HDPE; in other words, currently no methods are known which could be applied to purifying the HA-*co*-HDPE (i.e., removing unreacted constituents). The removal of DMSO was the result of its miscibility with water. Also, as a result of the solubility study, residual unreacted MA-*g*-HDPE was not removed due to the thermal degradation of the graft copolymer (i.e., a heated xylene solution could not be used to remove unreacted MA-*g*-HDPE). However, the wash with acetone may have been successful in removing ungrafted MA.[23] It was assumed that performing the hydrolysis procedure at 24°C would not degrade the newly formed graft copolymer. Generally, temperatures greater than 70°C are required for trans-esterification

to occur, which is the process of breaking ester bonds and forming a new ester with alcohols or water. The swelling properties of HA in water resulted in a loss of physical crosslinks and the HA backbone of the graft copolymer swelled in the polar solvent. However, the HDPE side chains are not soluble in water and remained suspended in solution.

The elemental analysis results did show that as the HA weight percent increased so did the weight percentages of oxygen and nitrogen; however, this does not prove that a reaction took place. The hydrolysis method was intended to regenerate HA from HA-CTA, and any unbound HA will be retained with the precipitated product throughout the hydrolysis of HA-CTA-*co*-HDPE. This said the elemental analysis results did not take into account by-product contamination. Only selected elements were targeted for analysis based on cost constraints. The results from elemental analysis showed that the carbon percentage calculated for the copolymers was lower than expected for both molar ratios. It was also shown that the oxygen and nitrogen had lower percentage values for the copolymer with 85-HA versus the copolymer with 98-HA.

In addition to distinct differences in peak intensities, the peaks at 110-50 ppm occur in *all* samples. By simply examining the current ssNMR spectra it is not possible to observe a definitive separate resonance (i.e., peak) due to the ester formation; the peaks may be superimposed and spectral subtraction of the control and copolymer sample may confirm the occurrence of a reaction. Additionally, the MA-*g*-HDPE:HA molar ratio will be calculated from their respective signal intensities for various HA-*co*-HDPE samples. The

relaxation time profile associated with the contact time arrays indicates a difference in the profiles of the control and HA-*co*-HDPE samples. The difference in the contact array profiles insinuates that the mobility of the MA-*g*-HDPE and HA polymers was altered due to the reaction taking place (i.e., an ester formation); this change in mobility is expected not to change in the physical blend of the control sample. The results reported here for the control and test samples, although still inconclusive, provide further evidence that a reaction takes place between HA and MA-*g*-HDPE, resulting in the formation of a covalent bond between the two polymers and ultimately resulting in the formation of the graft copolymer HA-*co*-HDPE .

The introduction of HA alters the  $T_m$  and  $\%X_c$  of refluxed MA-*g*-HDPE; however, more analysis (e.g., DMA) will need to be conducted to determine how the physical properties are affected by changes in network structure. The  $T_m$  of the different graft copolymers was used to develop the compression molding cycle for HA-*co*-HDPE. Due to the crystalline nature of HDPE, the  $\%X_c$  of the HA-*co*-HDPE was assumed to be equivalent to the weight percent corresponding to the MA-*g*-HDPE, assuming the HA portion of the copolymer did not contribute to the melt endotherm and the degree of crystallinity, which is discussed briefly by Zhang.[4] This assumption made it possible to calculate the crystallinity using the theoretical  $H_f$  of 100% HDPE. The endotherm of the first scan is very broad; this is due to bound water being released from the HA portion of the copolymer as it is being heated. It is hypothesized that the double peaks in the endotherm of the second run represent crystalline domains of HDPE and HA; however, further analysis via DMTA will allude to whether or not this is the case. Further FTIR analysis

confirmed that the endothermic abnormality (at approximately 170°C) of the HA-*co*-HDPE DSC scan, shown in Figure 14, was not the result of additional chemical reactions taking place, shown in Figure 19; FTIR spectra HA-*co*-HDPE before and after DSC analysis were nearly identical and it was concluded that no chemical modifications took place during DSC.

The melting temperature-composition relations of HA-*co*-HDPE are discussed. It is important to understand that in addition to different chemical repeating units, structural irregularities such as stereo-irregularity, branch points, head-to-head structures, and geometric irregularities all behave as copolymeric units when they are incorporated into a chain of a semi-crystalline copolymer.[22] When interpreting the melting temperature of a copolymer, it must be decided *a priori* whether the crystalline state remains pure (i.e., whether the co-unit enters the lattice). In the case of most copolymers, including HA-*co*-HDPE, the co-units or structural irregularities do not participate in the crystallization, i.e., the crystalline phase remains pure. Thus, the melting temperature of a copolymer does not depend directly on its composition, but rather depends on the nature of its sequence distribution (a consequence of the chain-like character of polymers). As the content of the crystallization component decreases, due to the grafting of HA onto HDPE units, the fusion occurs over a broader temperature range; it can be difficult to recognize the crystallinity and the fusion of copolymers that have high contents of structural irregularities.[22] Also, it is expected that the grafting (or branching) of HA onto the HDPE backbone will decrease the melting temperature of the homopolymer (i.e., MA-*g*-HDPE).

Compression molding the HA-*co*-HDPE powder and 90:10 and 75:25 HA-*co*-HDPE:UHMWPE powder blends decreased the heat of fusion and thus the crystallinity compared to the powder properties. Compression molding the 60:40 HA-*co*-HDPE:UHMWPE powder blend increased the heat of fusion and thus the crystallinity. The two different outcomes are the result of the UHMWPE content; at 40% UHMWPE the composite contains more crystalline regions, below 40% the effect is not seen. The effects of chemically crosslinking the HA and/or HDPE portions of HA-*co*-HDPE and HA-*co*-HDPE/UHMWPE blends vary on the amount of PE in the composite. The 90:10 powder blend composite that was chemically crosslinked with diisocyanate exhibited an increased heat of fusion compared to the powder form, whereas the opposite was true for the other powder blend composites in which the HA portions were crosslinked.

In past reports, an antioxidant has been shown to reduce further oxidation by incorporation of the chemical (0.25% (w/w)) with UHMWPE resin.[24] Vitamin E has gained popularity as an antioxidant to prevent oxidation of ultra high molecular weight polyethylene (UHMWPE) orthopaedic materials due to gamma radiation sterilization and crosslinking.[25-30] Vitamin E, or  $\alpha$ -tocopherol, is a phenolic antioxidant that traps residual free radicals. Vitamin E is generally biocompatible and therefore more acceptable to clinicians than Irganox® antioxidants;[31-33] for this reason vitamin E was utilized instead of Irganox® for the prevention of oxidative degradation of HA-*co*-HDPE. The effect of pressure during actual compression molding is evident from the change in color that occurs during processing. After the compression molding cycle is duplicated

with TGA, the powder samples still remain white in color. Although the above TGA scans do show a drastic difference in weight % loss, the difference between the basic HA-*co*-HDPE and HA-*co*-HDPE doped with vitamin E exists. The degradation temperature of HA is approximately 200°C. However, TGA is performed in the absence of oxygen and without the addition of pressure; during compression molding, some degradation of HA occurs at temperatures much lower than that (i.e., 150°C). In the future, electron paramagnetic resonance may be performed to determine the free radical content of HA-*co*-HDPE and thus the amount of vitamin E required for complete quenching and thermal protection.

The higher graft percent MA-*g*-HDPE had a lower molecular weight, which made the compression molded HA-*co*-HDPE weak in comparison to the higher molecular weight MA-*g*-HDPE. Compression molded HA-*co*-HDPE fabricated with 121.5 kg/mol MA-*g*-HDPE exhibited structural integrity in the solid and hydrated states, while HA-*co*-HDPE fabricated with 15 kg/mol did not hold together in the hydrated state. The mechanical integrity of HA-*co*-HDPE in the hydrated state was greatly improved by blending HA-*co*-HDPE powder with UHMWPE powder pre-compression molding. The mechanical integrity of HA-*co*-HDPE and HA-*co*-HDPE/UHMWPE blends were also improved by chemically crosslinking both the HA and PE constituents of the copolymer.

Sample groups H and XL H are misleading because the composite is composed of only HA-*co*-HDPE; the addition of the MA-*g*-HDPE (15 kg/mol) was unsuccessful due to the low molecular weight and the MA-*g*-HDPE flowed out of the mold during compression

molding. The compression molded cycles of sample groups XL G and I should be modified to improve consolidation and enhance the effects of the chemical crosslinking of the polyethylene portions of the composites; this may be accomplished by extending the melt soak time and increasing the melt soak temperature. Upon soaking in distilled water, all of the samples resembled sponges and not hydrogels. Sample group XL B was successful compared to the other HA-*co*-HDPE composites (i.e., not the composite blends); improvements in this sample group may consist of increasing the chemical crosslinking of the HA portion. Plain HA-*co*-HDPE, that was compression molded, fell apart when hydrated because the entanglement of the HDPE was not great enough to hold the material together. Crosslinking the HA portion of the copolymer after compression molding helped, but the swelling properties of HA also worked against the consolidation of the HDPE chains and the compression molded copolymer fell apart. Blending the HA-*co*-HDPE powder with UHMWPE powder before compression molding increased the strength of the material after compression molding because the UHMWPE entangled with the HDPE chains and the composite held together better after hydration; however, once swollen in water or PBS, the integrity of the blended materials decreased (see discussion below).

Material properties and mechanical performance of thermoplastic polymers are largely influenced by thermal history and processing methods.[34, 35] Specifically, the molding cycle times and temperatures used to compression mold UHMWPE products influence the mechanical properties of the final product, depending on the degree of consolidation (i.e., chain entanglement) and crystallinity achieved. The compression molding cycle

developed for HA-*co*-HDPE was not sufficient in fully consolidating the UHMWPE blending composites due to the melt soak temperature. UHMWPE is too tough; molding parameters degrade the HA too much. Blending with UHMWPE required a high melt soak temperature be used during compression molding; this resulted in advanced degradation of the HA, which decreased the swelling properties of the composite. Also, the UHMWPE only increased the structural integrity of the compression molded composites a small amount. The molecular weight between entanglements ( $M_e$ ) of polyethylene is 1250.[36, 37] The brittle fracture mechanism of polymeric materials depend on the molecular weight and  $M_e$ ; polymers with lower  $M_e$  ( $MW < 2M_e$ ) will exhibit macromolecular chain sliding adjacent to the fracture plane compared to long chain polymers which contain chain entanglements across fracture planes and scission of chain segments occurs.[36] It is also known that the fracture strength is linearly dependent on the molecular weight of the polymer. An increase in molecular weight also causes an increase in the zero shear viscosity and a decrease in the frequency at which shear thinning begins.[37] Thus, the structural integrity of the HA-*co*-HDPE compression molded material may be improved by using a maleated polyethylene with a higher molecular weight. If a chain segment, between two consecutive entanglements, is located about the fracture plane it behaves as a crosslink.

It is evident from the SEM images that soaking compression molded HA-*co*-HDPE in water created a more porous structure compared to the non-soaked control (middle column). This is more evident on the 2000x images comparing the HA-*co*-HDPE samples. Swelling in water and subsequent freezing and or drying methods can affect the

properties of hydrogels. Therefore, future compression molding parameters will have to take into account the high melting temperature and low melt flow index of UHMWPE and or other PE resins (e.g., HDPE) used to blend with copolymer. The affect of swelling and drying operations after molding will also be investigated.

The effect of compression molding melt temperature is shown in the water content differences of HA-*co*-HDPE composites fabricated from 640,000 Da HA, with a weight ratio of 50:50. An increase in HA degradation was expected as a result of increasing the compression molding melt temperature; however, the large decrease in water content was not expected. Due to the water contents of the HA-*co*-HDPE:UHMWPE blends, the addition of UHMWPE, and the necessary melt processing parameters, proved detrimental to the integrity and overall appearance of the HA-*co*-HDPE materials. It would be optimum to retain high water contents and improve upon the mechanical integrity of the compression molded composite. It was not intuitive to decrease the amount of HA in the copolymer materials to achieve increased water contents; it was discovered, however, that a small amount of HA goes a long way. This can be seen in Figure 31 of the last batch of HA-*co*-HDPE materials made. Decreasing the amount of HA in the material and chemically crosslinking the HA to itself improved the integrity of the compression molded materials by increasing the entanglement of the HDPE, increasing crystallinity.

In the future, different solvent variations and techniques may be investigated to optimize the interfacial esterification reaction, possibly taking advantage of the thermoplastic nature of the PE component; reducing the total reaction time would be advantageous for

reducing thermal degradation of the HA component. It is hypothesized that the structural integrity of the material can be increased by increasing the molecular weight of HDPE. Post-molding crosslinking was incorporated in the current study in order to maintain melt-flow properties of the HA-*co*-HDPE thru the PE portion; however, crosslinking during compression molding of the HA and PE portions should be investigated for optimizing the mechanical properties *in vivo*.

## 2.5 Conclusions

HA-*co*-HDPE is melt processable and amenable to tissue engineering scaffold fabrication or direct molding of medical implants; however, the novel material is vulnerable to thermal and/or pressure induced degradation of the biological component (i.e., HA) during compression molding. A small amount of HA (e.g., 10% by weight) will increase the compliance of HA-*co*-HDPE materials compared to HDPE while maintaining structural integrity of the compression molded materials. Free, or non-covalently bound, forms of HA and HDPE remain entangled within copolymer networks after fabrication; molar ratio and molecular weight calculations are essential precursors in predicting and understanding the reaction purity of HA-*co*-HDPE materials.

## 2.6 References

1. Bastow ER, Byers S, Golub SB, Clarkin CE, Pitsillides AA, Fosang AJ. Hyaluronan synthesis and degradation in cartilage and bone. *Cellular and Molecular Life Sciences* 2008;65:395-413.
2. Armarego WLF, Perrin DD. *Purification of Laboratory Chemicals*. Oxford: Reed Educational and Professional Publishing Ltd, 1996.
3. Shriver DF, Drezdron MA. *The Manipulation of Air-sensitive Compounds*. Toronto: John Wiley & Sons, 1986.

4. Zhang M. Surface Modification of Ultra High Molecular Weight Polyethylene With Hyaluronan For Total Joint Replacement Application [Doctor of Philosophy Mechanical Engineering]: Colorado State University Dissertation; 2004.
5. Zhang M, James SP. Novel Hyaluronan Esters for Biomedical Applications. Rocky Mountain Bioengineering Symposium, Biomedical Sciences Instrumentation 2004:238-242.
6. Zhang M, James SP. Synthesis and properties of melt-processable hyaluronan esters. Journal of Materials Science: Materials in Medicine 2005;16:587-593.
7. Zhang M, James SP. Silylation of hyaluronan to improve hydrophobicity and reactivity for improved processing and derivatization. Polymer 2005;46:3639-3648.
8. James SP, Zhang M, Beauregard GP, Kurkowski RA, inventors. Outer layer having entanglement of hydrophobic polymer host and hydrophilic polymer guest. United States of America, 2003.
9. Kurkowski RA. Chemical crosslinking, compatibilization, and direct molding of an ultra high molecular weight polyethylene and hyaluronic acid microcomposite. Fort Collins: Colorado State University Thesis; 2007.
10. James SP, Oldinski RK, inventors. Copolymer synthesized from modified glycosaminoglycan, GAG, and an anhydride functionalized hydrophobic polymer. USA, 2007 30.10.2008.
11. Oldinski RA, Harris JN, Godek ML, James SP. A novel hyaluronan-polyethylene copolymer for orthopaedic applications. 54th Annual Meeting of the Orthopaedic Research Society. San Francisco CA, 2008.
12. Kurkowski RA, James SP. Melt-processable hyaluronan ester scaffolds for articular cartilage tissue engineering. American Society of Mechanical Engineerings Summer Bioengineering Conference. Amelia Island FL, 2006.
13. James SP, Oldinski RA, Zhang M, Schwartz H. UHMWPE/Hyaluronan microcomposite biomaterials. In: Kurtz SM, editor. UHMWPE Handbook. 2nd ed: Elsevier, 2009.
14. Jung Y, Kim SS, Kim Y, Kim S-H, Kim B, Kim S, et al. A poly(lactic acid)/calcium metaphosphate composite for bone tissue engineering. Biomaterials 2005;26 6314-6322.
15. Li S, Burstein AH. Ultra-High Molecular Weight Polyethylene. The Journal of Bone and Joint Surgery 1994;76-A(7):1080-1090.
16. Shen FW, McKellop HA, Salovey R. Morphology of chemically crosslinked ultrahigh molecular weight polyethylene. Journal of Biomedical Materials Research 1998;41 71-78.

17. Ajji A, Utracki LA. Interphase and Compatibilization of Polymer Blends. *Polymer Engineering and Science* 1996;36 (12):1574-1585.
18. Odian G. *Principles of Polymerization*. Hoboken: Wiley-Interscience, 2004.
19. Zhai H, Xu W, Guo H, Zhou Z, Shen S, Song Q. Preparation and characterization of PE and PE-g-MAH/montmorillonite nanocomposites. *European Polymer Journal* 2004;40:2539-2545.
20. Zhang F, Qiu W, Yang L, Endo T, Hirotsu T. Mechanochemical preparation and properties of a cellulose-polyethylene composite. *J Mater Chem* 2002;12:24-26.
21. Wagner CD, Naumkin AV, Kraut-Vass A, Allison JW, Powell CJ, Rumble Jr JR. <http://srdata.nist.gov/xps>. 2006 [cited 2006/12/28/]; Available from:
22. Mark J, Ngai K, Graessley W, Mandelkern L, Samulski E, Koenig J, et al. *Physical Properties of Polymers*. Third ed. Cambridge: Cambridge University Press, 2004.
23. Chandra R, Rustgi R. Biodegradation of maleated linear low-density polyethylene and starch blends. *Polymer Degradation and Stability* 1997;56:185-202.
24. Kurtz SM, Pruitt LA, Jewett CW, Foulds JR, Edidin AA. Radiation and chemical crosslinking promote strain hardening behavior and molecular alignment in ultra high molecular weight polyethylene during multi-axial loading conditions. *Biomaterials* 1999;20 1449-1462.
25. Bracco P, Brunella V, Zanetti M, Luda MP, Costa L. Stabilisation of ultra-high molecular weight polyethylene with Vitamin E. *Polymer Degradation and Stability* 2007;92:2155-2162.
26. Oral E, Wannomae KK, Rowell SL, Muratoglu OK. Diffusion of vitamin E in ultra-high molecular weight polyethylene. *Biomaterials* 2007;28:5225-5237.
27. Reno F, Caplan AI. UHMWPE and vitamin E bioactivity: An emerging perspective. *Biomaterials* 2006;27:3039-3043.
28. Teramura S, Sakoda H, Terao T, Endo MM, Fujiwara K, Tomita N. Reduction of wear volume from ultrahigh molecular weight polyethylene knee components by the addition of vitamin E. *Journal of Orthopaedic Research* 2007.
29. Wolf C, Macho C, Lederer K. Accelerated ageing experiments with crosslinked and conventional ultra-high molecular weight polyethylene (UHMW-PE) stabilised with  $\alpha$ -tocopherol for total joint arthroplasty. *Journal of Materials Science Materials in Medicine* 2006;17:1333-1340.

30. Wolf C, Maninger J, Lederer K, Fröhlich-Smounig H, Gamse T, Marr R. Stabilisation of crosslinked ultra-high molecular weight polyethylene (UHMW-PE)-acetabular components with  $\alpha$ -tocopherol. *Journal of Materials Science Materials in Medicine* 2006;17:1323-1331.
31. Oral E, Rowell SL, Muratoglu OK. The effect of  $\alpha$ -tocopherol on the oxidation and free radical decay in irradiated UHMWPE. *Biomaterials* 2006;27:5580-5587.
32. Wolf C, Lederer K, Bergmeister H, Losert U, Bück P. Animal experiments with ultra-high molecular weight polyethylene (UHMW-PE) stabilised with  $\alpha$ -tocopherol used for articulating surfaces in joint endoprostheses. *Journal of Materials Science Materials in Medicine* 2006;17:1341-1347.
33. Wolf C, Lederer K, Pfragner R, Schauenstein K, Ingolic E, Siegl V. Biocompatibility of ultra-high molecular weight polyethylene (UHMW-PE) stabilized with  $\alpha$ -tocopherol used for joint endoprostheses assessed in vitro. *Journal of Materials Science Materials in Medicine* 2007;18:1247-1252.
34. Ramani K, Parasnis NC. Process-Induced Effects in Compression Molding of Ultra-High Molecular Weight Polyethylene (UHMWPE). *Fatigue and Fracture Mechanics* 1998;1307(28):5-23.
35. Windau JF, Mackin TJ. The effects of processing and sterilization on ultra high molecular weight polyethylene. 1996.
36. Mikos AG, Peppas NA. Polymer chain entanglements and brittle fracture. III. Critical fracture strength of macromolecular materials. *Journal of Materials Science Letters* 1989;8 833-834.
37. Wood-Adams PM, Dealy JM. Effect of molecular structure on the linear viscoelastic behavior of polyethylene. *Macromolecules* 2000;33:7489-7499.

## Chapter 3. Viscoelastic Characterization of HA-co-HDPE

### 3.1 Introduction

The main functions of articular cartilage are to mediate the transfer of load within the joint to the underlying subchondral bone and to provide a smooth, near frictionless articulating surface. Biomaterials designed for use *in vivo* to repair and/or replace damaged articular cartilage should ideally demonstrate mechanical properties which support, or match, those of the tissues at the site of implantation. A series of amphiphilic, HA-co-HDPE copolymers were evaluated for the repair and/or replacement of articular cartilage. A major advantage of these materials is that by varying the amount and the length of the constituents, an entire family of polymer systems can be obtained. Dynamic mechanical thermal analysis (DMTA) is a technique in which the elastic and viscous response of a sample under oscillating load, are monitored against frequency, time or temperature.[1] The response of a polymeric material to an applied stress exhibits both an elastic and viscous component; a polymer behaves viscoelastic due to a molecular rearrangement in the solid induced by the stress. Time effects in the strain as the mobile sections of the macromolecules flow are the result of an applied mechanical stress. The viscoelastic properties of polymers are highly temperature-dependent.[2]

The tensile modulus (E) or shear modulus (G) can be measured with DMTA equipment; during testing the polymer samples are assumed to behave linearly viscoelastic (i.e., the stress-strain relation is only a function of time). A sinusoidal strain,  $\epsilon(t) = \epsilon_0 \sin \omega t$ , during such a DMTA experiment results in a sinusoidal stress:  $\sigma(t) = \sigma_0 \sin(\omega t + \delta)$

with a phase difference  $\delta$  due to the viscoelastic behavior of the polymer. The ratio of the loss modulus to the storage modulus (i.e.,  $\tan \delta$ ) reflects the viscoelastic behavior of the material.  $E'$  is equal to  $(\sigma_0/\epsilon_0) \cdot \cos(\delta)$  while  $E''$  is equal to  $(\sigma_0/\epsilon_0) \cdot \sin(\delta)$ .  $E'$  is the in-phase or elastic (i.e., storage) component of modulus and  $E''$  is the out-of-phase or viscous (i.e., loss) component of modulus. The storage modulus and the loss modulus are related to the complex modulus  $E^* = E' + iE''$  and indicate the ability of the polymer to store and return energy (elastic, recoverable deformation) and dissipate energy through molecular chain interactions, such as internal friction and rearrangement of the chains due to deformation.[3]  $E'$  gives information about the energy storage capability of the material as well as a measure of its stiffness,  $E''$  informs about the energy dissipation capacity of the material, and  $\tan \delta$  presents the information about the damping ability of the material. DMTA was conducted in order to investigate the hypothesis that by varying the constituent weight ratios materials can be engineered with different mechanical properties.

It is hypothesized is that by adjusting the molecular weights of the PE and HA portions of the copolymer the mechanical properties can be optimized for permanent articular cartilage implants. In order to test this hypothesis, the viscoelastic properties will be evaluated relative to current hydrogel biomaterials for articular cartilage replacement and the native tissue using dynamic mechanical analysis.

## 3.2 Materials and Methods

Experiment samples were prepared by using a 4 mm diameter biopsy punch on hydrated 1.5 – 2.5 mm thick compression molded HA-*co*-HDPE disks (please see Chapter 2); samples were then vacuum dried and rehydrated again directly before testing.

### 3.2.1 Dynamic Unconfined Compression

The dynamic storage modulus ( $E'$ ), loss modulus ( $E''$ ) and mechanical loss tangent  $\delta$  were measured with a Perkin Elmer Pyris Diamond Dynamic Mechanical Analyzer (DMA). HA-*co*-HDPE and MA-*g*-HDPE samples ( $n=3$ ) were soaked in phosphate buffered saline (PBS) at room temperature overnight prior to testing to allow for hydration and swelling. The samples were compressed between two impermeable, unlubricated, parallel platens and immersion tested in PBS at 37°C in unconfined compression mode. The dynamic stiffness properties were determined by applying a dynamic compressive load (approximately 600 mN) at frequencies of 0.1, 1 and 10 Hz. The displacement amplitude was 10 micrometers, the minimum compression force was 300 mN, the tension and compression gain was 1.5, and the force amplitude default was 100 mN. The results will be expressed in terms of  $E'$ ,  $E''$  and  $\tan \delta$  as a function of frequency. Statistics were not performed due to the low sample sizes of the test materials.

### 3.2.2 Dynamic Temperature Sweep

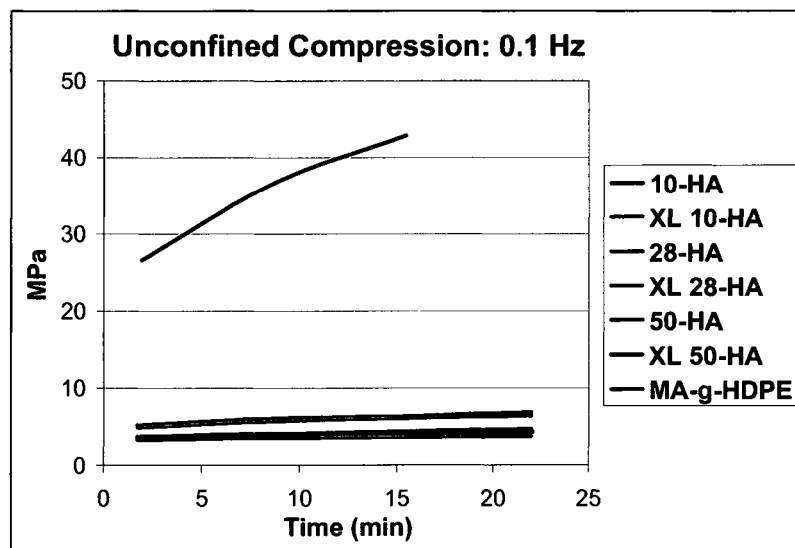
Dry HA-*co*-HDPE and MA-*g*-HDPE samples ( $n=1$ ) were placed between two impermeable, unlubricated, parallel platens and loaded in compression. The samples were heated from -140°C to 90°C at a heating rate of 2°C per minute, at frequencies of 1 and

100 Hz. Due to the excessive softness of the experimental and control samples at temperatures beyond 90°C, it was not possible to measure the dynamic mechanical properties near the softening point (i.e., melting point). Statistics were not performed due to the low sample sizes of the test materials.

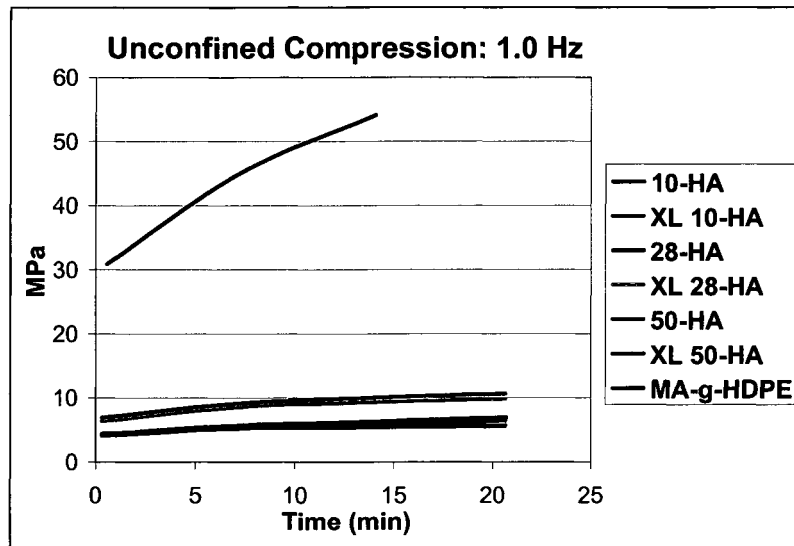
### 3.3 Results

#### 3.3.1 Dynamic Unconfined Compression

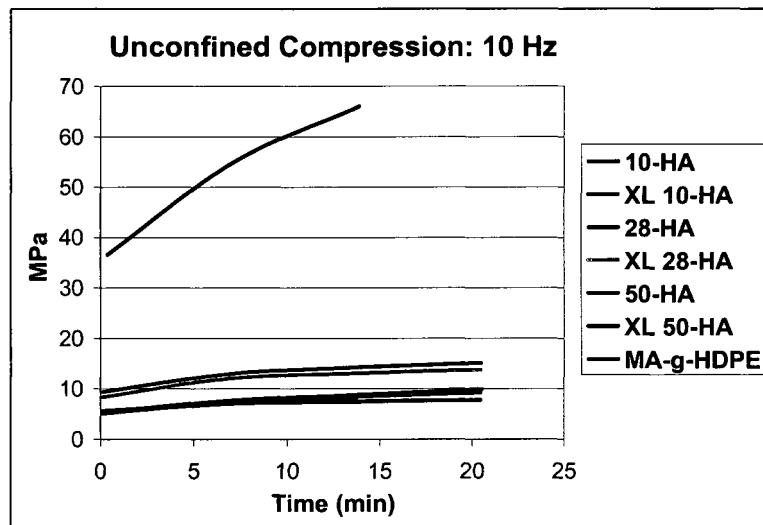
Figure 1 shows the effect of frequency versus time on the storage modulus of the composites with various contents of HA. As shown in Fig. 1,  $E'$  values of all the composite samples increase with an increase in test frequency. The increase of  $E'$  with the rise of frequency implies that the HA-co-HDPE composites maintain a comparatively strong network structure.



(A)



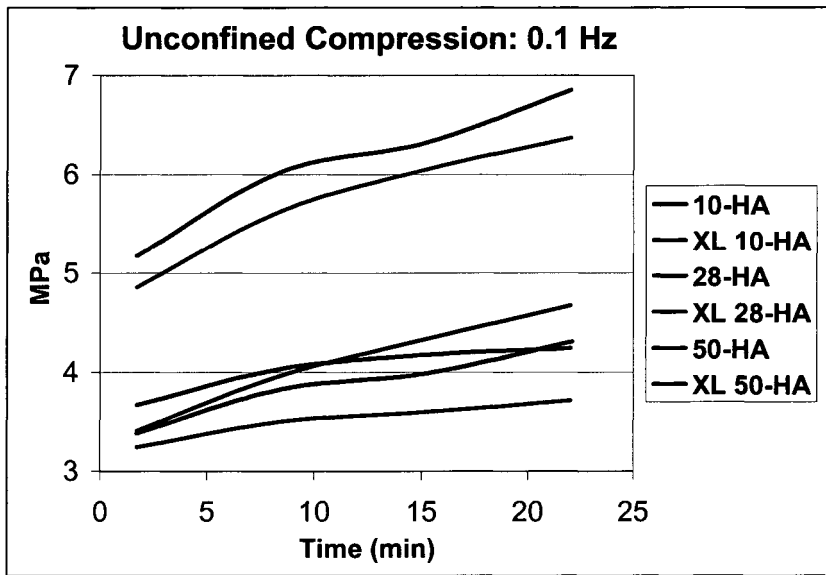
(B)



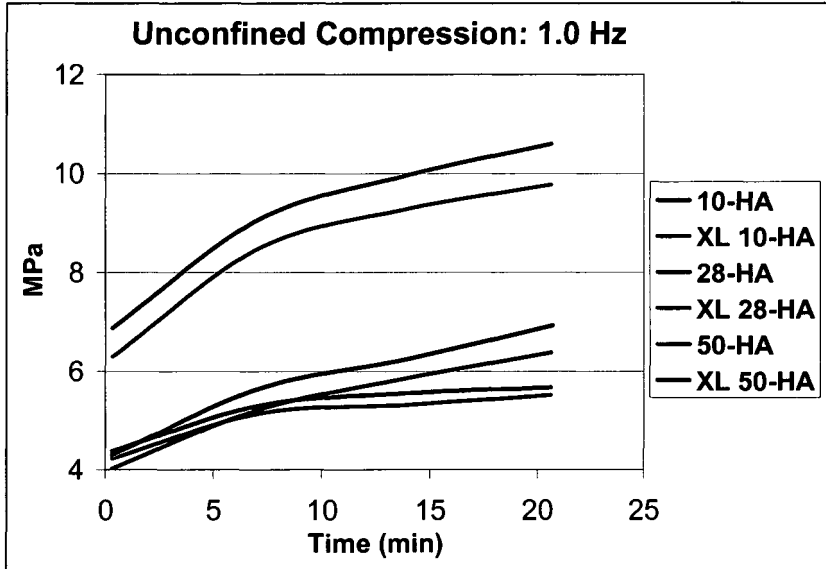
(C)

**Figure 1. Storage modulus ( $E'$ ) versus time for HA-co-HDPE and MA-g-HDPE samples under unconfined compression at loading frequencies of 0.1 (A), 1.0 (B) and 10 Hz (C).**

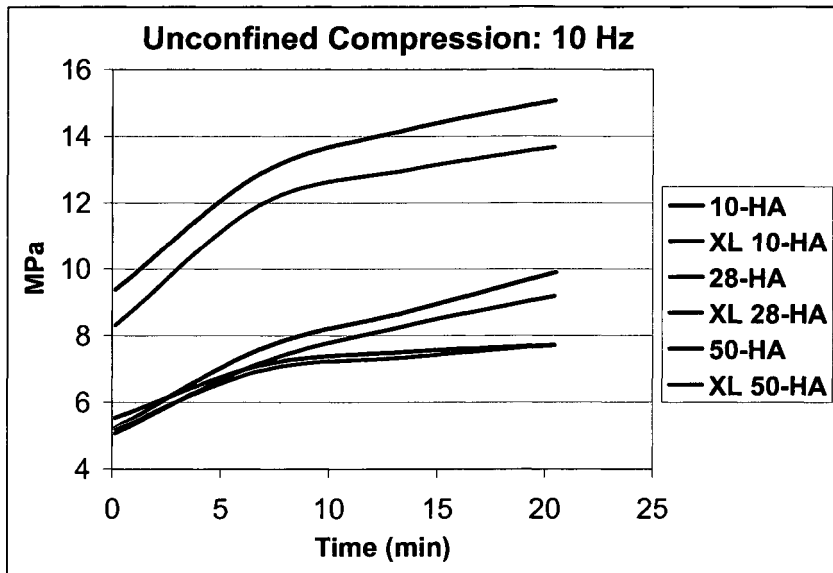
The loss modulus shows a weak relationship with frequency.



(A)



(B)



(C)

**Figure 2. Storage modulus ( $E'$ ) versus time for HA-co-HDPE samples only under unconfined compression at loading frequencies of 0.1 (A), 1.0 (B) and 10 Hz (C).**

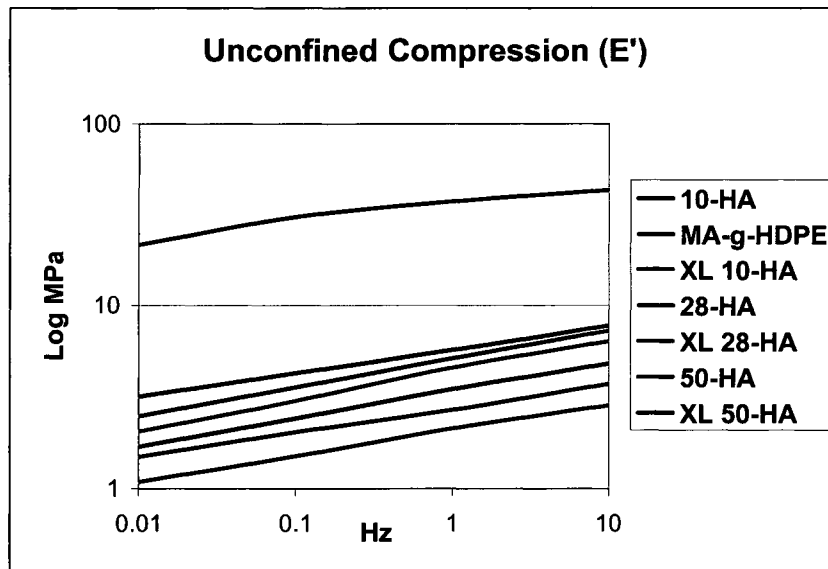


**Figure 3. Storage modulus ( $E'$ ) of HA-co-HDPE and MA-g-HDPE samples under unconfined compression at loading frequencies of 0.01-10 Hz.**

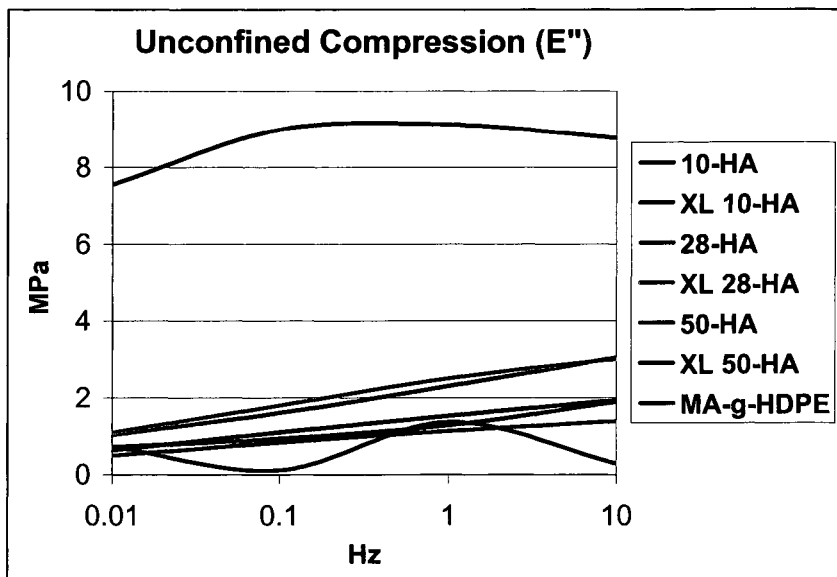


Figure 4. Loss modulus ( $E''$ ) of HA-co-HDPE and MA-g-HDPE samples under unconfined compression at loading frequencies of 0.01-10 Hz.

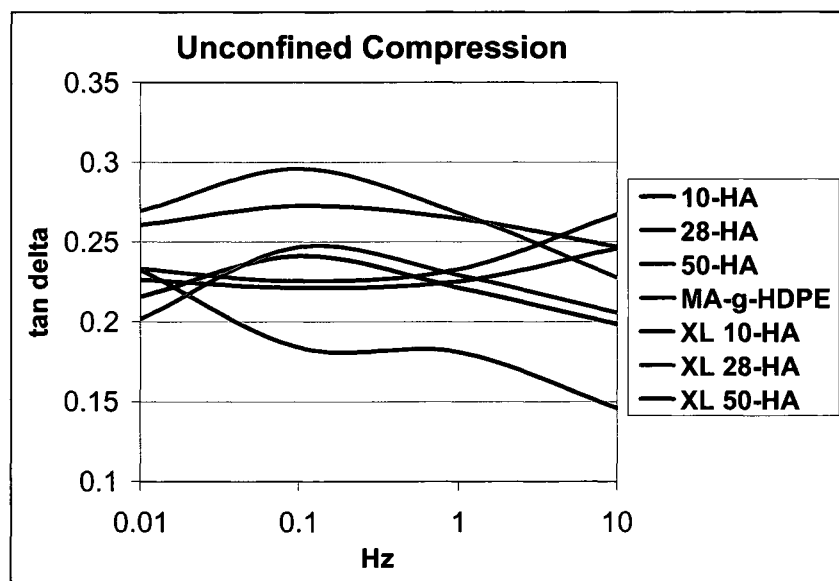
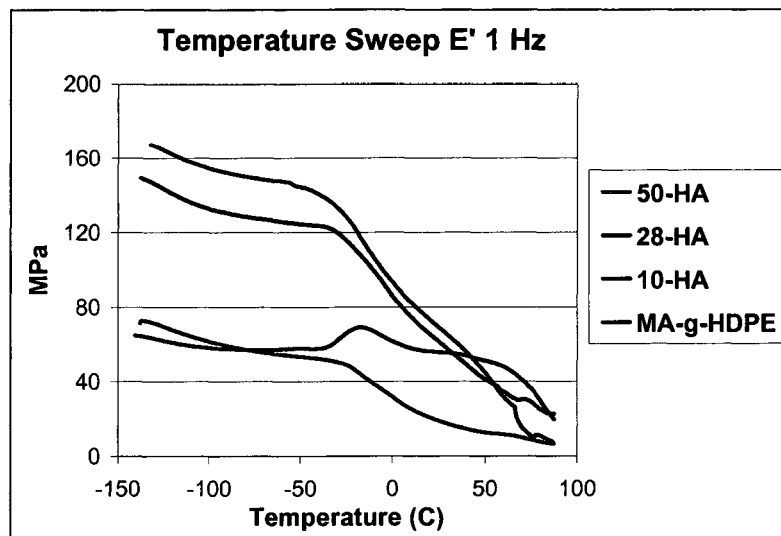


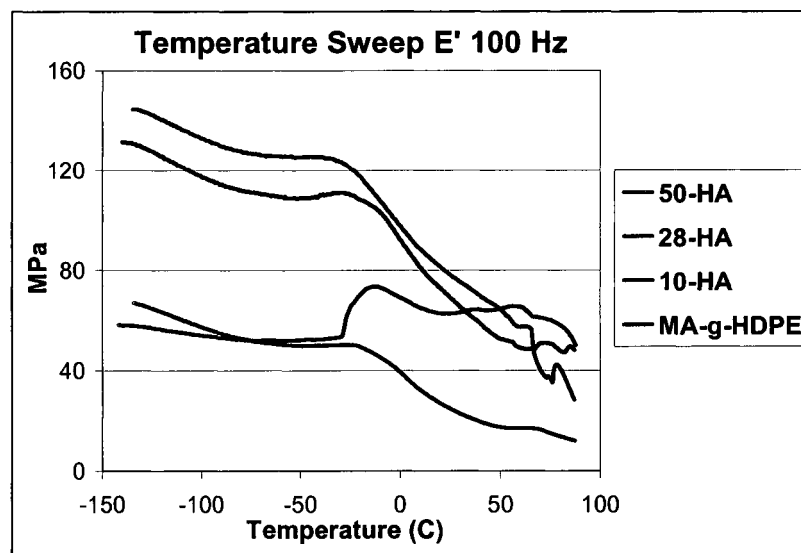
Figure 5. Tan delta of HA-co-HDPE and MA-g-HDPE samples under unconfined compression with loading frequencies 0.01-10 Hz.

### 3.3.2 Dynamic Temperature Sweep

Figures 6-8 shows the  $E'$ ,  $E''$  and  $\tan \delta$  values of all the dry copolymer samples with increases in temperature.

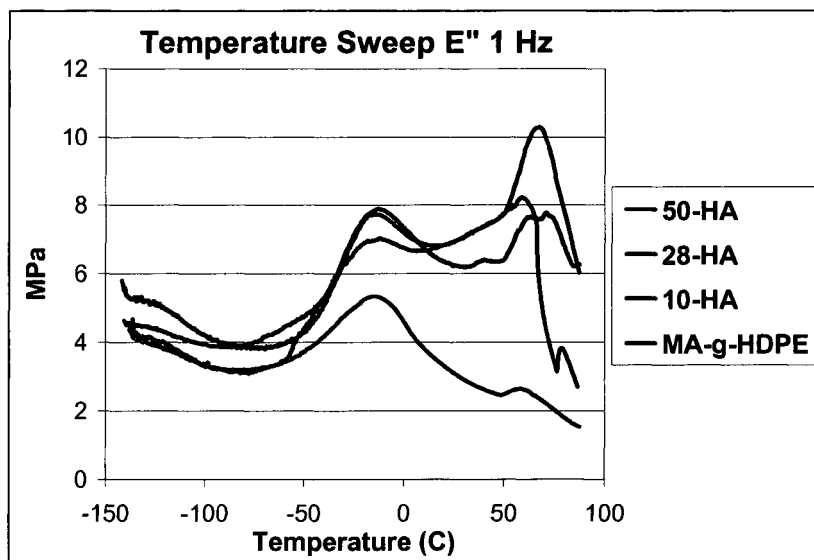


(A)

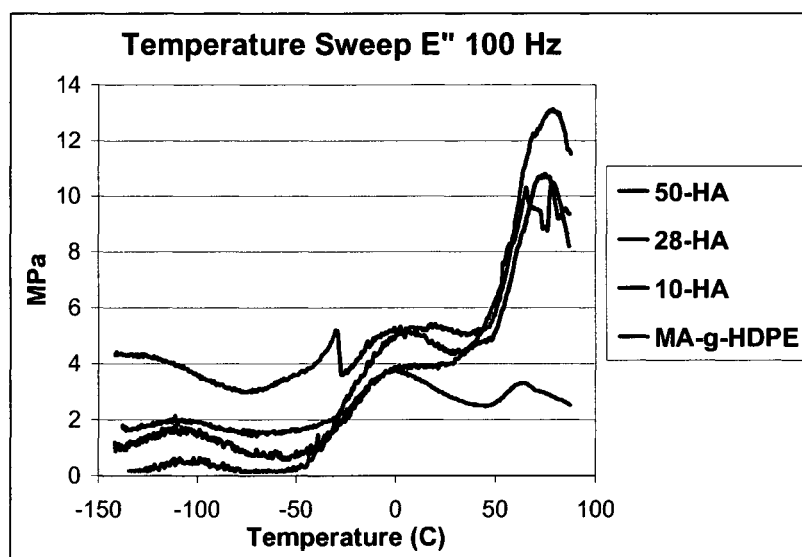


(B)

**Figure 6. Storage modulus ( $E'$ ) of HA-co-HDPE and MA-g-HDPE samples versus temperature at loading frequencies of 1 (A) and 100 Hz (B).**



(A)



(B)

Figure 7. Loss modulus ( $E''$ ) of HA-co-HDPE and MA-g-HDPE samples versus temperature at loading frequencies of 1 (A) and 100 Hz (B).

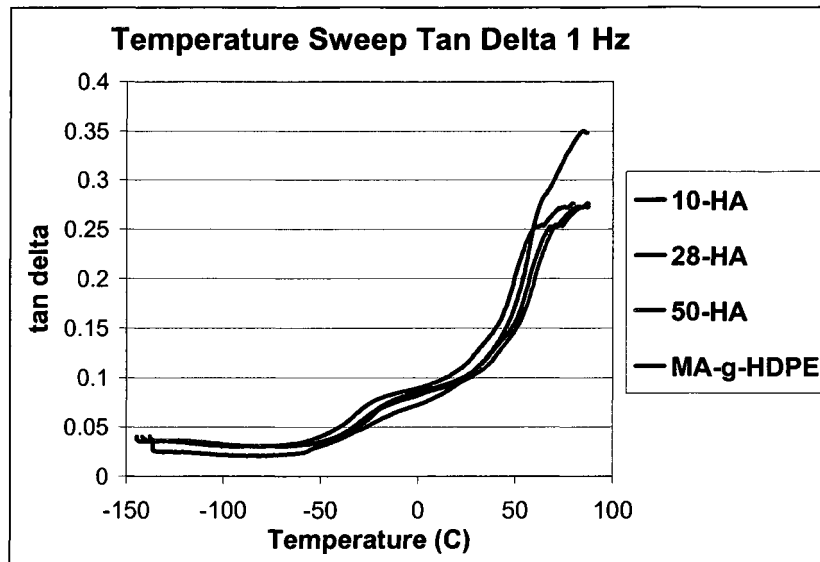


Figure 8. Tan delta of HA-co-HDPE and MA-g-HDPE samples under versus temperature at a loading frequency of 1 Hz.

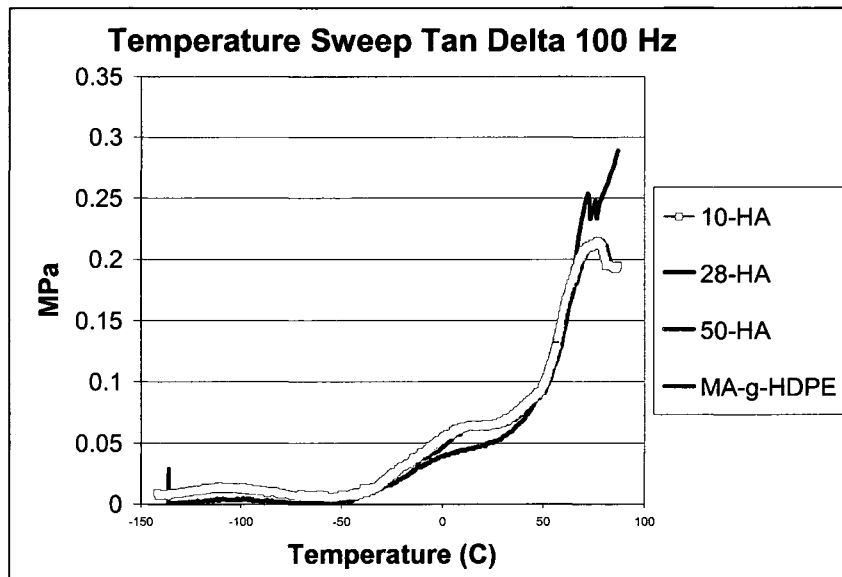


Figure 9. Tan delta of HA-co-HDPE and MA-g-HDPE samples under versus temperature at a loading frequency of 100 Hz.

For all the test samples, the results show that the  $E'$  values are approximately one order of magnitude higher than  $E''$  values, showing that the elastic characteristic plays a principal role in the materials structure.

### 3.4 Discussion

No pre-conditioning load was applied to the samples; preconditioning is normally conducted at a single frequency meant to reduce the influence of surface artifacts and changes in structure due to preconditioning. Figure 1 graphically depicts the slope of  $E'$  versus time for 0.1 Hz and 10 Hz for all of the HA-*co*-HDPE groups alone or compared to MA-*g*-HDPE (i.e., the control). The increase in the storage modulus with time is most likely the result of changing porosity (i.e., changing density); the increase in storage modulus, or density, is shown more with increasing amounts of HA, comparing the 50-HA and 10-90 samples, crosslinked and noncrosslinked. If the samples had been preconditioned, the increase with time would likely have been eliminated. In other words, rather than preconditioning the samples were tested for 10 minutes or more and the data taken from the longer time points when most samples appeared to reach a consistent value. The MA-*g*-HDPE exhibited a steeper slope compared to all the HA-*co*-HDPE samples; this may be the result of a well-formed network microstructure. This coincides with the percent crystallinity of the materials too; the materials with higher crystallinity percents exhibited the highest slope, with increasing  $E'$  with time. Therefore, one would be led to believe that the 28-HA and XL 28-HA copolymers formed more of a network microstructure compared to the microstructures of 10-HA, XL 10-HA, 50-HA and XL 50-HA. For 1 and 10 Hz the copolymer believed to have the most *unbound* HA exhibited the flattest slope; the loss of HA lead to the permanent deformation of the HDPE by water uptake of HA. A change in volume would also be associated with the swelling of HA-*co*-HDPE and respective loss of water.

Damping (i.e., energy dissipation) affect of cartilage with increasing frequency of loading – compare to HDPE and analyze viscoelastic properties (effect of biomechanical response *in vivo*). Due to the incorporation of HA, HA-*co*-HDPE materials exhibit the behavior of a hydrodynamic cushion, characteristic of healthy articular cartilage. The differences in conditioning effects with time at various frequencies may also be the result of low sample size and non-parallel surfaces.

Dynamic mechanical compression showed differences in storage modulus ranging from 1.0819 – 3.1635 MPa at 0.01 Hz, 1.4920 – 4.2415 MPa at 0.1 Hz, 2.1134 – 5.6719 MPa at 1 Hz, and 2.8259 – 7.7036 MPa at 10 Hz, respectively, based on copolymer composition. The storage modulus for the plain MA-g-HDPE ranged from 21.5351 – 42.9394 MPa at 0.01 – 10 Hz, respectively. The unconfined storage modulus for the HA-*co*-HDPE samples were close to the unconfined dynamic stiffness of bovine articular cartilage: 4.10 MPa at 0.1 Hz in PBS at 37°C [4], and 470 – 1010 kPa at 0.1 – 10 Hz, respectively, in bovine serum at 37°C [5]. The variations in solution properties between PBS and bovine serum may cause the material to behave differently (i.e., to exhibit different stiffness values).

Knowledge of the temperature dependence of the modulus gives an important clue to the engineering application of a polymer. The temperature sweep measurements were made at constant frequency over an extremely wide range of temperature. The low temperature process  $\gamma$ , observed in several polysaccharides, was attributed to conformational variations due to local motions of either the main chain or methyl groups.[6] The glass-

to-rubber relaxation ( $\alpha$ -relaxation) is the mechanical manifestation of the glass transition; the  $T_g$  is associated with large-scale motion of the molecular chain segments, also known as the upper use temperature. The  $\alpha$ -relaxation is observed when a time constant for a specific molecular motion passes through the time constant of the mechanical experiment, detected most easily by a peak in  $\tan \delta$ . [2] The temperature dependence of all of the samples, including the MA-g-HDPE control, was characterized by a shallow decline of  $E'$  with  $T$ . The shallow decline is due to thermal expansion: the molecules in the solid move further apart as the temperature increases, and this lowers the modulus. Each abrupt drop is generated by a viscoelastic relaxation process due to a specific type of molecular movement. The plateau region, where the  $E'$  levels off, identifies the material is in a rubber phase. The increase in  $E'$  of the 28-HA copolymer sample is indicative of crystallization; heating a semi-crystalline material polymer above the  $T_g$  of the amorphous fraction will always permit additional crystallization (i.e., recrystallization) to occur (if the specimen is not initially at equilibrium). [2] This also helps to explain why the 28-HA absorbs the least amount of water during swelling experiments: water molecules absorb into the amorphous region and so the higher the crystallinity the less the absorption. [2] The HA phase of the HA-co-HDPE copolymers decreased the modulus of HDPE, assuming that HDPE is the continuous phase. The low sample number ( $n=1$ ) in these experiments limits the ability to interpret this data as truly representative of the copolymer.

The  $\gamma$  process of a dry HA film (molecular weight = 146 kDa) occurred at about  $-85^{\circ}\text{C}$  and the  $T_g$  occurred around  $14^{\circ}\text{C}$ . [7] The  $E'$  of HA showed a simple discontinuity around  $25^{\circ}\text{C}$ ; this phenomenon has been considered to account for a strain-induced crystallization with an increase in the number of intermolecular and/or intramolecular hydrogen bonds. [8] Amorphous polymers exhibit fewer mechanical relaxations than crystalline polymers due to the substantial difference in properties between crystalline and amorphous polymers. The relaxation temperatures also often mark transitions in ductility; the polymer becomes increasingly brittle as it is cooled. [2]

Under compression, articular cartilage behaves like a poroelastic material, in which its response to compressive loads is frequency and strain dependent. These properties are governed by the interrelationship between solid extracellular matrix (ECM) constituents (e.g., collagen type II) and interstitial fluid flow. [9] The biomechanical properties of cartilage rely on the intact collagen network and a high concentration of aggrecan. [10] The viscoelastic behavior of the composites in which the storage modulus (i.e., stiffness) increases with an increase in loading frequency is similar to that of natural articular cartilage. Articular cartilage deforms at low stress levels by enlarging the contact area thus uniformly distributing endured stresses *in vivo*. At high loading rates articular cartilage has little time to deform and it presents excellent resistance to compressive stress due to its increased stiffness. The long chain molecule HA in solution behaves as a stiffened random coil with large hydrated volume, such that each molecule interacts with its neighbors resulting in viscoelastic solutions. [10] Segmental mobility of HA chains is restricted owing to a local stiffness induced by the existence of intramolecular hydrogen

bonds. This stiffness is responsible for the large hydrated volume of HA chains. The stiffening of HA is due to a range of dynamic hydrogen bonds between adjacent saccharides, thus forming a dynamic network which restricts the movement of other macromolecular chains.

In diarthrodial joints, HA acts as a lubricant because of its rheological properties. As a comparison to *in vivo* proteoglycans, HA-*co*-HDPE is stiffer due to the continuous PE network and PE crystalline regions. The stiffness from crystalline regions is the result of physical crosslinks via PE crystals not chemical crosslinks; however, chemical crosslinking of the PE portion could be introduced to further optimize the dynamic properties of HA-*co*-HDPE materials. The dynamic cushioning comes from the polyanionic component, HA, branching off and lightly crosslinked to each other within amorphous regions. Graft copolymers (e.g., HA-*co*-HDPE) have mechanical spectra quite different from random copolymers. Graft copolymers form two-phase solids, in which each constituent aggregate to form domains. Random copolymers form single-phase solids. Thus, by varying the proportions of comonomer it is possible to synthesize families of copolymers with significantly different mechanical properties.[2]

DMTA was utilized to give perspective on the crystalline state and microstructure of HA-*co*-HDPE and MA-*g*-HDPE; the material properties give insight into the molecular morphology of the material thus crystallization mechanisms may be investigated.[11] The crystalline state is characterized by three-dimensional order over at least a portion of the chains, i.e., molecules organized into a regular three-dimensional array. The storage

moduli values for the HA-*co*-HDPE materials are promising for use in repairing or replacing articular cartilage; however, the mechanical integrity of the materials needs to be improved for *in vivo* use, since the material was inclined to fall apart when swollen (see Chapter 2 swell data).

It would be worthwhile to repeat the DMTA (1 and 10 Hz at 37°C) with wet and dry samples to investigate the effect of water flux through HA-*co*-HDPE during unconfined compression. Strength properties of HA-*co*-HDPE would be valuable to consider for future investigations in improving the structural integrity of the materials. In addition, it would be interesting to perform wear tests and calculate the coefficient of friction (COF) of HA-*co*-HDPE against cartilage, UHMWPE, CoCr and PVA-H.

### **3.5 Conclusion**

Through the novel synthesis and fabrication of HA-*co*-HDPE materials, a biomaterial was engineered which incorporates stiffness (via the crystalline network of the PE) and hydrodynamic properties (via water flux and attraction properties of the HA). DMTA analysis supports that the HA-*co*-HDPE is a viscoelastic behavior. HA-*co*-HDPE is a compliant material with mechanical stiffness properties similar to articular cartilage. The storage modulus of HA-*co*-HDPE is higher compared to crosslinked HA gels and lower compared to MA-*g*-HDPE compression molded disks. It has been shown by adjusting the amount of HA in the final composite (covalently bound and/or excess HA) and incorporating chemical crosslinking of the HA phase of the material the mechanical properties can be optimized for a variety of applications. The properties may be further

optimized by adjusting the molecular weights and weight ratios of the HA and PE phase and incorporating different polyethylenes (e.g., LDPE, LLDPE, UHMWPE) or possibly any maleated thermoplastic. This offers extensive possibilities in the design of systems with tailor-made properties, such as swelling, degradability and stiffness.

### 3.6 References

1. Groenewoud WM. *Characterisation of Polymers by Thermal Analysis*. First ed. Amsterdam: Elsevier 2001.
2. McCrum NG, Buckley CP, Bucknall CB. *Principles of Polymer Engineering*. Oxford: Oxford University Press, 1988.
3. Chakravartula A, Komvopoulos K. Viscoelastic properties of polymer surfaces investigated by nanoscale dynamic mechanical analysis. *Applied Physics Letters* 2006;88(131901):1-3.
4. Woodfield TBF, Malda J, de Wijn J, Peters F, Riesle J, Van Blitterswijk CA. Design of porous scaffolds for cartilage tissue engineering using a three-dimensional fiber-deposition technique. *Biomaterials* 2004;25:4149-4161.
5. Schwartz CJ, Bahadur S. Investigation of articular cartilage and counterface compliance in multi-directional sliding as in orthopedic implants. *WEAR* 2007;262:1315-1320.
6. Bradley SA, Carr SH. Dynamics of macromolecular chains. III. Time-dependent fluorescence polarization studies of local motions of polystyrene in solution. *Journal of Polymer Science: Polymer Physics Edition* 1976;14(1):11-27.
7. Dave V, Tamagno M, Focher B. Hyaluronic acid-(hydroxypropyl)cellulose blends: a solution and solid state study. *Macromolecules* 1995;28(10):3531-3589.
8. Rials TG, Glasser WG. Thermal and dynamic mechanical properties of hydroxypropyl cellulose films. *Journal of Applied Polymer Science* 1988;36(4):749-758.
9. Mow VC, Guo XE. Mechano-Electrochemical Properties of Articular Cartilage: Their Inhomogeneities and Anisotropies. *AnnuRevBiomedEng* 2002;4:175-209.
10. Bastow ER, Byers S, Golub SB, Clarkin CE, Pitsillides AA, Fosang AJ. Hyaluronan synthesis and degradation in cartilage and bone. *Cellular and Molecular Life Sciences* 2008;65:395-413.

11. Mark J, Ngai K, Graessley W, Mandelkern L, Samulski E, Koenig J, et al. *Physical Properties of Polymers*. Third ed. Cambridge: Cambridge University Press, 2004.

## Chapter 4: *In Vitro* Biological Assessment of HA-co-HDPE

### 4.1 Introduction

Different molecular engineering strategies have led to the development of a variety of synthetic and modified natural polymers aimed at reaching the highest level of compatibility in the physiological environment, i.e., optimal performance of function, low toxicity and suitable degradation rate. Being a natural component of extracellular matrix, hyaluronan (HA) has recently emerged as a potential candidate for biomaterials and connective tissue applications.

HA-co-HDPE materials were developed for the repair or replacement of articular cartilage, which has a limited capacity for self-regeneration. The most common conventional surgical treatments of damaged articular cartilage confined to a small area, or osteochondral lesions (which includes the cartilage and the vascularized subchondral bone), include:

- Grafts of periosteum or perichondrium
- Creating micro-fractures in the subchondral bone area to allow bone marrow stem cells to invade the damaged cartilaginous cavity, creating fibrocartilage; however, fibrocartilage does not have the same mechanical properties as normal cartilage.
- Osteochondral grafts or mosaic plasty [1]

Mesenchymal stem cells (MSC) are the most promising for bone defect restoration.[2] MSC have the ability to differentiate to osteoblastic cells.[3] Osteoblast compatibility was evaluated because articular cartilage replacements are often anchored in place by enhancing osseointegration through a porous portion of the construct. Bone marrow contains MSC or bone marrow stromal cells (BMSC), which may allow for a better understanding of bone remodeling.[4]

In this work, the aim was to evaluate the short-term and long-term degradation properties and osseocompatibility of the biosynthetic material (i.e., the proliferation and differentiation of bone marrow derived mesenchymal stem cells on a hyaluronan and polyethylene copolymer (HA-*co*-HDPE)).

## **4.2 Materials and Methods**

### **4.2.1 HA-*co*-HDPE Fabrication**

HA-*co*-HDPE sample groups consisted of 10, 28 and 50% (w/w) HA with [OH: AH] molar ratios of [1:1] (*10-HA*), [4:1] (*28-HA*) and [10:1] (*50-HA*), respectively. For the enzymatic degradation study, HA-*co*-HDPE specimens (*10-*, *28-*, *50-HA*) with an average thickness of 3 mm and diameter of 4.0 mm were punched from compression molded HA-*co*-HDPE samples using a 4.0 mm diameter biopsy punch and dried at 50°C under vacuum for 12 hours. Chemically crosslinked HA-*co*-HDPE specimens (XL *10-*, XL *28-*, XL *50-HA*) were fabricated by placing in a 10% (v/v) poly(diisocyanate) (Sigma-Aldrich) solution (*which creates crosslinks between hydroxyl groups on neighboring HA segments*) for 24 hours and cured in a 50°C vacuum oven for 3 hours.

Residual poly(diisocyanate) was removed by rinsing in acetone and vacuum drying for a few hours at room temperature until all of the acetone was evaporated off.

For the human osteoblast cell line study, compression molded HA-*co*-HDPE samples (10-, 28-, 50-HA) with an average thickness of 1.2 mm and diameter of 6 mm were wiped with 100% (v/v) ethanol (n=3 for each group per time point per experiment). The HA-*co*-HDPE specimens were then placed inside a disinfected bio safety cabinet. The HA-*co*-HDPE specimens were rinsed with 70% (v/v) ethanol before being placed in sterile costar® (Corning) 24 well tissue culture plates (1.9 cm<sup>2</sup> culture area/well). One clear bottom 96-well plate was used for the 24 hour cytotoxicity test, the 7 day cytotoxicity test and the osseocompatibility test, respectively. Tissue culture polystyrene (TCPS) was used as the positive control (n=3). Each experimental and control specimen was placed in a single well. The experimental and control samples were further disinfected by exposing them to ultraviolet (UV) light for 10 minutes and preconditioned in sterile phosphate buffered solution (PBS) for 24 hours at room temperature.

For the BMSC study, compression molded HA-*co*-HDPE (n=4) and chemically crosslinked HA-*co*-HDPE (n=4) (10-HA, XL10-HA), TCPS (positive control, n=3) and MA-*g*-HDPE (complimentary controls, i.e., no HA, n=3) specimens were punched out of disks with an 8.0 mm stainless steel punch, with an average thickness of 1mm and a diameter of 8.0 mm. Specimens were adhered to the bottom of the well with medical grade adhesive (Nexaband®, Abbott Laboratories) to ensure the samples remain submerged. The samples were sterilized by soaking in 70% ethanol and exposing them to

UV light for 10 minutes. The substrates were then soaked in sterile PBS and exposed to an additional 10 minutes of UV light. The PBS was aspirated off and the samples were allowed to dry overnight at room temperature. Samples were soaked in media 2 hours prior to seeding the cells.

#### 4.2.2 HA-co-HDPE Enzymatic Degradation

The biostability of HA-co-HDPE was determined by weighing samples after soaking in a hyaluronidase (i.e., enzyme) solution and control PBS solution.[5] Three HA-co-HDPE samples were taken from each of the test groups for each time point (day 0, 1, 7, 28 and 56) and the weight was recorded. The control was HA-co-HDPE and MA-g-HDPE samples suspended in PBS without the enzyme.[6] The hyaluronidase solution concentration was 100 units/mL in PBS.[7] The samples were dried at room temperature in a vacuum oven for 24 hours prior to testing. After drying, an initial weight was recorded (day 0). The samples were then placed in the enzyme solution and stored in a shaker-incubator at 37°C. The enzyme solution and PBS was replaced every 48 hours. After 1, 7, 28 and 56 days the samples were rinsed with deionized and distilled (DI) water and vacuum dried until no change in weight occurred then the weight was recorded. Degradation was reported as the lost weight divided by the original weight.

The enzymatic degradation of HA, and crosslinked HA, can be measured using UV spectroscopy or weight loss percentages. In order to utilize UV spectroscopy, it was necessary to first determine the lower detection limit of stained HA. Sodium HA was added to a 20% (v/v) poly(hexamethylene diisocyanate) acetone solution; the HA soaked

in the crosslinking solution for 10 minutes then vacuum dried for 3 hours at 50°C. The crosslinked HA was soaked in acetone for 10 minutes, to remove residual un-cured crosslinker, and vacuum dried at room temperature for 1 hour. The crosslinked, dried HA was then dyed using Coomassie Brilliant Blue R-250 (CBB). The 0.25% (w/v) CBB solution was prepared using the following methods: 0.0125 g CBB, 0.5 mL glacial acetic acid, 2.0 mL methanol and 2.65 mL DI water were mixed together at room temperature immediately before use. The crosslinked HA was placed in the CBB solution for 10 minutes at room temperature then rinsed with DI water until all of the unbound dye was removed (the water remained clear). The dyed, crosslinked HA was then placed in a room temperature vacuum oven until dry. The dyed, crosslinked HA powder was added to a 24 well polystyrene plate with well capacity of 1 mL in the following amounts: 1, 2, 3 and 5 mg (n=3). To each well, 0.5mL of hyaluronidase (HAase) solution was added. The HAase solution was prepared using the following methods: 8.22 mg of HAase was added to 50 mL of PBS resulting in a 100 units/mL concentration. The dyed crosslinked HA powder soaked in the HAase solution for 6 hours at 37°C. Three hundred µL of the supernatant was aliquoted out of each well and transferred to a 1.5 mL microcentrifuge tube.

#### 4.2.3 Secondary Origin Cell Study

##### *Cell Culture*

Cells from the human osteoblast cell line, HFOB1.19 (ATCC, Manasses, VA) were utilized for a quantitative assessment of cytotoxicity (cell viability after 24 hours and seven days). One mL of frozen cells ( $2 \times 10^6$  cells/mL, 10% (v/v) DMSO in FBS) was

removed from cryogenic storage (in liquid nitrogen) and quickly thawed in a double-boiler water bath. The cells were added to a sterile cell culture flask (75 cm<sup>2</sup> culture area) followed by 20 mL of pre-heated 37°C media. The base medium used for this cell line was a 1:1 mixture of Ham's F12 Medium Dulbecco's Modified Eagle's Medium, with 2.5mM L-glutamine (without phenol red). Growth medium was prepared by adding the following components to the base medium: 0.3 mg/mL G418, FBS to a final concentration of 10% (v/v). Cells were propagated at 34.0°C and 5.0% (v/v) CO<sub>2</sub> and were observed daily under an inverted microscope. Media was changed every 2-3 days. The cells were sub-cultured at a ratio of 1:4 using the following procedure: media was aspirated off and the cell layer was rinsed with 5 mL of 0.25% (w/v) Trypsin- 0.53mM EDTA solution. The flask was incubated for 15 minutes at 34.0°C and 5.0% (v/v) CO<sub>2</sub>. Four mL of the cell and trypsin solution was transferred to a sterile cell culture flask (125 cm<sup>2</sup> culture area); 20 mL media was added to the 75 cm<sup>2</sup> flask while 40 mL media was added to the 125 cm<sup>2</sup> flask.

Pre-osteoblast cells were matured at 39.5°C 24 hours prior to seeding. The cells were detached from the flask with trypsin and re-suspended in 5 mL media. Ten µL of the cell suspension was mixed with an equal volume of trypan blue O dye (Thermo Scientific HyClone, Fisher) in a microcentrifuge tube. A hemacytometer and phase-contrast light microscope were used to view and count the cells; the number of cells per mL was calculated by multiplying the average number counted by  $2 \times 10^4$ . The PBS was aspirated off the specimens and one ml of cell solution was added to each well. HFOB1.19 cells were seeded at a density of approximately 9000 cells/cm<sup>2</sup>; the same number of cells was

seeded into each culture well. Some of the samples were not completely sunk but all of the specimens were completely submerged. All three plates were placed in the incubator at 39.5°C and 5.0% (v/v) CO<sub>2</sub>. Media was changed on day 3 only for the hFOB1.19 study.

### *Cell Viability*

HFOB1.19 cell viability (Molecular Probes' LIVE/DEAD® Viability/Cytotoxicity Kit for mammalian cells) was evaluated day 1 and 7 post-seeding. Twenty µL of 2mM EthD-1 stock solution was added to 10mL of sterile, tissue culture-grade D-PBS and vortexed to ensure mixing. Five µL of 4mM calcein AM stock solution was added to the EthD-1 solution and the solutions were vortexed. Media was aspirated from each well and 0.5 mL of the LIVE/DEAD® stain was added to each well containing a specimen. The cells were then incubated for 30 minutes at room temperature. Following incubation, the specimens were removed from the solution, rinsed in PBS, and viewed under a fluorescence microscope (Carl Zeiss). Images were taken of live (green) and dead (red) HFOB1.19 cells and live cells only at 4 and 10x magnification.

### *Osteoblast Phenotype Expression*

Relative short/long-term ALP expression (BioAssay Systems' QuantiChrom alkaline phosphatase assay kit) was measured from cell extracts to determine the different amounts of ALP present on HA-co-HDPE (10-, 28-, 50-) and control (TCPS) samples. Intracellular extraction was achieved via CellLytic™-M (Sigma mammalian cell lysis/extraction reagent); the media was aspirated off of each well, samples were rinsed

with sterile PBS, and transferred to non-seeded wells in which the lysing solution was then added. Samples were incubated in the lysate for 20 minutes at room temperature. Remaining lysate was stored at -70°C. All end-point assays for HFOB1.19 cells were conducted 7 days post-seeding and executed at room temperature. Samples were assayed in triplicate (n=3) using a clear bottom 96-well plate. The ALP activity of the samples (IU/L) was measured by performing the following calculation (n=9):

$$= \frac{[(OD_{\text{SAMPLE } t} - OD_{\text{SAMPLE } 0}) \cdot 1000 \cdot \text{Reaction Volume}]/[(OD_{\text{CALIBRATOR}} - OH_{\text{H}_2\text{O}}) \cdot \text{Sample Volume} \cdot t]}{40.4}$$

OD<sub>SAMPLE t</sub> and OD<sub>SAMPLE 0</sub> are OD<sub>405nm</sub> values of sample at time t (*the incubation time*) and 0 minutes measured using a plate reader (FLUOstar Omega, BMG LABTECH). The incubation time for this study was 4 minutes. The factor 1000 converts IU/mL to IU/L. The reaction volume was 150 µL and the sample volume was 50 µL.

#### 4.2.4 Primary Origin Cell Study

##### *BMSC Isolation and Culture*

BMSC were isolated from Wistar rats (*Rattus norvegicus*) supplied by Harlan Sprague Dawley, Inc. Limbs were aseptically removed from recently euthanized animals. Soft tissue was removed and the bones were briefly stored in cold PBS before isolating cells. Metaphyseal ends of the bones were removed to expose the bone marrow cavity. In a 50 mL conical tube, marrow was repeatedly flushed with culture media (αMEM with 10% fetal bovine serum (FBS, Sigma) and 1% penicillin/streptomycin (Pen/Strep, Sigma)) using 10 mL syringes with 18 and 25 gauge needles. Media containing cells and debris

was filtered with a 70  $\mu\text{m}$  nylon filter into a clean tube. Cells were counted using a hemocytometer before seeding. Cells were seeded on samples (surface area: 50  $\text{mm}^2$ ) in a 24-well plate at a density of 1.2 million/well. Cells were cultured in the same media described above. Cultures were incubated at 37.0°C and 5%  $\text{CO}_2$  for the duration of the study. Half of the media was changed at day 4. On day 7, all the media were replaced with an osteogenic differentiation media consisting of  $\alpha$ -MEM supplemented with 10% FBS, 1% Pen/Strep, dexamethasone ( $10^{-8}\text{M}$ ) (D-8893, Sigma), ascorbic acid (50 mg/mL) (255564, Sigma), and  $\beta$ -glycerol phosphate (8 mmol) (G-6251, Sigma). A  $10^{-5}\text{M}$  concentration of dexamethasone in ethanol was prepared ahead of time and stored in a -4°C freezer. Before adding to media, the dexamethasone solution was diluted  $10^{-5}\text{M}$  1:1000 in media and then immediately added to media. For  $\beta$ -glycerol phosphate, 54 g was added to 250 mL of DI water to make 1M concentration; the phosphate aqueous solution was then filtered with a 0.2  $\mu\text{m}$  nalgene filter unit. The phosphate aqueous solution was prepared ahead of time and stored in a -4°C freezer. Three mL of the phosphate aqueous solution was added to 500 mL of the original media. For ascorbic acid, 25 mg of acid was added to 5 mL of media and immediately added to media. Twenty seven  $\mu\text{L}$  (with syringe) was added for every 500 mL of media (5-6  $\mu\text{L}$  per 100 mL media). The media were changed every 2 or 3 days with osteogenic media up to 21 days. Long-term studies were conducted in duplicate using different animals as the MSC source for each study.

### *Cell Viability and Proliferation*

BMSC cell viability (Molecular Probes' LIVE/DEAD® Viability/Cytotoxicity Kit for mammalian cells) was evaluated days 1, 4 and 7 post-seeding. Twenty  $\mu\text{L}$  of 2mM EthD-1 stock solution was added to 10mL of sterile, tissue culture-grade D-PBS and vortexed to ensure mixing. Five  $\mu\text{L}$  of 4mM calcein AM stock solution was added to the EthD-1 solution and the solutions were vortexed. Media was aspirated from each well and 0.5 mL of the LIVE/DEAD® stain was added to each well containing a specimen. The cells were then incubated for 30 minutes at room temperature. Following incubation, the specimens were removed from the solution, rinsed in PBS, and viewed under a fluorescence microscope (Carl Zeiss). Images were taken of live (green) and dead (red) BMSC and live cells only at 4 and 10x magnification. BMSC cell viability was evaluated days 1, 4 and 7 post-seeding via the LIVE/DEAD® stain.

The activity of living cells via mitochondrial dehydrogenase activity can be analyzed using a MTT system (key component is 3-[4,5-dimethylthiazol-2-yl]-2,5-diphenyl tetrazolium bromide or MTT). BMSC viability was quantitatively assessed via a MTT assay (Cayman's MTT Proliferation Assay Kit, #10009365) conducted 1 and 4 days post-seeding. Samples in culture plates were removed from the incubator, placed in a disinfected bio safety cabinet, and transferred to a new 24-well culture plate. Samples were rinsed with sterile PBS. One mL of PBS and 100  $\mu\text{L}$  of MTT mixture was added to each culture well. The culture plates were incubated for 6 hours at 37°C. The MTT mixture was aspirated off and 1 mL of the crystal dissolving solution with 10% (v/v) Triton® X-100 (Sigma) was added to each well. The culture plate was placed on a shaker

table at room temperature for 2 hours then the absorbance at 570 nm was spectrophotometrically (FLUOstar Omega, BMG LABTECH) measured.

Total protein content of differentiated BMSC seeded specimens *post*-differentiation was quantitatively assessed via a protein assay (BCA™ Protein Assay Kits, ThermoFisher Scientific, Pierce Biotechnology). Intracellular extraction was achieved via CelLytic™-M (Sigma mammalian cell lysis/extraction reagent); the media was aspirated off of each well, samples were rinsed with sterile PBS, and transferred to non-seeded wells in which the lysing solution was then added. Samples were incubated (on a shaker table) in the lysate overnight at room temperature. A set of protein standards was prepared by diluting a 2.0mg/mL albumin (BSA) standard solution in triplicate; the final BSA concentrations were as follows: 2000, 1500, 1000, 750, 500, 250, 125, 25 and 0 µg/mL. The working solution was prepared by mixing 50 parts of BCA Reagent A with 1 part of BCA Reagent B. Twenty five µL of each standard or unknown sample (i.e., lysate solution) was pipetted into a microplate well, followed by 200 µL of the working solution to each well and the plate was mixed thoroughly on a plate shaker for 30 seconds. The plate was then incubated at 37°C for 30 minutes and cooled to room temperature. The absorbance was read using a plate reader (FLUOstar Omega, BMG LABTECH) at 562 nm. The average 562 nm absorbance reading of the blank standard was subtracted from the 562 nm absorbance reading of all other individual standard and experiment samples. A standard curve was prepared by plotting the average blank-corrected 562 nm reading for each BSA standard verse its BSA concentration in µg/mL. The standard curve was used to determine the protein concentration of each experimental and control sample.

### *Osteoblast Phenotype Expression*

Relative short/long-term ALP expression (BioAssay Systems' QuantiChrom alkaline phosphatase assay kit) was measured from cell extracts to determine the different amounts of ALP present on HA-co-HDPE (10-, XL 10-HA) and control (TCPS, MA-g-HDPE, UHMWPE) samples *post*-differentiation. Intracellular extraction was achieved via CellLytic™-M; the media was aspirated off of each well, samples were rinsed with sterile PBS, and transferred to non-seeded wells in which the lysing solution was then added. Samples were incubated (on a shaker table) in the lysate overnight at room temperature. Remaining lysate was stored at -70°C. All end-point assays for MSC were analyzed 1, 2 and 3 weeks *post*-differentiation. Samples were assayed in triplicate (n=3) using a clear bottom 96-well plate.

### *Biom mineralization*

A qualitative measurement of calcium concentration (BioAssay Systems' QuantiChrom calcium assay kit) on BMSC seeded materials was performed on weeks 1, 2 and 3 *post*-differentiation. Calcium deposited on the surface of the samples was dissolved via soaking in 12N HCl solution overnight at room temperature (on a shaker table). Diluted standard solutions were prepared ahead of time and stored at 4°C for future use. Standard solution calcium concentrations (mg/dL) were as follows: 20, 16, 12, 8, 6, 4, 2 and 0 mg/dL. Five µL of the standard and sample solutions was transferred into wells of a clear bottom 96-well plate, followed by 200 µL of working reagent (1:1 ratio of Reagent A and Reagent B, at room temperature). The plates were then incubated for 3 minutes at room temperature and the optical density was read at 612 nm using a plate reader (FLUOstar

Omega, BMG LABTECH). A standard curve was prepared by plotting the average blank-corrected 612 nm reading for each calcium standard verse its calcium concentration in mg/dL. The standard curve was used to determine the calcium concentration of each experimental and control sample.

Surface calcium and phosphate staining were conducted separately at weeks 1, 2 and 3 post-differentiation. For calcium staining, the media was aspirated off and the experimental (10-, XL 10-HA) and control (TCPS, UHMWPE and MA-g-HDPE) specimens were rinsed with cold (4°C) ringer solution (Sigma K4002). The MSC were fixed in a 4% (w/v) paraformaldehyde solution in PBS (4°C) for 10 minutes. Then the samples were washed in cold DI water twice. Two percent (w/v) Alizarin Red S solution (Sigma A5533) was added in 10% (v/v) ammonium hydroxide (pH 4.2) and the samples were soaked in the staining solution for 10 minutes. Finally, the samples were rinsed with DI water three times and images were taken of the stained samples. For phosphate staining, the media was removed and the samples were rinsed with cacodylate buffer (pH 7.2; 54.6 mL 1M cacodylic acid (137.99 g/L), 50.0 mL 1N NaOH (40 g/L), 895.4 mL DI water). The cultures were fixed with 2% (w/v) paraformaldehyde in cacodylate buffer; samples were soaked in the solution for 10 minutes then rinsed twice with DI water. The samples were then soaked in 5% (w/v) silver nitrate (S-6506, Sigma) aqueous solution for 1 hour in a light box. The silver nitrate solution was removed; the samples were rinsed with DI water, and then images were taken of the stained samples.

BMSC-seeded samples were also fixed for scanning electron microscopy (SEM) and energy dispersive spectroscopy (EDS) analysis at each time point (days 1, 4, 7 post-seeding and weeks 1, 2, 3 post-differentiation). The specimens were rinsed two times in PBS for 5 minutes to leach out media. The specimens were then placed in the primary fixative solution (3% (w/v) vglutaraldehyde in 0.1M sodium cacodylate and 0.1M sucrose) for 45 minutes at room temperature. The primary fixative was then replaced with buffer solution (0.1M sodium cacodylate and 0.1M sucrose) and the samples were allowed to soak for 5 minutes; this process was repeated an additional two times. The specimens were next dehydrated with ethanol using the following concentrations in the listed order and allowing the specimens to soak for 10 minutes in each solution: 35%, 50%, 70%, 95%, 100% and 100%. Finally, the ethanol was replaced with hexamethyldisilazane (HMDS) for 10 minutes and dried in a room temperature vacuum oven until characterization. The samples were coated with 20 nm of gold. Prepared specimens were stored under vacuum at room temperature prior to imaging; images were taken using a JOEL JSM-6500F field emission SEM (Tokyo, Japan). Images of the cell-seeded surfaces were taken at 25, 150, 500, 1000 and 8000x at 5.0 keV. Energy-dispersive x-ray spectroscopy (EDS) was also performed; EDS images were taken during SEM analysis using ThermoNORAN software at 15.0 keV.

#### 4.2.5 Statistics

Statistics were analyzed using Statistical Analysis Software (SAS® Institute Inc.). A normality test was performed on the ALP from the immortalized cell line; both the intracellular and extracellular sample sets were non-normal. Therefore, a Wilcoxon rank-

sum test with a 95% confidence interval ( $\alpha=0.05$ ) was performed; multiple comparisons were performed using the least square means. Correlation tests were also performed on the experimental groups only, comparing weight percent of HA to the ALP activity for the intracellular and extracellular data points. The average value and standard error of the mean (s.e.m.) for each experimental and control group population was calculated.

### 4.3 Results

#### 4.3.1 Enzymatic Degradation

The results of the enzymatic degradation study performed on HA-co-HDPE materials and a MA-g-HDPE control are shown in Figures 1 and 2.

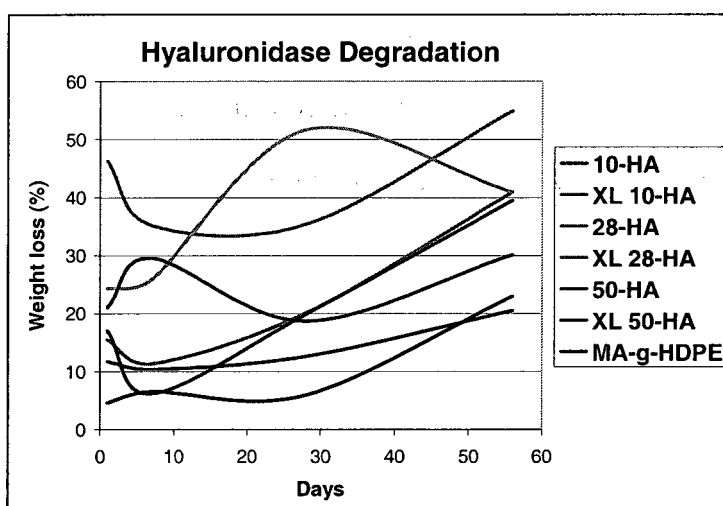
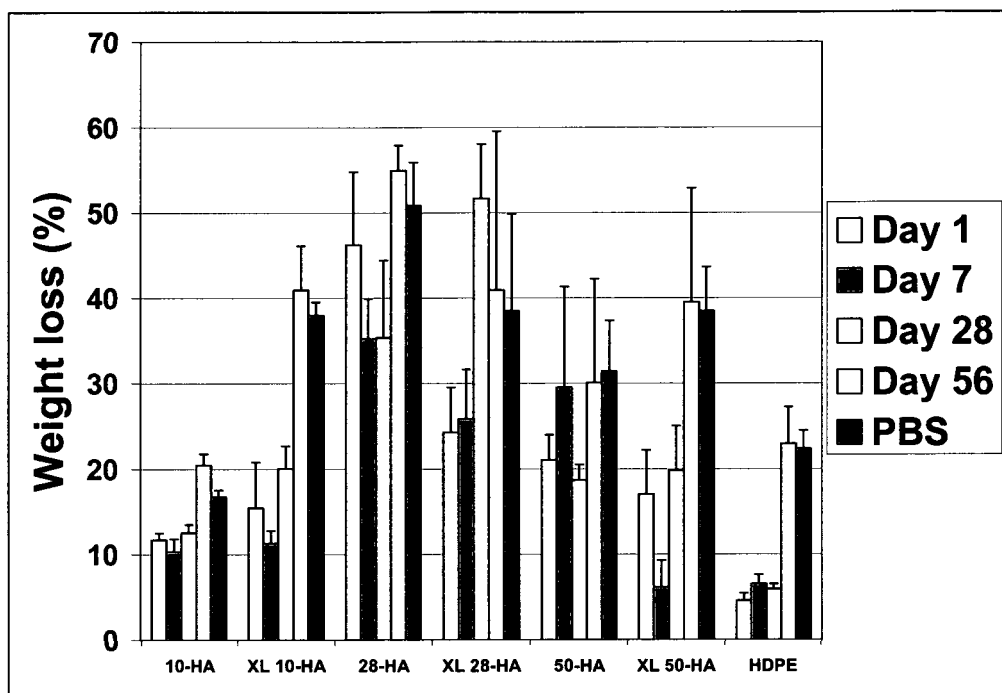


Figure 1. Weight loss (%) of HA-co-HDPE materials and a control group (MA-g-HDPE) over a 2 month period suspended in a hyaluronidase aqueous solution.



**Figure 2. Weight loss (%) of HA-co-HDPE materials and a control group (MA-g-HDPE) over a 2 month period suspended in a hyaluronidase aqueous solution, compared to samples suspended in PBS solution alone for 2 months.**

#### 4.3.2 Secondary Origin Cell Study

##### *Cytotoxicity*

The fluorescent LIVE/DEAD® images of HA-co-HDPE sample groups (10-, 28-, 50-,) and control group (TCPS) will not be shown due to: 1) poor image quality (due to the fluorescent dye binding to the HA molecules) and 2) the inability to image cells inside of the HA-co-HDPE materials. Viable cells were shown on all of the groups at each time point.

##### *Osseocompatibility*

The ALP activity (IU/L) of the 10-, 28- and 50-HA HA-co-HDPE sample groups and TCPS controls is shown in Figure 3. The intracellular ALP activity of the TCPS control

( $0.57 \times 10^3$ ) was significantly ( $p \leq 0.0021$ ) lower than all the HA-co-HDPE sample groups (10-HA= $2.13 \times 10^3$ ; 28-HA= $1.89 \times 10^3$ ; 50-HA= $1.46 \times 10^3$ ). The HA-co-HDPE sample groups were not significantly different from each other; no significant correlation existed between the weight percent of HA in a HA-co-HDPE sample and the corresponding intracellular ALP activity.

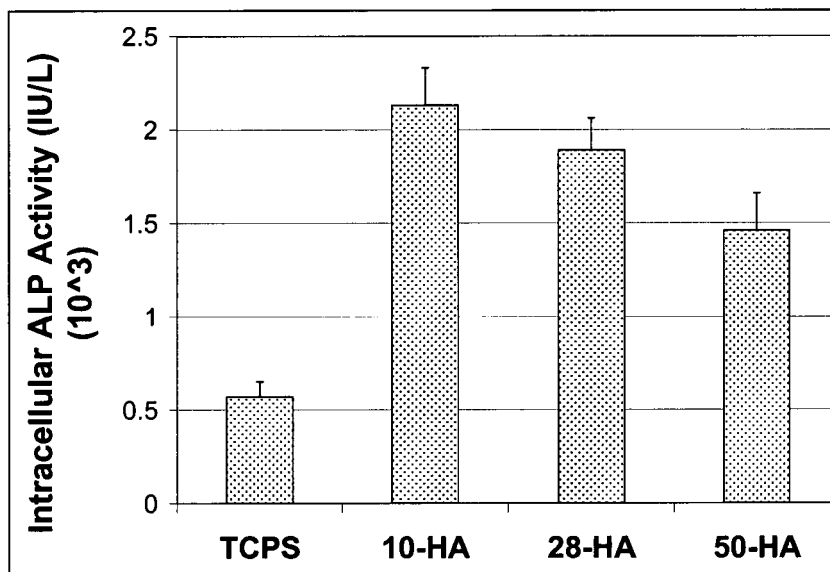


Figure 3. Alkaline phosphatase (ALP) activity (IU/L) for HA-co-HDPE sample groups and TCPS controls 7 days post-seeding HFBOB1.19 [average + s.e.m. ( $n=9$ )].

#### 4.3.3 Primary Origin Cell Study

##### *Cytotoxicity*

The fluorescent LIVE/DEAD® images of HA-co-HDPE sample groups (10-, XL 10-HA), control group (TCPS) and complimentary control groups (MA-g-HDPE and UHMWPE) will not be shown due to: 1) poor image quality (due to the fluorescent dye binding to the HA molecules) and 2) the inability to image cells inside of the HA-co-HDPE materials. Viable cells were shown on all of the groups at each time point;

however, the number of cells shown on the surfaces of complimentary controls exponentially decreased with time.

### *Osseocompatibility*

The results of the MTT assay at days 1 and 4 are shown in Figure 4. All of the materials except for the UHMWPE group exhibited increased cell proliferation from day 1 to day 4.

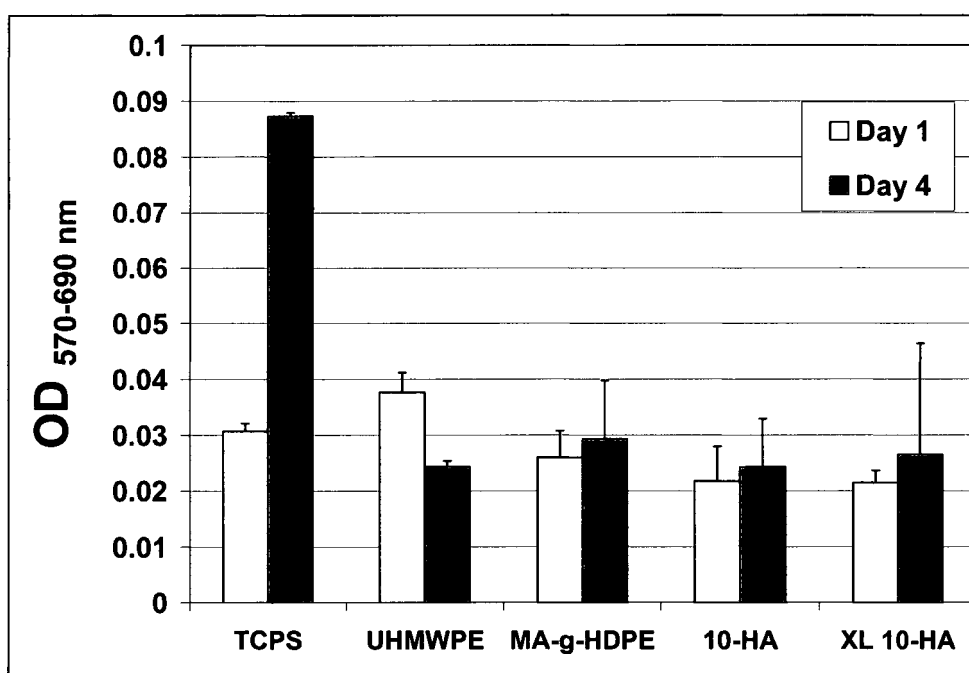


Figure 4. MTT assay optical density for experimental and control samples 1 and 4 days post-seeding [average + s.e.m.].

The protein assay measuring the BSA (i.e., albumin) concentration (Figure 5) and the intracellular ALP concentration (Figure 6) were measured from the same lysate solution. The BSA concentration of the experimental samples is higher compared to the controls at weeks 1 and 2. The BSA concentration was negative for all samples three weeks post-differentiation. The ALP concentration was negative for all experimental groups at all time points.

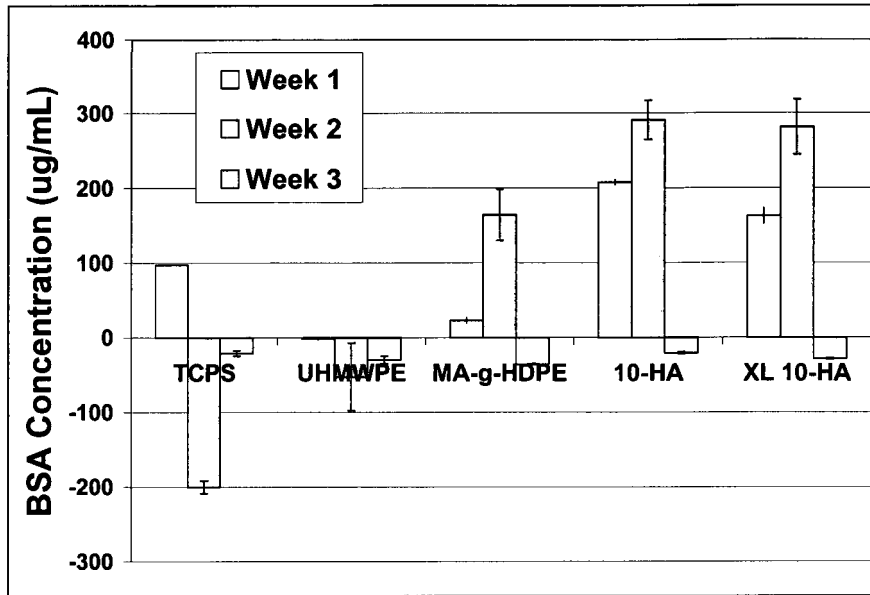


Figure 5. The albumin (BSA) standard curve and BSA concentration ( $\mu\text{g/mL}$ ) for experimental and control samples 1, 2 and 3 weeks post-differentiation.

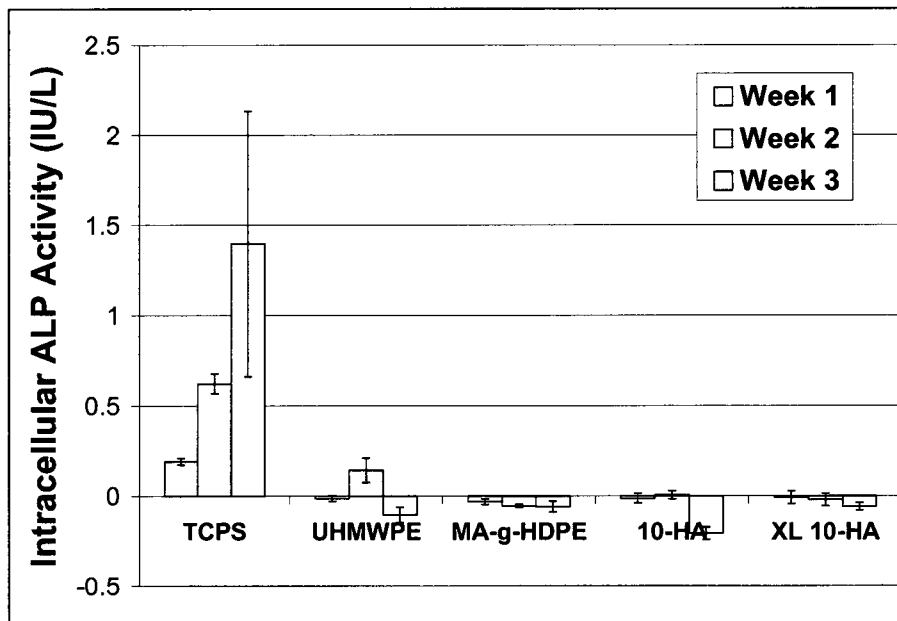


Figure 6. Intracellular ALP activity (IU/L) for experimental and control samples 1, 2 and 3 weeks post-differentiation.

To investigate the maturation of the differentiated MSCs to the osteoblasts, total calcium content was measured of the experimental and control samples. The calcium assay data is shown in Figure 7.

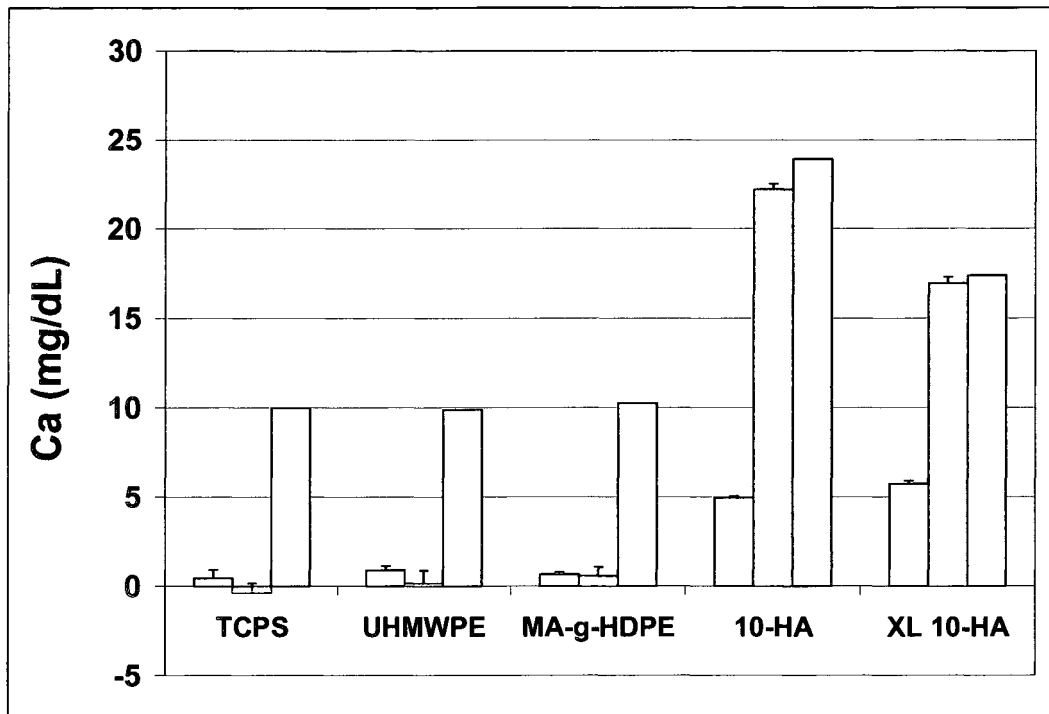


Figure 7. The calcium assay standard curve and  $\text{Ca}^{2+}$  values (mg/dL) for experimental and control samples 1, 2 and 3 weeks post-differentiation.

The experimental and control samples stained for surface calcium and phosphate at 1, 2 and 3 weeks post-differentiation are shown in Figures 8-10. The intensity of the stain for the samples looks very similar for all three time points.

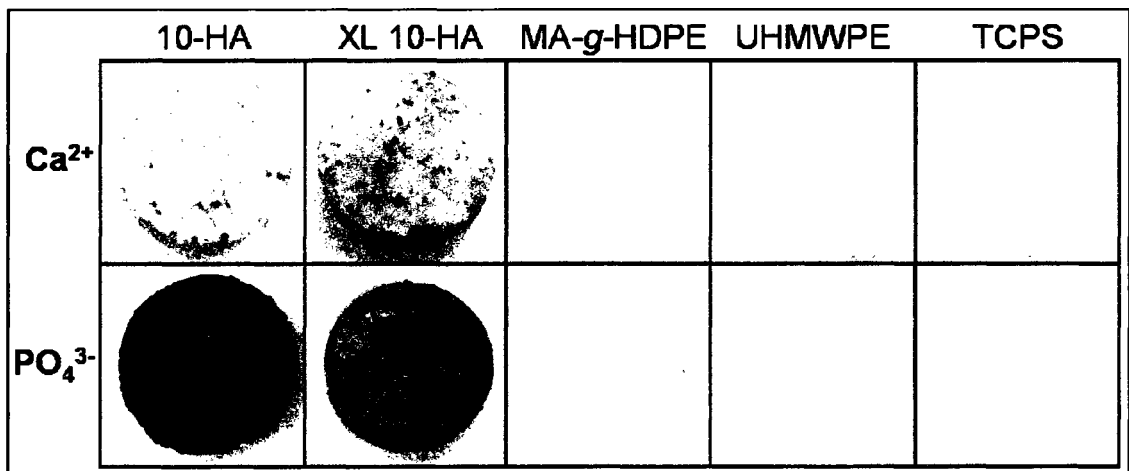


Figure 8. Experimental and control samples stained for calcium and phosphate 1 week post-differentiation.

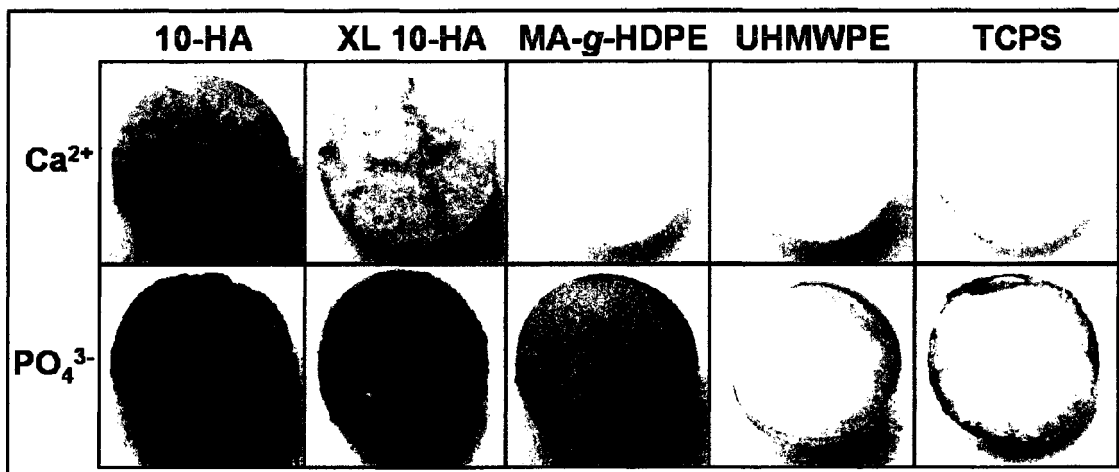


Figure 9. Experimental and control samples stained for calcium and phosphate 2 weeks post-differentiation.

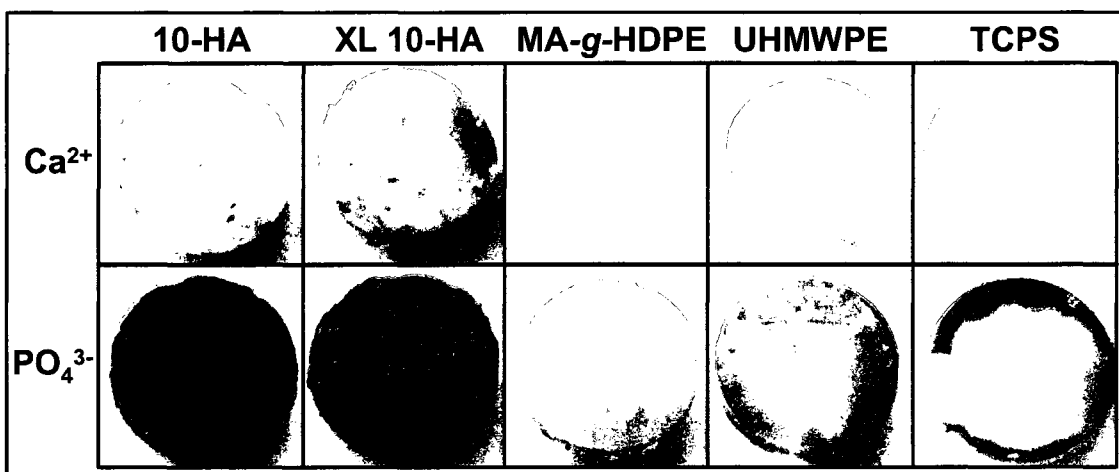


Figure 10. Experimental and control samples stained for calcium and phosphate 3 weeks post-differentiation.

SEM images were taken after 1, 4, and 7 days of culture and weeks 1, 2 and 3 after differentiation with osteogenic media to visualize morphological changes in adhered MSC. The SEM images of experimental and control samples were taken; however, the results for the controls were as expected (*round morphology of MSC on complimentary controls compared to spread out, thin, cells on TCPS control*) and most are not included in this report. SEM images of HA-co-HDPE materials can be found in **Appendix A**. EDS was performed on cell-seeded materials post-differentiation to determine if mineralization was occurring on the surface of the samples; analysis was also performed

on a HA-*co*-HDPE material pre-differentiation to show that no calcium or phosphorus was present on the sample. The EDS electron maps and spectra can be found in **Appendix B**. The EDS elemental spectra for MA-*g*-HDPE and UHMWPE are shown in Appendix B; cells are present on the complimentary controls and are laying down matrix.

#### **4.4 Discussion**

The long-term stability of an implant will determine its clinical utility. *In vivo*, HA is degraded by oxygen free radicals and hyaluronidase.[8] Hyaluronidase exists in many forms – two forms have been well characterized in the literature; one can degrade HA to intermediate-sized fragments of ~20 kDa while the other has the ability to degrade HA to its constituent monosaccharides. In the HA-*co*-HDPE and crosslinked HA-*co*-HDPE groups, the more remarkable degradation was noted in the presence rather than in the absence of hyaluronidase, due to the exogenous enzymatic degradation of the HA portion of the materials. Modification of the HA-*co*-HDPE materials was achieved via chemical crosslinking of the HA portion of the copolymer. However, most surprising, was the amount of weight loss seen in the MA-*g*-HDPE samples; the PBS and hyaluronidase solution weight loss values were approximately the same, which was expected because hyaluronidase has no affect on polyethylenes. The weight loss associated with the MA-*g*-HDPE is the result of low molecular weight species becoming untangled and coming out of the construct. This could be prevented in the future by choosing a thermoplastic with a higher molecular weight, which would in turn reduce the weight loss associated with HA-*co*-HDPE materials. The byproducts of HA degradation induce different affects depending on the size of the fragments; HA fragments of relatively low molecular weight

are inflammatory, angiogenic and immunomodulatory; on the other hand, relatively high molecular weight fragments are non-inflammatory, non-angiogenic and immunomodulatory.[8] An analysis on the hyaluronidase solution removed every other day may provide information on the HA fragments in solution.

Previous work indicated the suitability of HA-*co*-HDPE for chondrocyte viability.[9] After evaluating the HFOB1.19 data, it was determined that the HA-*co*-HDPE samples were non-cytotoxic 7 days post-seeding. The LIVE/DEAD® stain images of HA-*co*-HDPE samples 24 hours and 7 days post-seeding show viable (green) cells growing on all of the samples at each time point; however, the morphology and number of osteoblasts attached to the TCPS control is more distinct and higher compared to the HA-*co*-HDPE sample groups. The lower cell count on the surface of HA-*co*-HDPE specimens may be the result of the surface topography of the specimens. When the HA-*co*-HDPE materials are hydrated, either by water, PBS or cell media, the hydrophilic portion of the compression molded copolymer (i.e., the HA portion) swells and unfolds, creating a porous surface layer. Cells are able to attach to the material on any plane of the material's porous surface layer; therefore, the microscope images of the HA-*co*-HDPE samples are only showing viable cells within a single plane even though multiple planes contain attached cells. This is one reason why the TCPS control shows many more viable cells because the TCPS is a very flat material and all of the cells are attached in a single plane.

Up-regulation of endogenous cellular ALP activity is commonly used as an intracellular marker for assessing the differentiation of osteoprogenitor cells into an osteoblastic

phenotype.[10, 11] The intracellular ALP activity is 10x lower than the extracellular ALP activity. This may be the result of the lysing solution that was used to break down the cell membrane for ALP extraction. The extracellular ALP activity levels for the HA-co-HDPE samples are positive and indicate that viable osteoblasts were present on those samples; however, this data is not representative of the ALP activity for the duration of the study because the media was replaced on day 3. No significant correlation existed between the weight percent of HA in the HA-co-HDPE samples and the intra- and extracellular ALP activity levels. Therefore, it may be possible to alter the weight percent of HA to optimize the mechanical properties of HA-co-HDPE without affecting its osseocompatibility. This may be evaluated in the future by including a negative control (i.e., a material that is known to be cytotoxic). Irregardless of the amount of HA in HA-co-HDPE, the material has been shown to support phenotypic behavior, which has also been shown in the literature.

The use of HFOB1.19 fulfilled the first cytotoxicity screening and provided proof of concept. Therefore, a more physiologically relevant BMSC study was conducted to more rigorously test the osseocompatibility of HA-co-HDPE; one HA-co-HDPE copolymer was chosen for the BMSC study.

The idea is to look for the same trend in BMSC and HFOB1.19 data. The BMSC are more exact to *in vivo* scenario compared to the secondary immortalized cell line because the differentiated MSC are more physiologically relevant; MSC migrate to the site of a bone tissue injury. Bone marrow was collected and BMSC were filtered and were later

signaled via complete media to differentiate to osteoblasts. Traditionally, MSC have been isolated from the cell population of bone marrow based on their selective adherence.[3]

The MTT method is useful in the measurement of cell growth in response to mitogens, antigenic stimuli, growth factors and other cell growth promoting reagents, cytotoxicity studies, and in the derivation of cell growth curves. The reagent, MTT, is enzymatically cleaved within the mitochondria of living cells to produce a dark blue/purple formazan product. An increase in cell number results in an increase in the amount of MTT formazan formed and an increase in absorbance. The MTT method is a cell proliferation assay; growth factors bind to the cell surface during proliferation. The MTT assay will not work outside the log-phase of cell growth thus it is not used as a measure of cell number once the cells have been differentiated and are confluent. The MTT assay will not work once the cells are confluent because they are not working as hard to produce growth promoting reagents. Traditionally, the determination of cell growth is done by conducting a cell count via vital dye staining and microscopy; however, in situations where cell visibility is compromised (e.g., trypsin unsuccessful or view is obstructed) further methods must be employed. Visual cell counting techniques are only approximate and controversial. Alternative methods include radioisotope measure of DNA synthesis, automated cell counters and other techniques which rely on dyes and cellular activity.

The first round of MTT assays were performed following the manufacturer's protocol. The optical density values, however, were very low and a surfactant (Triton® X-100) was incorporated for the second round of MTT assays in order to increase the dissolution of

the formazan crystals. After incubation in the reagent, HA-co-HDPE samples clearly contained purple formazan crystals (indicating viable cells within the material); however, due to the porous nature of the HA-co-HDPE the crystals were incompletely dissolved which may have resulted in artificially low MTT optical densities compared to the controls.

It is hypothesized that the porous structure of the HA-co-HDPE behaved like a scaffold and the cells are migrating into the material rather than adhering to the surface; however, some cells do remain adhered to the surface copolymer materials. This hypothesis is supported by the detection of calcium and phosphate on cracks that have penetrated the surface and the round morphology of osteoblasts on the surface of the material, exhibited in the SEM images of the materials at all time points. Positive protein assay results for weeks 1 and 2 also suggest that viable cells were present in the material 2 weeks post-differentiation. The negative protein assay results for week 3 post-differentiation may be explained by the entrapment of the cell materials (used for ALP and protein assay analysis) in the porous structure; it is evident from the SEM images at week 3 that cells are present on the HA-co-HDPE materials. Also, a large amount of nitrogen, compared to a non-differentiated control, appeared on the elemental scans of cell-seeded samples 3 weeks post-differentiation. It has been reported in literature that MSC seeded on porous hydrogels showed a round morphology on the surface of the materials and tended to aggregate inside the pores.[12] The outer layer, or surface, of the HA-co-HDPE possibly contains a lower weight percentage of HA compared to the interior due to the loss of low molecular weight species which developed due to thermal degradation during

compression molding. It is recommended that the melt processing parameters (including sample depth and temperature gradients) be optimized for consistent results and homogenous materials.

The porous structure of XL HA-*co*-HDPE would be altered with chemical crosslinking, thus having an affect on MSC phenotype expression.[12] The degree of crosslinking, whether for the HA or PE portions of the copolymer, is yet another parameter that can be varied to optimize the osteogenic properties of the HA-*co*-HDPE materials (MSC attachment and differentiation). Mercury intrusion porosimetry is often employed to quantitatively determine the porosity and average pore size of materials; however, the high pressure associated with this technique is not suitable for hydrogel-type scaffolds, like HA-*co*-HDPE, because it could rupture the scaffold.

Bioactivity can be retained in a composite which incorporates a bioactive phase. The effect of HA, in the form of HA-*co*-HDPE, was analyzed on the osteogenic differentiation and mineralization in rat-derived mesenchymal cell cultures. HA-*co*-HDPE was developed for use as an orthopaedic biomaterial due to the bioactive natural component, HA. A wide variety of cell types express the archetypal HA receptor, CD44; the cell-signaling function of HA is mediated through the CD44 receptor. Chondrocytes express the standard isoform of CD44; CD44-HA interactions are essential for maintaining normal cartilage homeostasis (e.g., modulating cartilage metabolism) by linking cells with their extracellular environment.[8] CD44 is also expressed in bone in haematopoietic marrow cells, osteoclasts (degrade bone matrix) and osteocytes

(responsible for mechanosensory functions), osteoblasts (synthesize bone) and osteoprogenitor cells; CD44-HA interactions may play roles in inter-osteocyte and osteocyte-osteoclast communication.[8] HA-cell surface receptor interactions activate a series of intracellular signaling pathways, including transforming growth factor (TGF)- $\beta$  receptor I, and participate in regulation of cell migration, proliferation, condensation and differentiation.[13] HA plays an important role in both the early and later stages of bone formation. HA has the capacity to modify osteoblast behavior; high molecular weight HA has been shown to be osteoinductive (accelerating new bone formation) *in vivo*[8] while low molecular weight species increase osteogenic differentiation of mesenchymal cells *in vitro*. [13] High molecular weight HA (300 kDa) has been shown to stimulate MSC proliferation and significantly increase ALP activity and bone mineralization (i.e., calcium deposition increased).[10] Although HA makes up 3% of the total GAG content in bone[13], cell adhesion is adversely affected by the presence of HA.[14]

In order to determine the toxicity potentials of HA-co-HDPE materials *in vivo*, a leachable cytotoxicity assay may be performed to determine if excess solvents or other cytotoxic leachables were trapped in the material as a result of fabrication and processing. In the future confocal laser microscopy should be investigated as an alternative to epifluorescence microscopy, using a depth profiling characterization.[12] The freeze-thaw method may be applied to the HA-co-HDPE materials in the future to lyse the cells and deform the structure of the material, releasing the cell content into solution for UV spectroscopy analysis.[11] Additional molecular markers that could be targeted include: TGF- $\beta$ 1 (a biomarker for osteoblast proliferation) and PGE<sub>2</sub>, an indicator of osteoblast

differentiation and maturity). Immunoblotting of focal adhesion proteins can be performed to determine levels of cytoplasmic proteins relating to focal adhesion (e.g., focal adhesion kinase, FAK). A cytoskeletal stain may also be used to show differences due to surface (or interior material) properties such as surface energy (hydrophobic versus hydrophilic surfaces). Osteocalcin, a biomarker for mature osteoblasts, can be semi-quantitatively measured using standard Western blot techniques (primary antibody: anti-human osteocalcin, Biogenex # AM-386-5M) and a chemi-luminescent detection system.

#### **4.5 Conclusion**

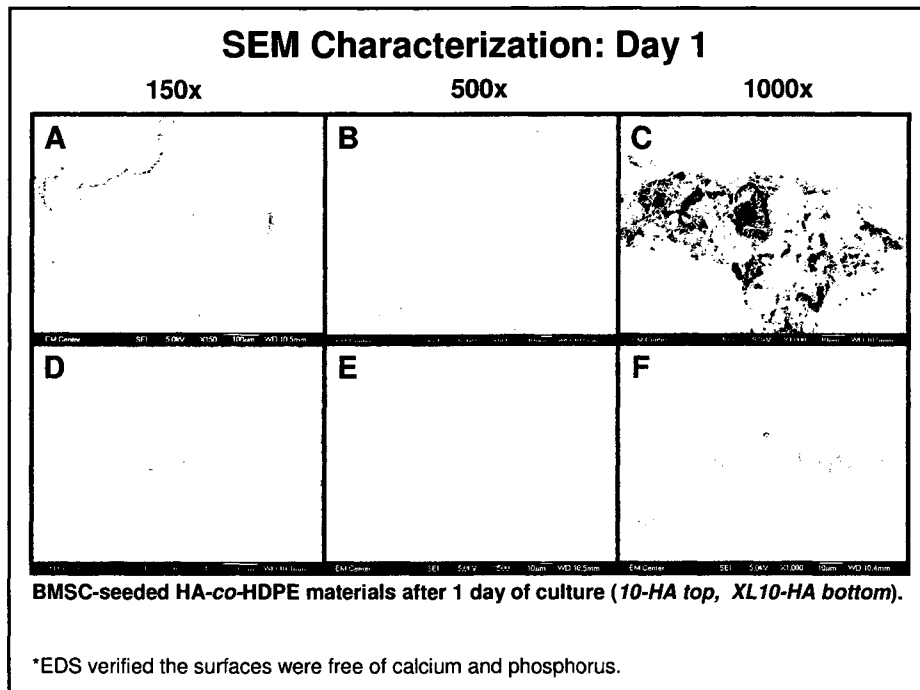
Various *in vitro* studies have demonstrated both the non-cytotoxicity and osseocompatibility of HA-co-HDPE materials. HA-co-HDPE materials, in their crosslinked and non-crosslinked states, provide a superior microenvironment to support BMSC differentiation into osteoblasts. The HA-co-HDPE materials retain the osteoinductive properties native to HA. These findings suggest that HA-co-HDPE may be successfully used for treating osteochondral defects and enhancing osseointegration, but also as cell delivery applications to bone defects *in vivo*.

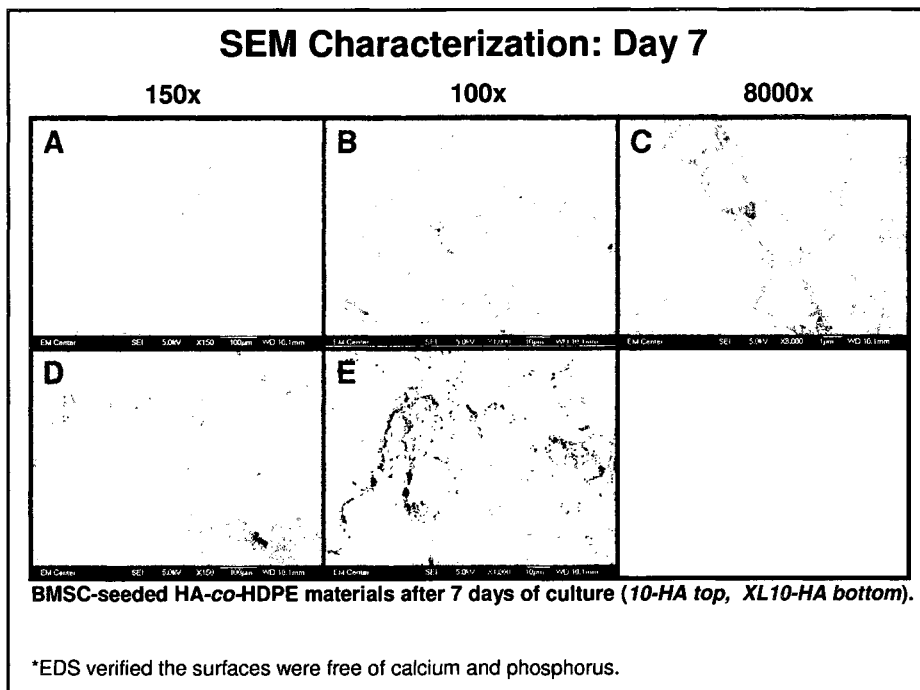
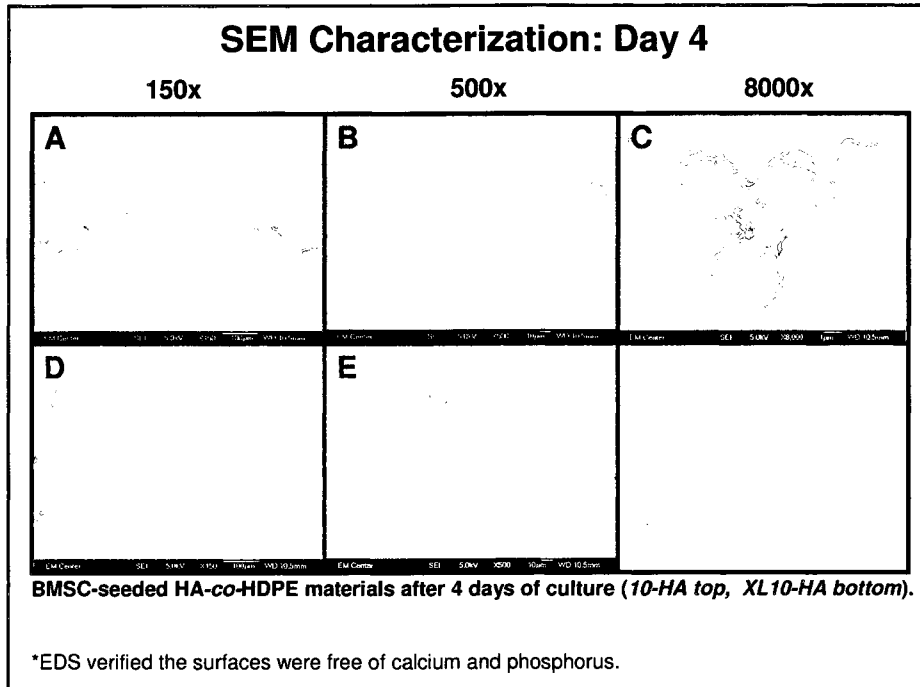
#### **4.6 References**

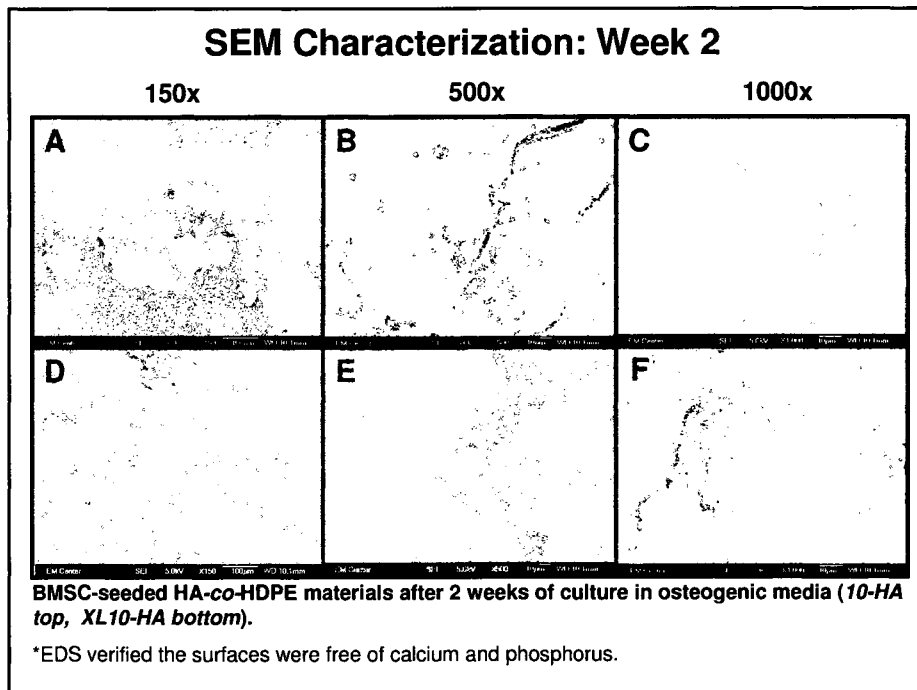
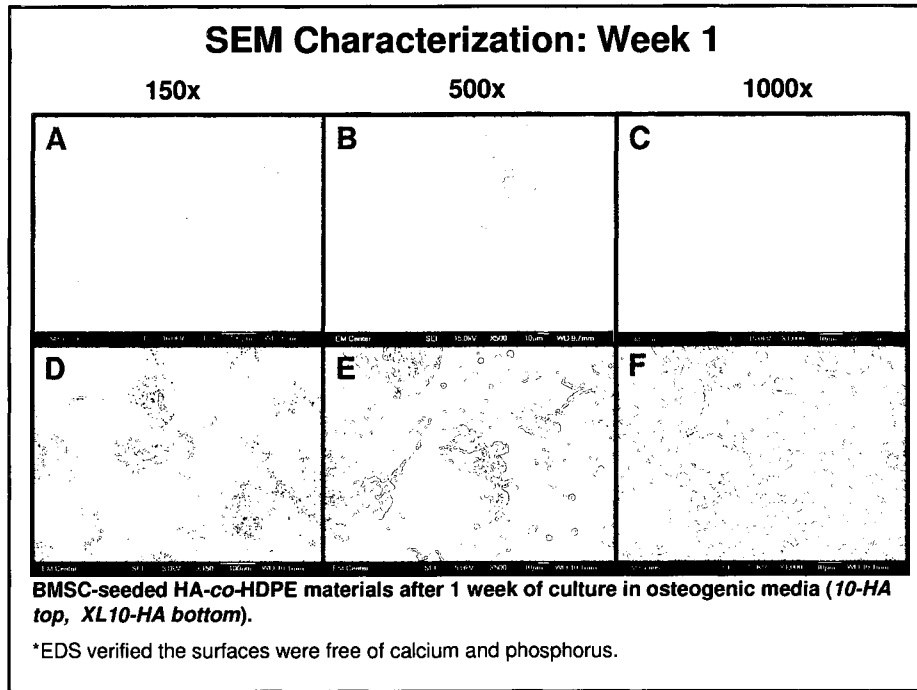
1. Chajra H, Rousseau CF, Cortial D, Ronziere MC, Herbage D, Mallein-Gerin F, et al. Collagen-based biomaterials and cartilage engineering. Application to osteochondral defects. *Bio-Medical Materials and Engineering* 2008;18:S33-S45.
2. Machado CB, Ventura JMG, Lemos AF, Ferreira JMF, Leite MF, Goes AM. 3D chitosan-gelatin-chondroitin porous scaffold improves osteogenic differentiation of mesenchymal stem cells. *Biomedical Materials* 2007;2:124-131.
3. Kassem M, Abdallah BM, Saeed H. Osteoblastic cells: differentiation and trans-differentiation. *Archives of Biochemistry and Biophysics* 2008;473:183-187.

4. Modder UI, Khosla S. Skeletal stem/osteoprogenitor cells: current concepts, alternate hypothesis, and relationship to the bone remodeling compartment. *Journal of Cellular Biochemistry* 2008;103:393-400.
5. Lu P-L, Lai J-Y, Ma DH-K, Hsiue G-h. Carbodiimide cross-linked hyaluronic acid hydrogels as cell sheet delivery vehicles: characterization and interaction with corneal endothelial cells. *Journal of Biomaterials Science Polymer Edition* 2008;19(1):1-18.
6. Woodfield TBF, Malda J, de Wijn J, Peters F, Riesle J, Van Blitterswijk CA. Design of porous scaffolds for cartilage tissue engineering using a three-dimensional fiber-deposition technique. *Biomaterials* 2004;25:4149-4161.
7. Segura T, Anderson BC, Chung PH, Webber RE, Shull KR, Shea LD. Crosslinked hyaluronic acid hydrogels: a strategy to functionalize and pattern. *Biomaterials* 2005;26(4):359-371.
8. Bastow ER, Byers S, Golub SB, Clarkin CE, Pitsillides AA, Fosang AJ. Hyaluronan synthesis and degradation in cartilage and bone. *Cellular and Molecular Life Sciences* 2008;65:395-413.
9. Oldinski RA, Harris JN, Godek ML, James SP. A novel hyaluronan-polyethylene copolymer for orthopaedic applications. 54th Annual Meeting of the Orthopaedic Research Society. San Francisco CA, 2008.
10. Huang L, Cheng YY, Koo PL, Lee KM, Qin L, Cheng JCY, et al. The effect of hyaluronan on osteoblast proliferation and differentiation in rat calvarial-derived cell cultures. *Journal of Biomedical Materials Research Part A* 2003;66A(4):880-884.
11. Huang J, Di Silvio L, Wang M, Tanner KE, Bonfield W. In vitro mechanical and biological assessment of hydroxyapatite-reinforced polyethylene composite. *Journal of Materials Science: Materials in Medicine* 1997;8:775-779.
12. Dadsetan M, Hefferan TE, Szatkowski JP, Mishra PK, Macura SI, Lu L, et al. Effect of hydrogel porosity on marrow stromal cell phenotypic expression. *Biomaterials* 2008;29:2193-2202.
13. Zou L, Zou X, Chen L, Li H, Mygind T, Kassem M, et al. Effect of hyaluronan on osteogenic differentiation of porcine bone marrow stromal cells in vitro. *Journal of Orthopaedic Research* 2008;26(5):713-720.
14. Chua PH, Neoh KG, Shi Z, Kang ET. Structural stability and bioapplicability assessment of hyaluronic acid-chitosan polyelectrolyte multilayers on titanium substrates. *Journal of Biomedical Materials Research Part A* 2008;87A:1061-1074.

# Appendix A





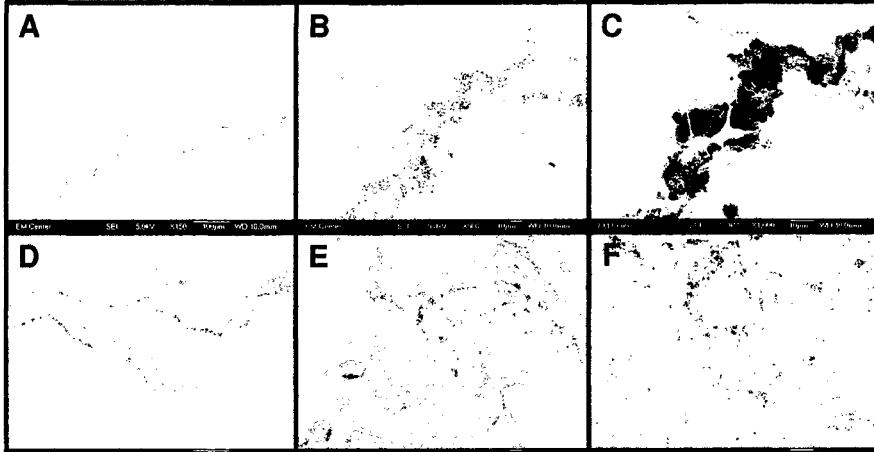


### SEM Characterization: Week 3

150x

500x

1000x

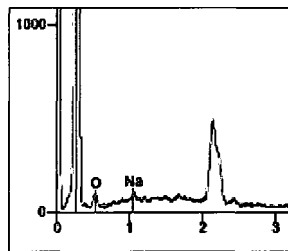


**BMSC-seeded HA-co-HDPE materials after 3 weeks of culture in osteogenic media (10-HA top, XL10-HA bottom).**

\*EDS verified the surfaces were free of calcium and phosphorus.

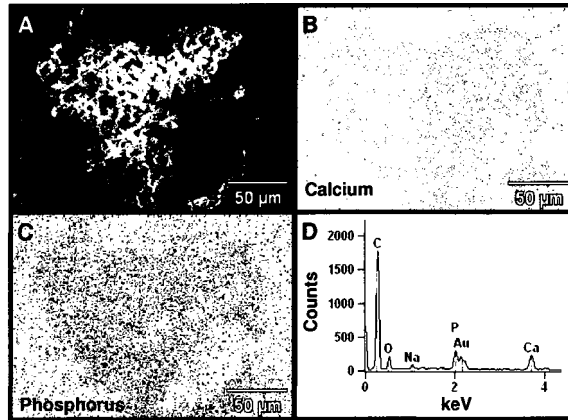
## Appendix B

### HA-co-HDPE: Day 7



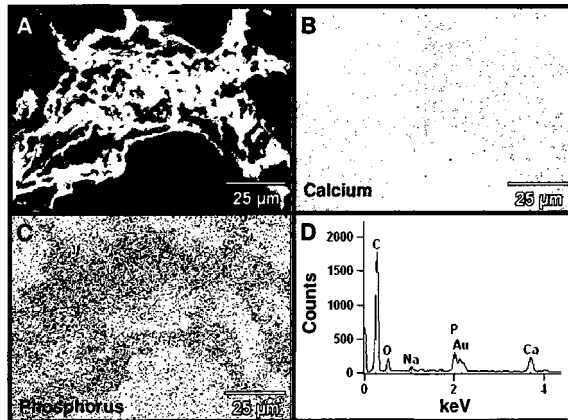
EDS spectrum of HA-co-HDPE surface 7 days after culture; no calcium or phosphorus exists on the surface of the sample.

### HA-co-HDPE: Week 1



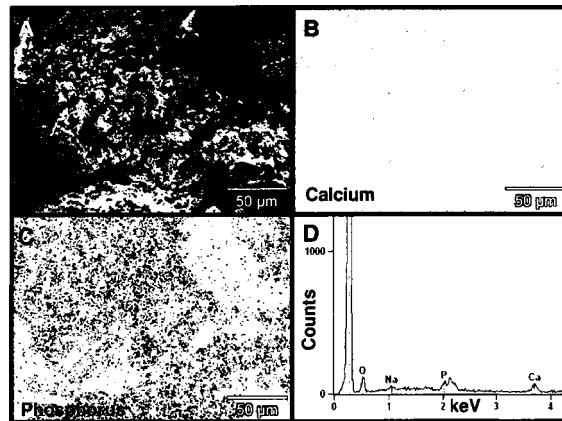
SEM (A), EDS color map (B,C) and EDS spectrum (D) of HA-co-HDPE surface 1 week after culture in osteogenic media. In the center of the SEM image is a pore lined with calcium-phosphate spherulites.

### XL HA-co-HDPE: Week 1



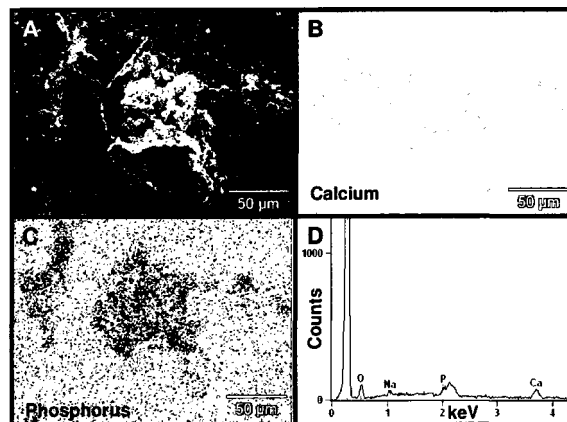
SEM (A), EDS color map (B,C) and EDS spectrum (D) of XL HA-co-HDPE surface 1 week after culture in osteogenic media. In the center of the SEM image is a pore lined with calcium-phosphate spherulites.

### HA-co-HDPE: Week 2



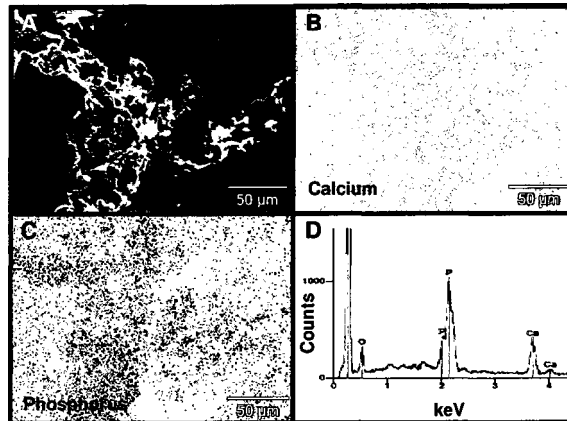
SEM (A), EDS color map (B,C) and EDS spectrum (D) of HA-co-HDPE surface 2 weeks after culture in osteogenic media. In the center of the SEM image is a pore lined with calcium-phosphate spherulites.

### XL HA-co-HDPE: Week 2



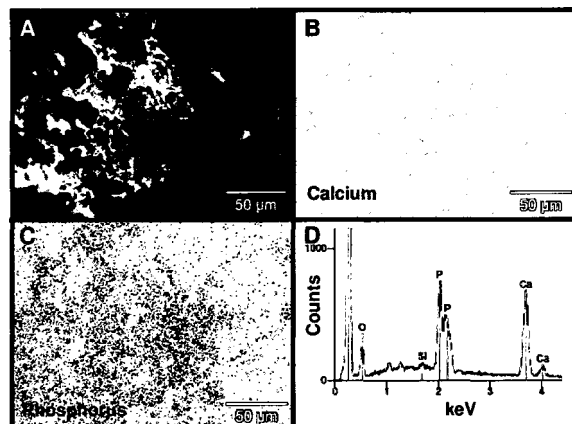
SEM (A), EDS color map (B,C) and EDS spectrum (D) of XL HA-co-HDPE surface 2 weeks after culture in osteogenic media. In the center of the SEM image is a pore lined with calcium-phosphate spherulites.

### HA-co-HDPE: Week 3



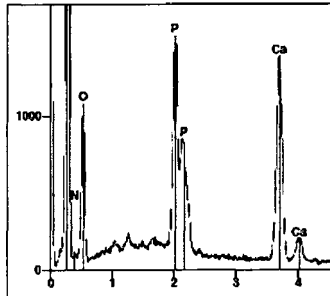
SEM (A), EDS color map (B,C) and EDS spectrum (D) of HA-co-HDPE surface 3 weeks after culture in osteogenic media. In the center of the SEM image is a pore lined with calcium-phosphate spherulites.

### XL HA-co-HDPE: Week 3



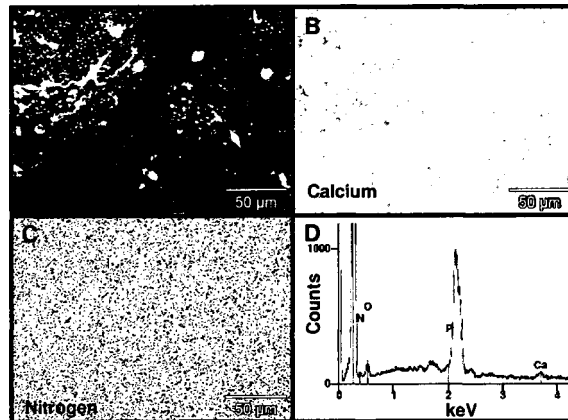
SEM (A), EDS color map (B,C) and EDS spectrum (D) of XL HA-co-HDPE surface 3 weeks after culture in osteogenic media. In the center of the SEM image is a pore lined with calcium-phosphate spherulites.

### MA-g-HDPE: Week 3



EDS spectrum of MA-g-HDPE surface 3 weeks after culture in osteogenic media.

### UHMWPE: Week 3



SEM (A), EDS color map (B,C) and EDS spectrum (D) of UHMWPE surface 3 weeks after culture in osteogenic media.